Injection Matching of Antenna

By

Yasin Kabiri

A Thesis Submitted to
The University of Birmingham
for the Degree of
Doctor of Philosophy

School of Electronic, Electrical
and System Engineering
College of Engineering
and Physical Sciences
The University of Birmingham
April 2016

Abstract

One of the most important modules of the current and next generation of the wireless communications is the antenna. The coexistence of the machine and human in the next communication system will open-up a vast range of new applications and communication services which need to be supported by the antenna.

Moreover, the forthcoming 5G technology vision is prognosticated on the use of multiple communication bands and standards in a seamless fashion.This can force the mobile devices to have multiple antennas on a single device which will add significant complexity or using an antenna with wideband reconfiguration capability. On the other hand, switched-off analogue communications provides the opportunity for re-using prime spectrum in UHF bands. Considering the size of hand-held devices, this will need strong miniaturization. To address these requirements, electrically small, tunable, wideband and highly efficient antenna technology is strongly desired.

In this thesis a new area of research in antenna design is introduced which has been unexplored by the other researchers. A new theory called Injection Matching Theory (IMT) is proposed which uses multi-port configuration. This will enable to control current distribution on the antenna structure at its extremities and couple a wave length, much larger than what the antenna dimensions naturally allow. Apart from electrically small operation this can be used for improving band width and efficiency, and providing reconfiguration capability.

To illustrate the versatility of the proposed theory, for every feature mentioned above a chapter is provided which demonstrates the potential capability of the proposed theory via simulation and fabrication of the prototyped examples.

Contributions

1. Patent

   Y. Kabiri, P. Gardner, and C. Constantinou "Electrically small antenna," , U.K Patent application GB1603154.4, 24th February 2016.

2. Proposal

   EPSRC grant proposal (£1.2m), "TEMPEST: Tunable, efficient, multi-port electrically small antenna" , 2015

3. Invited Book Chapter

   Modern Antenna Systems, INTECH, 2016

4. Publications

   (a) Y. Kabiri, P. Gardner, and C. Constantinou "Fabrication and measurement of Simultaneous Injection matched Patch antenna," Transaction on Antennas and Propagation, IEEE. (Submitted)

   (b) Y. Kabiri, P. Gardner, and C. Constantinou "A miniaturized highly efficient injection matched antenna," Transaction on Antennas and Propagation, IEEE, (Submitted)

   (c) Y. Kabiri, P. Gardner, and C. Constantinou "Frequency reconfigurable injection matched antenna," Antennas and Wireless Propagation Letters, IEEE. (Submitted)

   (d) Y. Kabiri, P. Gardner, and C. Constantinou, , "Wideband miniaturized Injection Matched patch Antenna," in Radio Science Meeting (Joint with AP-S Symposium), 2015.

(e) Y. Kabiri, P. Gardner, and C. Constantinou, "Simultaneous Injection Matched Antenna," in Antennas and Propagation (EuCAP), 2015 9th European Conference.

(f) Y. Kabiri, P. Gardner, and C. Constantinou "Injection matched approach for wideband tunable electrically small antennas," Microwaves, Antennas Propagation, IET, vol. 8, no. 11, pp. 878 - 886, August 2014.

(g) Y. Kabiri, P. Gardner, and C. Constantinou, "Radiation Investigation From An Injection Matched Antenna," in Antennas and Propagation (LAPC), 2014 10th Loughborough Conference.

(h) Y. Kabiri, P. Gardner, and C. Constantinou, "A novel approach for wideband tunable electrically small antennas," in Antennas and Propagation (EuCAP), 2014 8th European Conference on, April 2014, pp. 3633 - 3637.

(i) P. Gardner, A. Feresidis, P.S. Hall and Y. Kabiri, "Frequency reconfiguration in single and dual antenna modules," in Antennas and Propagation (EuCAP), 2013 7th European Conference on, April 2013, pp. 2006 - 2009

This thesis is dedicated to my parents

for their endless love, support

and encouragement

Acknowledgements

I praise God for all His mercy and grace, the beauties of the world and the chance that he has given us to discover its laws. I would like to thank Prof. Peter Gardner and Dr. Costas Constantinou, the supervisors of this research, for the scientific and moral guidance of this work. I would like to thank my parents, my brothers Mohsen and mohammad hosein(sedmilad), and my wife, for all their support and encouragement throughout my life. I would like to thank all the teachers and professors that I have had throughout my life. I would also like to thank my dear friends and colleagues, especially Mohammadreza, Mahdi, Hessam, Omid who helped me through completion of my work.

Contents

List of Figures

List of Abbreviations

GSM Global System for Mobiles

UHF Ultra High Frequency

FM Frequency Modulation

IMT Injection Matching Theory

SIMT Simultaneous Injection Matching Theory

SIM Simultaneous Injection Matching

IM Injection Matching

PF Power Factor

MTM Meta-material

ENG Epsilon Negative

ESA Electrically Small Antenna

MNG μ negative

NFRP Near-Field Resonant Parasitic

NIC Negative Impedance Converter

MIMO Multiple Input Multiple Output

PIFA Planar Inverted F Antenna

UWB Ultra Wide Band

CPW Co Planar Waveguide

CP Circular Polarization

DRA Dielectric Resonator Antenna

CCCS Current Control Current Source

VNA Vector Network Analyzer

Chapter 1

Introduction

1.1 Background

The need for small antenna terminals to meet specific demand for mobile communications initiated with the birth of the 1st generation (1G) of mobile communication in the 1990s. The mobile phone services opened new tasks and requirements for the antennas which significantly differ from conventional portable radio link systems. The revolutionary applications and capabilities which became available with the rise of 1G, guaranteed a significantly broad market.

In 1G mobile communication the devices should be hand held and thus the size was a challenging constraint with few degrees of freedom imposed by the low operating frequency band in the 1G. To meet this challenge the only practical solution was the use of whip antennas. However, this constraint was relaxed with the advent of the Global System for Mobiles (GSM) standard and the adoption of higher operating bands [1].

Further developments in mobile communication enabled users to have access to a range of wireless standards including blue-tooth, WiFi, FM radio and etc. Considering the voracious demand for connectivity and the new requirements, more standards and services are and will be set out to handle this trend. Therefore, the range of requirements for mobile antennas has significantly broadened. These requirements could be in accordance to the

user's need such as small dimension, low cost, light weight or the service provider's need such as high efficiency, enough channel bandwidth, multi-band operation and robustness to the environmental change. Moreover, nowadays, the demarcation between various devices such as mobile, telephone and computers has faded and the most important goal for the communication system is to provide universal connectivity any where, and any time via enabling wireless access to private or public networks. For such a system, the higher data rate and enhanced quality of service will be two indispensable factors entangled with the advent of forthcoming standards and applications [2]. Consequently, the future antennas, which connect the terminals to free space, to be able to fully support this system, will have to have some specific features including, small size, easy fabrication, wideband width with frequency tuning capability and high efficiency.

A frequency reconfigurable antenna with sufficiently wide bandwidth can be used in a mobile device instead of multiple antennas to cover multiple frequency. This will save space and will reduce the cost of the design. On the other hand highly, efficient antennas are highly desired as they can save the battery life [3–6].

The significant growth in mobile communication systems was made feasible by the evolution of the semi-conductor technologies. It allows to decrease the physical size while increasing the functionality of the electronic devices in mobile terminals. Consequently this trend compels the antenna designer to miniaturize the size. However, in contrast to the electronic chips, antenna miniaturization is not determined by the technology used, while it is limited by the laws of physics; the antenna size relative to the radiation wavelength is the predominant factor which influences the characteristics of an antenna. This can be readily conceived considering an antenna as a transformer which transforms the guided wave to the radiating wave. Therefore, for an efficient transformation the size of the antenna should be large enough compared with the guided wave length to allow the coupling of the guided wave. Surely, the antenna can be made smaller but this is a challenging demand which will be described in depth in this thesis [2, 7].

Deriving the relationship between the antenna characteristics and its geometry an-

tenna, has been an important research topic from the early radio days. This is discussed in depth in chapter 2.

1.1.1 predicted future requirements

Among the most important components of the current and next generation of the wireless communications are the antennas. The forthcoming 5G technology vision is prognosticated on the use of multiple communication bands and standards in a seamless fashion. This forces the mobile devices to have multiple antennas on a single device and some believe that to achieve the optimum operation there will be a need for 20 antennas on a single device [8]. This will add severe complexity to the antenna design in mobile devices that already suffer from lack of enough space to locate multiple antennas with sufficient isolation between them.

On the other hand due to the current traffic of the available spectrum for use of mobile communication, there is strong demand to re-use the spectrum available in UHF bands freed recently by the abolishment of analogue communication. Therefore, the complexity of antenna design is intensified as these bands are incompatible with the size of mobile devices if strong miniaturization has not been accomplished [2, 9].

In summary, considering current and future requirements in mobile communication systems, antennas with the following features are highly desirable and vital for the establishment of the next generation of the mobile communication: electrically small operation: wide bandwidth: tuning capability and high efficiency. In this thesis, a new theory is introduced which can address these requirements for the current and future of mobile communication. It opens up a completely new research area using a technique that has been unexplored by other researchers.

1.2 Objectives and hypothesis

In a conventional antenna, the current flows over the structure via one excitation port. Generally, the currents fall down to zero or have a local maximum amplitude at the antenna's extremities. This current distribution limits the size of the wavelength which can be coupled and naturally resonate on the antenna structure.

However, if the endpoint restriction on the current distribution is relaxed, the antenna size and the operating wavelength can be decoupled via a forced resonance on the antenna structure. The investigation of how to realize such an operation and its potential benefits, are discussed in this thesis. The forced resonance is constructed on the antenna by introducing an extra excitation port close to the antenna extremities. This new proposed approach is called Injection Matching Theory (IMT). The operation of this new class of antennas with an associated design methodology for electrically small, wideband width and frequency tunable operation is also discussed. Furthermore, it will provide an opportunity for improving the efficiency of the antennas which suffer inherent low total efficiency.

One unique advantage of this approach, is that it is not limited by the operating frequency. Therefore, the subject of this thesis not only addresses the requirements of the mobile communication industry, but also can be used to provide green communication by significantly improving the efficiency of highly inefficient transmitters/receivers used in FM broadcast radio bands.

To the best of the author's knowledge the introduced technique, has never been investigated before and as such it opens a fundamentally new area. The thesis then will address the theory, simulation and experiment of the proposed concept.

1.3 Layout of the thesis

The thesis consists of eight chapters. While chapter 2 reviews the literature and related works to this thesis, the main contributions are presented in Chapters 3 to 7, and a conclusion is provided in Chapter 8. Figure 1.1 depicts the conceptual links between different chapters of the manuscript. In the following, a brief overview of each chapter is provided.

1.3.1 Chapter 2

The main purpose of this chapter is to review the parts of the literature which are related to this thesis and to introduce the developed theory. It starts with the description of the fundamental limitations of an electrically small antenna and how the physical size of an antenna can affect its characteristics such as band width, efficiency and quality factor. This is described from the highly cited papers which addressed these limitations back in 1947 to the most recent ones.

Once the physical limitation which causes the poor performance of the electrically small antennas is described, the more recently developed techniques in the literature to address this challenge, are covered.

The impedance matching technique for wideband operation, is also a topic entangled with electrically small antenna design. Therefore these techniques are also reviewed. Moreover the constraints and the limitation of the reviewed techniques are investigated.

As the IMT uses the multi-port configuration, to show the uniqueness of this technique and for better understanding of it, a review of the state of the art on multi-port antennas is provided and the main goal of such design is discussed.

Tuning capability is one of the most important requirements for the current and future mobile communication system. This is one of the potential benefits of the IMT. Therefore, some current techniques for making reconfigurable antennas are also discussed. This can illustrate the novelty being used in the developed technique in this thesis.

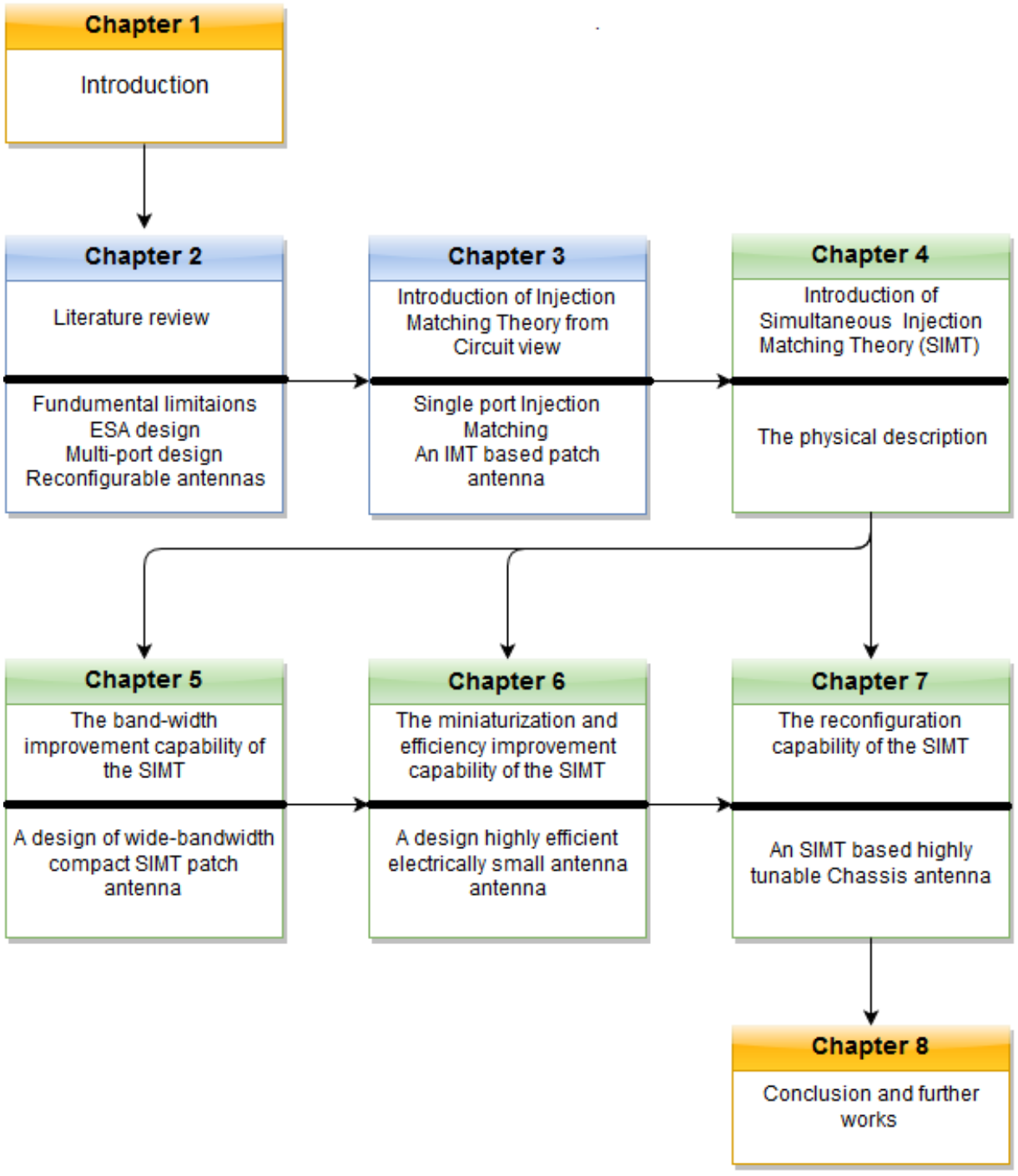

Figure 1.1: The hierarchical thesis structure

1.3.2 Chapter 3

In this chapter the theory of the IMT which does not suffer from the drawbacks and limitations associated with the available techniques in the literature, is presented. This technique enables electrically small operation with wide bandwidth and tuning capability at the same time which are the requirements of the current and the future of mobile communication.

The theory is introduced and derived via a circuit point of view. An injection matched patch antenna is fabricated and experimental validation of the IMT is performed. The radiated power from an injection matched patch antenna is also investigated.

The experimental results demonstrate that injection matching can significantly improve the radiation from an antenna at frequencies well below its natural resonance.

In this section one port is introduced to the antenna structure, to provide matching for the other port.

1.3.3 Chapter 4

Successful realization of the IMT, led on to investigation of the possibility of simultaneous injection matching of the excitation ports (SIMT). This is the topic of this chapter which is described via physical explanation. The forced resonant concept is described from presenting the current distribution, via elastic string analogy. Examples for better understanding of the physical concept behind the SIMT are also provided.

1.3.4 Chapter 5

This Chapter illustrates the bandwidth improvement capability of the SIMT initially described in chapter 4. This is investigated by applying the SIMT technique on a proximity fed patch which suffers from poor matching. The SIMT based proximity fed patch antenna shows considerably wider bandwidth and much better level of matching over frequency. The antenna is also fabricated and the experimental results agreed well with simulation

which validates the mentioned capability of the SIMT.

1.3.5 Chapter 6

In this chapter an electrically small antenna with wide bandwidth and high efficiency is fabricated via use of the SIMT. Moreover, the potential capability of the SIMT for improving the total efficiency of an antenna is investigated. This is described by showing how the SIMT can affect the input impedances of the port for an efficient radiation. The antenna is then fabricated and the experimental data show good agreement with the simulated data.

1.3.6 Chapter 7

In this chapter to address frequency reconfiguration capability which is strongly desired in mobile communication, the SIMT is used as a design methodology for making highly tunable antenna with wide band width of operation. This is investigated via a chassis antenna with current handset dimensions. The suitability of the developed methodology is then validated by comparing the results from conventional varactor tuning technique and the proposed technique.

The design is then fabricated and approaches for further improvements are discussed

1.3.7 Chapter 8

In this chapter current and future needs for mobile and wireless communication systems are discussed. Then, apart from outlining the achievements of each chapter, the potential capabilities of the developed theory for addressing these requirements are discussed. This chapter is finished by providing the further work that can be accomplished.

1.4 Conclusion

In this chapter the requirement for the current and future mobile communication are discussed. SIMT and IMT show considerable promise for making new types of electrically small, reconfigurable, wideband and highly efficient antennas which can address these requirements. In this chapter, the motivations of the study, the research needs and thesis contributions are discussed. The chapter is finished by providing the thesis structure and a brief summary of each chapter.

Chapter 2

Literature Review

Recently, great attention is concentrated on studying Electrically Small Antennas (ESA) due to their compact size and light weight - two highly attractive features. Moreover, due to the rapid growth in mobile communications technology, ESAs with several functional capabilities are even more desirable [10].

Electrically Small Antennas are much smaller than the conventional half-wavelength antennas. This is a challenging demand to meet as the physical size of the antenna with respect to wavelength is a parameter which essentially affects the radiation characteristics. Major studies have been suggested toward the analysis of the electrically small antennas in which the earliest and most influential ones were established by Chu [11] and Wheeler [12].

They have introduced the theoretical limits which state how bandwidth and electrical size are related. Subsequent studies and further refinements are mainly based on them, although more precise and more type specific. The common idea is that for a passive one-port radiator, the size reduction can only be achieved at the expense of efficiency or bandwidth.

There are also various guidelines presented in the literature to make an electrically small antenna operate close to the fundamental limits. Some of these approaches will be investigated in the further subsections. In summary, key design notes which guarantee

an optimum operation of electrically small antennas are, low dielectric constant, aspect ratio close to unity and the internal structure of the antenna such that the fields are as uniform as possible in the smallest enclosing sphere [13].

In this chapter, initially an introduction to small antenna fundamentals are provided. Then the state of the art in electrically small antennas and various recent matching techniques are investigated. These papers and the developed theoretical limits have been investigated for radiators with ***one excitation port***. However, due to the nature of this thesis which will utilize a multi-port antenna configuration, a subsection is allocated to summarize the available design notes for multi-port antennas.

Moreover, one important application of the electrically small antennas is in hand-held and mobile devices in which a tuning capability is a great advantage. This is also considered in the developed designs in this thesis. Therefore, a subsection of this chapter reviews the design guide lines for reconfigurable antennas.

2.1 Fundamentals of electrically small antennas

In this section, a summarized overview of small antenna analysis and its theoretical limits is provided. For the first time in 1947 Wheeler developed the relation between the bandwidth and the efficiency through studying two small antennas occupying the same volume; a cylindrical parallel plate capacitor and a cylindrical coil inductor [14]. He derived the radiation power factor for these antennas. The radiation power factor p_e for the capacitive (parallel plate) antenna is derived as

$$p_e = \frac{G_e}{\omega C} = \frac{1}{6\pi}\frac{k_a A b}{l^3} \tag{2.1}$$

and for the coil inductor antenna p_m as

$$p_m = \frac{R_m}{\omega L} = \frac{1}{6\pi}\frac{k_b A b}{l^3} \tag{2.2}$$

where G_e and R_m are radiation conductance in parallel and radiation resistance in series with the antenna, respectively and C and L are capacitance and inductance. A and b are the area of base and height of cylindrical volume, respectively. k_a is the shape factor of the capacitor which is the ratio of effective area and the actual area A, and k_b is the shape factor of the inductor which is the ratio of effective length and the actual length b and $l = \lambda/2\pi$ is the radian length.

He define that the fundamental limitation on bandwidth and the practical efficiency is related to the radiation power factor p_e or p_m. Due to the miniaturized size of the small antennas the radiation power factor is much less than unity.

By comparing (2.1) and (2.2) he concluded that the power factor has the same form for both antennas. Apart from the correction factor, it has also the same value and only depends on the ratio of the antenna volume (Ab) to radian cube (l^3). Therefore, the interceptable amount of power by the capacitor or inductor antenna is limited by the radiation power factor which is somewhat greater than $\frac{1}{6\pi}\frac{Ab}{l^3}$ on the assumption of no tuning loss [14].

In fact the radiation power factor describes the radiation of the real power from an antenna considerably smaller than its operating wavelength, which includes also large reactive power. It can be used for any highly reactive element in which the size of the element is the limiting factor for the maximum achievable radiation power factor.

In general two volume references are used for illustrating the size relative to the radian length, which are:

$$radiancube = V_c = (\frac{\lambda}{2\pi})^3 = V_s(\frac{3}{4\pi}) \tag{2.3}$$

or

$$radiansphere = V_s = (\frac{\lambda}{2\pi})^3(\frac{4\pi}{3}) = V_c(\frac{4\pi}{3}) \tag{2.4}$$

The latter is a hypothetical sphere with radius of a radianlength from the centre of an antenna, significantly smaller than the radiansphere. The radian sphere can be considered as the border between the near-field (inside) and the far-field (outside). The

radiated fields from the antenna at the centre, include stored energy and radiated power which are predominant in the near-field and far-field respectively [15].

The radiansphere is also important as it is easy to use where the antenna is spherical and as the effective volume is often expressed in spherical format. The radiation power factor can be expressed in terms of V_s and V_c as:

$$radPF = P = (\frac{1}{6\pi})(\frac{V'}{V_c}) = (\frac{2}{9})(\frac{V'}{V_s}) \tag{2.5}$$

where the $V' = k_a Ab$ or $k_b Ab$ in which k_a and k_b are bigger than zero. The effective volume V' is directly proportional to the radiation PF and an increase in its value will increase the latter. Therefore an approach for making efficient small antennas is to use structures with large effective volume.

To provide a better understanding of effective volume, Fig. 2.1 taken from Wheeler's work [16], is provided. The geometries of a modified dipole and a loop antenna and their corresponding effective volumes are illustrated. From these examples it can be concluded that more efficient use of volume (examples from left to right) will increase the effective volume.

The theoretical upper limit for the radiation PF can be achieved if a small spherical coil filled with perfect magnetic core is used. A spherical coil filled with air has a shape factor of 3/2 which will be multiplied by 3 if it is filled with a perfect magnetic core [17]. From (2.5) the radiation PF can be calculated as:

$$radP_m = (\frac{2}{9})(\frac{(3)(3/2)V}{V_s}) = (\frac{V}{V_s}) = (ka)^3 \tag{2.6}$$

The last part of the equation (2.6) can be readily derived by considering that $k = 2\pi/\lambda$ in (2.4) and the volume of a sphere is $V = (4/3).\pi a^3$, where a is the radius of the sphere enclosing the antenna and k is the wave number. This is the idealized case in which the avoidable stored energy is totally removed and there is no stored energy inside the antenna (sphere with radius a).

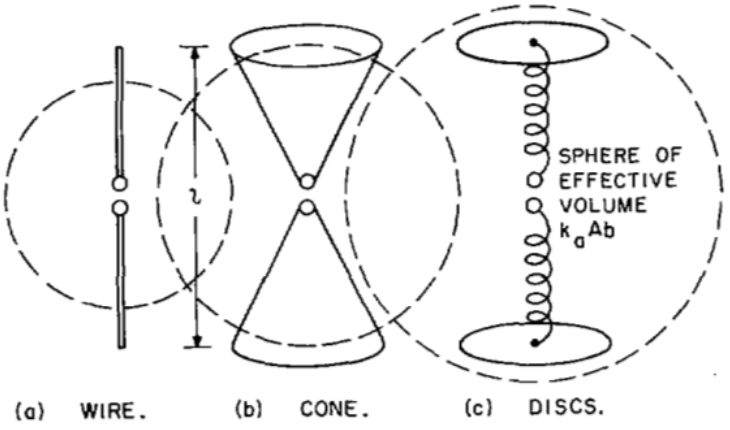

Effective volume of axial electric dipole.

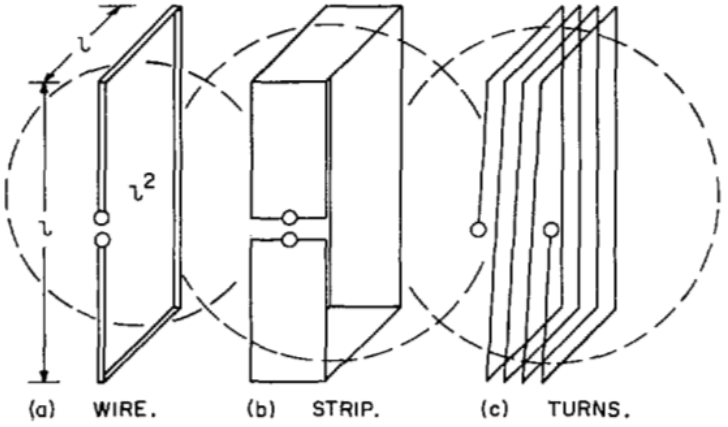

Effective volume of square loop.

Figure 2.1: The effective volume and various geometry of a dipole and a loop antenna [16].

Therefore, for **a single feed** antenna this rad PF can not be exceeded and is the upper limit. The reactive power or stored energy fills the rest of the radiansphere which is the unavoidable part of the stored energy. This will impose the fundamental limitation on achievable radiation power factor. This suggests that for an antenna, the radiation power factor can be increased by allowing the antenna structure to utilize as much as possible of the volume of a sphere with a diameter equal to the maximum dimension of the antenna.

The opposite bound can be achieved from (2.5) in which the effective volume is equal to the radian sphere with a power factor of 2/9.This is the case for a long inductor with air core or a flat capacitor with air-dielectric.

The Q-factors for RL and RC circuits are $R/\omega L$ and $1/\omega RC$, respectively [18]. Wheeler's

definitions of the power factor for inductive and capacitive antennas derived in (2.1 and 2.2) are recognizable as the inverse of the Q-factor for an RL and RC circuit. By inverting the physical upper limit for the radiation power factor derived for a spherical coil filled with perfect magnetic material in (2.6) will be also in good approximation to what Chu and other authors calculated for the minimum achievable Q using more rigorous methods [11].

Regarding the small antenna design Wheeler also showed the following guidelines: for a given volume adding an electrically large ground plane can almost double the radiation power factor, increasing μ_r can increase rad power factor by a factor of 3 while increasing ϵ_r inside the antenna will reduce the latter proportional to ϵ_r. In non-spherical antenna the radiation PF is decreased due to partial utilization of effective volume [13–16]

2.1.1 Q-factor calculation

In 1948 Chu derived the minimum achievable Q-factor from the field expansion with the use of spherical wave functions for a **one port** omni-directional antenna [11].

He showed that any radiating field can be expressed as a summation of orthogonal spherical modes such that each mode illustrates a spherical wave which travels in the outward radial direction.

As the spherical waves are orthogonal, energy associated with each of the spheres will not be coupled to the other spheres. Therefore, the summation of the energy and the complex power associated with each spherical wave will lead to the total stored energy outside the sphere and complex power transmitted across the closed spherical surface, respectively.

Consequently, the fields outside of the sphere can be represented by the equivalent circuits of the spherical modes. For a loss-less antenna each of the spherical modes can be expressed by an L-C circuit with a series C and a shunt L. Hence, the whole circuit might be modelled by a ladder network of L-C circuits that is terminated by a shunt resistor which represents the radiation resistance. Based on the simplified equivalent circuit, by

knowing the impedance of each sphere, the average dissipated power and the average energy stored for each sphere can be found. Consequently the Q which is the ratio of the stored energy to the radiated energy can be obtained [11].

After Chu's and Wheeler's initial works, regarding the minimum achievable Q, numerous authors have investigated this subject for various cases using different methods. Herein, some of the highly cited ones are mentioned.

The general description of the quality factor at the operating frequency ω is the ratio of the stored energy W to the dissipated power via radiation P. For a non-resonant network the input impedance is proportional to $P + 2j\omega(W_m - W_e)$ where W_m and W_e are the time averaged stored magnetic and electric energy [19]. For this reason Collin in 1964 defined the Quality factor for a network which includes an additional ideal lossless reactive element for reactance compensation, as:

$$Q = (\frac{2\omega W}{P}) \tag{2.7}$$

where

$$W = 2Max((W_m - W_e)) \tag{2.8}$$

Consequently, he defines (2.7) as the upper achievable bound for an antenna tuned to resonate with adding an external reactive element to compensate for the reactive part presented at input impedance. Any loss introduced by the tuning circuit will cause deviation of the Q from the limit presented in (2.7) [19].

He derived the reactive magnetic and electric energy by subtracting the energy density associated with power flow from the total energy density. Then he calculated Q from (2.7). He also calculated the limit for the Q for the cylindrical and spherical antenna.

In 1981 Hansen [20] further investigated the ladder network equivalent circuit for each spherical mode, presented by Chu. In accordance to the modal impedance (ratio of mode voltage to mode current in the equivalent circuit) and after considerable manipulation, he

derived an expression for the quality factor of the lowest TM mode as:

$$Q = \frac{1 + 3k^2r^2}{k^3r^3[1 + k^2r^2]} \tag{2.9}$$

In 1996 McLean [21] followed two techniques for calculating the Q. He derived the propagating and non-propagating fields, and Q as their ratio. Then he used Chu's equivalent circuit and showed that both approaches result in the same expression which was also derived by Collin as:

$$Q = \frac{1}{k^3a^3} + \frac{1}{ka} \tag{2.10}$$

In addition to this, he also derived an expression for a circularly polarized antenna as:

$$Q = \frac{1}{2k^3a^3} + \frac{1}{ka} \tag{2.11}$$

Many other authors have provided further expressions for the Q. However (2.10) and (2.11) are mostly accepted and the other author's results are within an acceptable agreement with (2.10) and (2.11).

2.1.2 Limits on radiation efficiency and bandwidth

Generally, electrically small antennas have low radiation resistance and high reactance and consequently they have high Q. The radiation efficiency of an antenna can be defined as:

$$e_r = \frac{R_r}{R_r + R_{ohmic}} \tag{2.12}$$

where R_r and R_{ohmic} are the radiation resistance and total ohmic losses of the antenna and any matching circuits, respectively [14].

As previously discussed, the radiation power factor defined by Wheeler, is the inverse of the quality factor. On the other hand, the bandwidth is defined as [20]:

$$Bandwidth = \frac{f_{upper} - f_{lower}}{f_{centre}} = \frac{1}{Q} \tag{2.13}$$

Therefore, in effect the radiation power factor is equivalent to impedance bandwidth and similar limitations are applied. The radiation efficiency presented in (2.12) can be rewritten in terms of radiation and loss power factor as:

$$e_r = \frac{P_{rad}}{P_{rad} + P_{loss}} \tag{2.14}$$

According to (2.14) in an electrically small antenna, as the P_{rad} is relatively small, existence of P_{loss} can significantly affect the efficiency of the antenna. In practice the P_{loss} is unavoidable as it will be present in the reactive source used for the purposes of reactance compensation and will also increase the input resistance at the input terminal of the small antenna.

In (2.9), (2.10), (2.11) and Wheeler's definition of the radiation power factor, P_{loss} is considered to be zero. The limits for the achievable Q may differ for a network with a non zero P_{loss}. The effect of the loss factor for lossy antennas can be modelled by inserting a loss resistance in series with the radiation resistance which will affect the Q. This has been investigated by Hansen in [20]. This is presented in Fig. 2.2 which illustrates the fundamental limitation for Q versus various efficiencies. The bandwidth then can be derived from (2.13). From this figure it is clear that the bandwidth can be increased at the expense of reducing the efficiency. More effective use of volume will also increase the bandwidth.

Moreover in Hansen's study, for the purpose of comparison between the Q for practical antennas and the minimum achievable Q, two examples are provided. The Q for a short dipole which is basically a 1-D structure and a more effective design using a three dimensional structure (a cover leaf dipole with coupling loops over a ground) designed by Goubau, are illustrated in Fig. 2.2 [20]. It is clear that the Goubau antenna [22] which has larger effective volume, is closer to the limit curve compared with the two dipoles

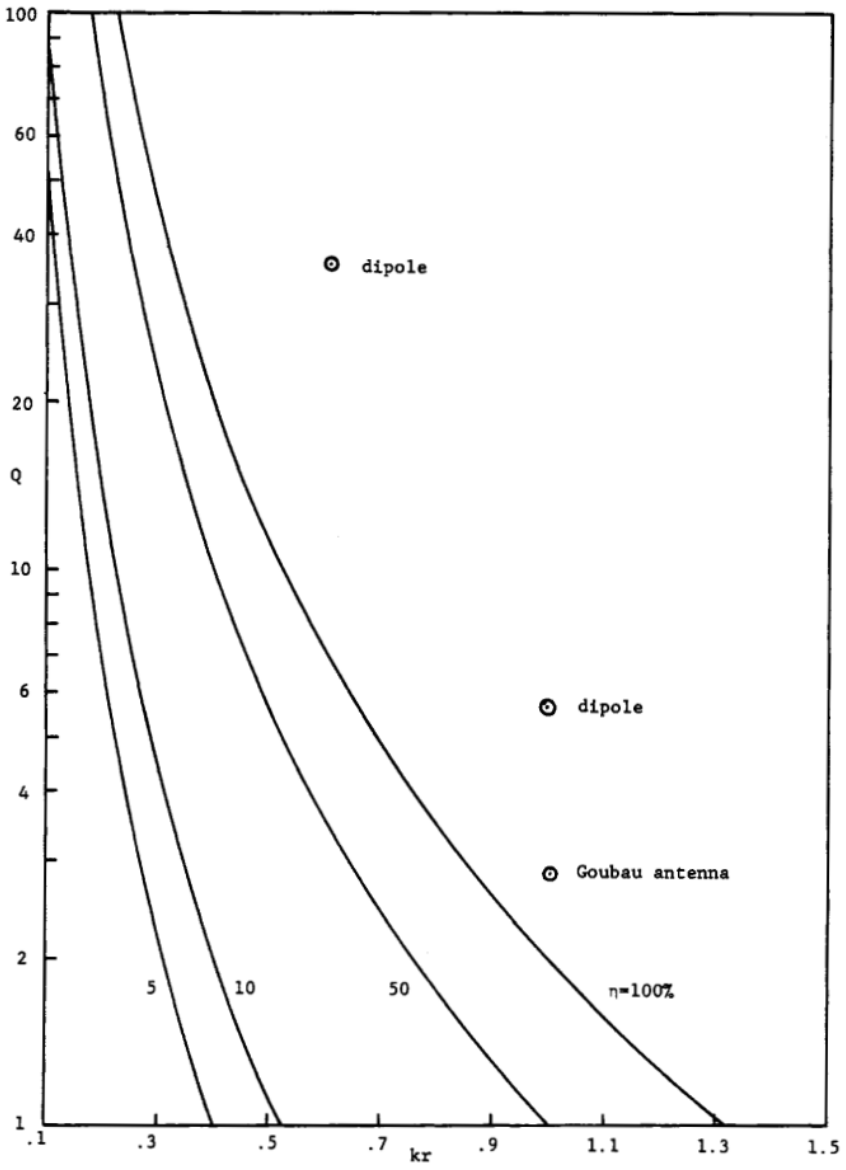

Figure 2.2: Fundamental limitation on radiation Q for various efficiencies [20].

illustrated in this figure for two values of kr.

2.2 State of the art in one port electrically small antennas

After reviewing the fundamental limitations of an electrically small antenna, herein the most common miniaturisation approaches are reviewed. Various approaches have been

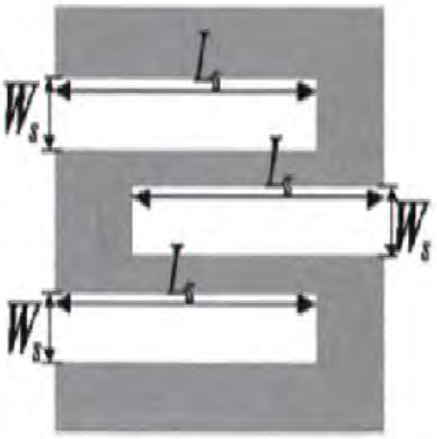

L_s (mm)	f_0 (GHz)	Q_z (Meas.)	Q_z (Simul.)	Q_{FBW} ($SWR = 2$)	Q_{exact} (Simul.)	E_s (L/λ_g)	a/λ_0	ka	Radiation Efficiency (%)
0	2.236	29.5	26.4	28.6	25.8	0.444	0.212	1.331	83.1
13	1.665	–	92.0	–	–	0.331	0.158	0.991	71.8
15	1.535	–	112.6	–	–	0.305	0.145	0.914	63.8
17	1.400	158.3	132.6	155.4	132	0.278	0.133	0.834	53.3
19	1.263	194.6	173.6	188.8	167	0.251	0.120	0.752	40.2
21	1.115	–	150.0	–	–	0.222	0.106	0.664	24.6
23	0.953	–	200.7	–	–	0.190	0.090	0.567	21.5
25	0.838	–	223.6	–	–	0.167	0.080	0.499	11.1
27	0.755	–	248.4	–	–	0.150	0.072	0.449	5.7
29	0.689	–	286.3	–	–	0.137	0.065	0.410	3.7
31	0.64	–	361.6	–	–	0.123	0.061	0.381	2.4

Figure 2.3: Different values for the width and length of the slots and their effect on the Q factor [23]

proposed to meet this challenge. These approaches are defined and practical examples for each of them are illustrated.

2.2.1 Electrical length

The overall antenna size can be condensed by maintaining the physical length, while increasing the electrical length. A rectangular patch antenna which exploits multiple slits parallel to its radiating edges is illustrated in Fig. 2.4 [23]. The slits force the current to flow in a meandering path on the patch. The meandering current path increases the electrical length of the patch antenna and as a consequence results in considerable decrease in the resonant frequency. The bandwidth and the Q are improved by optimizing

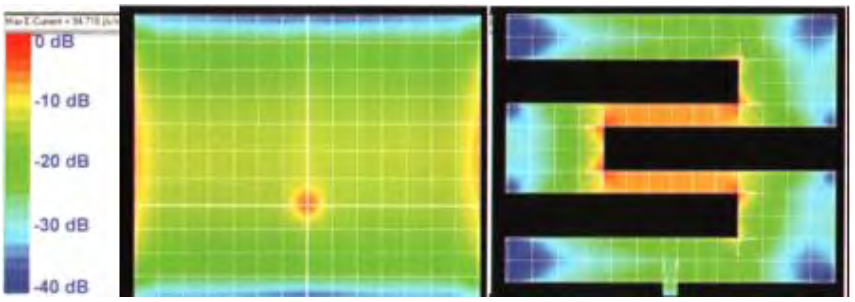

Figure 2.4: The current distribution on the basic patch and patch with slits [23].

the length and the width of the slits. An antenna with $ka < 1$ has been successfully fabricated for this approach in [23]. The geometry of this antenna and how the current is being distributed on the patch are illustrated in Fig. 2.4. In this figure the current distribution on the conventional patch (right hand figure) and the meander current on the patch with slits are illustrated in which significant increase in radiating length in the latter is visible (shaded area). The results achieved for different values for the width and length of the slots and their effect on the Q factor can be found in Fig. 2.3

Utilizing this approach, miniaturized antennas have been developed in [23–25]

2.2.2 Volumetric antenna

Increasing the radiation resistance of an antenna can significantly improve the radiation efficiency and such an antenna can readily match with the source impedance if its reactance is also close to zero. An important class of those which perform particularly well are antennas with complicated structure that have spherical shape or an aspect ratio close to one. The concept behind this technique is defined here through the following examples [26]. In [26] and [27] amendment on the dipole antenna is applied to achieve an electrically small self resonant dipole. The capacitive reactance of the conventional electric dipole can be tuned to zero by increasing the total length of the wire. A lower Q factor is achieved when the antenna structure uses the entire volume of the sphere which encloses the largest antenna dimension. To meet these two points the folded spherical dipole is designed. On the other hand to increase the input resistance of such an antenna, multiple

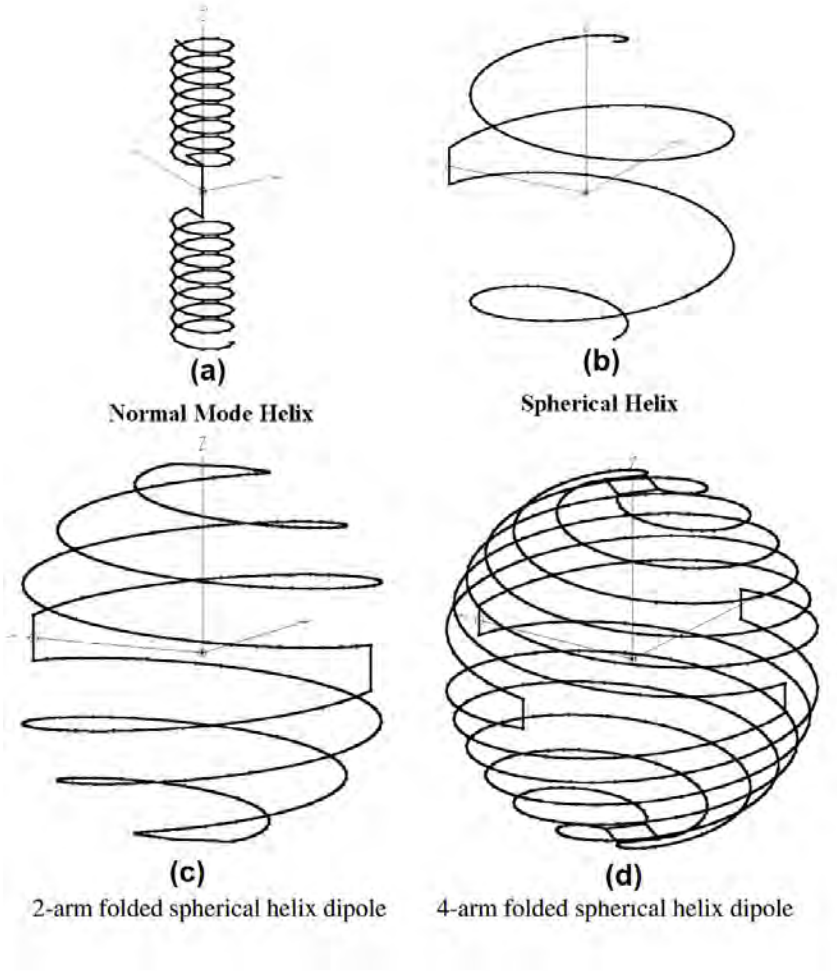

Figure 2.5: (a) Normal mode Helix, (b) Spherical Helix, (c) 2-arm folded spherical Helix and (d) 4-arm folded spherical Helix [26].

folded arms are added to the structure. These antennas are illustrated in (Fig. 2.5) [26]. The Q and the input impedance of four different antennas are compared with a straight wire dipole which has a feed point impedance equal to 1.1-j1015 and a Q of 950 at 300 MHz. The effective height and the spot frequency are almost the same in all examples which will lead to $ka = 0.27$, where k is the wave number and a is the radius of sphere enclosing the maximum dimension of the antenna. Fig. 2.5 (a) illustrates a normal helix with a self resonance close to 300 MHz, impedance of 4.6 Ω and Q of 216. The increase in the input resistance compared with the normal dipole is due to the increase in wire length.

Fig. 2.5 (b) shows a spherical helix. The input resistance of this antenna is 2.2 Ω

which is less than that of the normal helix. This is due to the significantly shorter wire length used for this antenna compared with the helix. However, the Q of this antenna is 193 which is substantially less than that a of helix. This can be clarified from what was discussed in section 1.1. The spherical helix occupies significantly larger volume than the normal helix which leads to substantially less reactive power surrounding the antenna. To increase the wire length and as a consequence increase the radiation resistance, folded arms can be added to the spherical helix, as illustrated in Fig. 2.5 (c). The 2-arm folded spherical helix has radiation resistance of 10.3 and Q of 101.1 which are considerably improved compared with the spherical helix. The radiation resistance and the Q are improved to 47.5 and 87.3 , respectively by adding 2 more folds. This is illustrated in Fig. 2.5 (d)

To further decrease the quality factor of this antenna, the arms are configured such that the antenna excites elliptical polarization. This will reduce the Q to half of that for the 4-arm spherical helix with linear polarization. Similar techniques following the same concept as defined in the latter examples have been used in many other papers to make electrically small antennas including [28–32]

2.2.3 Metamaterial inspired

Metamaterial (MTM) inspired antennas are another recently suggested approach which has introduced opportunities for research into new types of ESA.

The MTMs are artificial materials whose permeability and permittivity can be designed to be positive or negative. The MTM element is positioned in proximity to the driven element of the antenna, and via a strong magnetic or electric coupling between them, a good match to a 50 Ω impedance is obtained without the use of an external matching network [33]. Therefore, high radiation efficiency as well as size miniaturization are achieved. The main concept of this design is that an electrically small epsilon negative (ENG) material which is inductive in nature, is introduced at the very near field of an electrically small antenna, such as an electric dipole which is highly capacitive, to form

a composite resonant system. Similarly a μ negative(MNG) MTM which is capacitive in nature, can be used for the same purpose for a magnetic dipole (loop antenna). In theory it is also shown that using this technique, it is possible to achieve 50 Ω input impedance.

Fig. 2.7 taken from [10] illustrates the general concept of MTM based electrically small antennas. The middle part in Fig. 2.7 (a) realizes the effect of the shell with epsilon negative material. The coupling between the monopole and the shell is represented via the transformer N_1 and L which in this case shows the inductive effect of the ENG shell.

The C_0 component illustrates the capacitance associated with the infinitesimal electric dipole and its resistance is neglected because it is much smaller than the source impedance which is 50 Ω. N_2 is used to represent the coupling between the antenna shell and free space. By ignoring the conduction loss of the shell, R_0 represents the radiation resistance of the shell. To simplify this concept further the equivalent circuit in Fig. 2.7 (b) is developed. The coupling between the dipole and the shell is represented here by a transformer with turns ratio N. In this figure the value of the radiation resistance can be evaluated from $N^2 \times R = 50\Omega$. Therefore, the small radiation resistance and significant capacitance of the dipole can be compensated via the transformation of L and R. Consequently via this paradigm, a 50 Ω matching can be achieved at the input of the composite shell dipole antenna. Intuitively, this concept can be repeated for a magnetic dipole with a Mu negative shell at its very near field.

The above discussion illustrates the idealized concept of this technique. However, there is no ENG and MNG material in nature and producing them needs significant effort and still is an immature field of engineering. Even if they are successfully realized, there would be dispersion loss and conductive losses associated with them which are considerable at the scale of electrically small antennas. It is found that a near field resonant parasitic antenna (NFRP) which uses just one MTM unit cell and not a bulk medium, can be well matched to the source. As only one MTM is used within the structure of these antenna, they are called MTM-inspired rather than MTM-based.

Inspired by this concept, numerous MTM electrically small antennas are proposed.

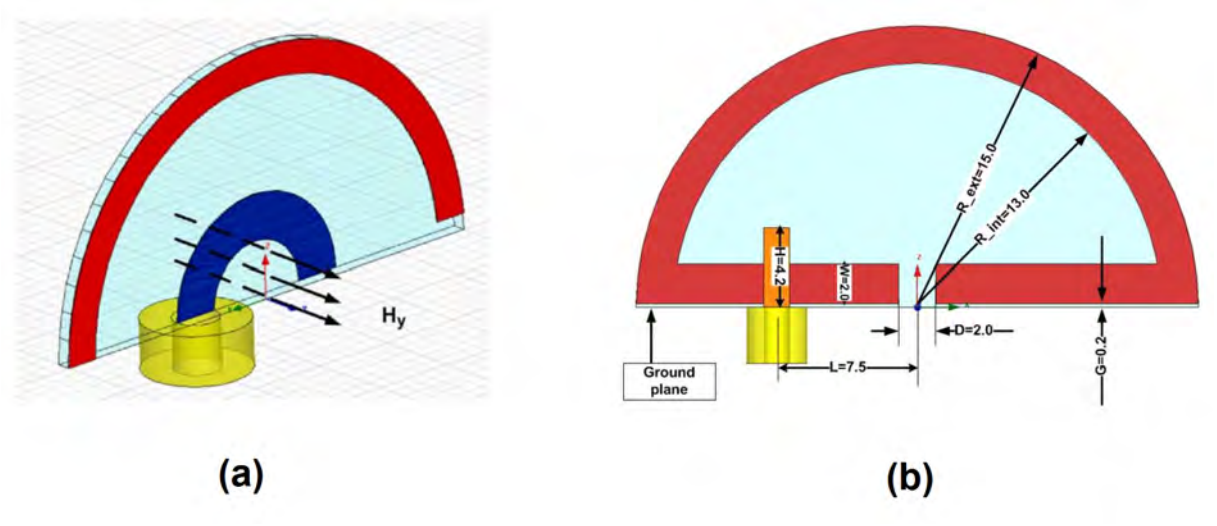

Figure 2.6: Two simple examples of the (a) magnetic [39] (b) electric NFRP antennas [40]

[34–38]. These antennas are well miniaturized, $ka < 1$, and demonstrate good efficiency at the centre frequency, however due to the dispersive nature of the NFRP element the bandwidth is narrow [39]. In Fig. 2.6 taken from [39, 40], two simple examples of the (a) magnetic (b) electric NFRP antennas are shown.

2.2.4 Non-Foster matching

Another class of matching technique which has been recently attracting the attention of antenna designers is active matching (non-Foster) matching. The performance of an antenna can be significantly improved when Non-Foster matching circuits are used as it is no longer limited by gain-bandwidth product constraint [41]. For this purpose active circuits are directly used in the antenna structure, and as a consequence matching will not be limited by the physical geometries of the antenna but mainly relies on the performance of the active circuitry [42].

Fig. 2.8 illustrates the concept of non-Foster matching and its advantage over passive matching [43]. The Foster theorem states that the reactance of a Passive network increases monotonically with frequency ($dX/d\omega > 0$) [44]. Therefore, to achieve zero reactance using a passive component, for a capacitive network, an admittance which behaves as an inductor is required and vice verse for a magnetic dipole. In this manner a net zero

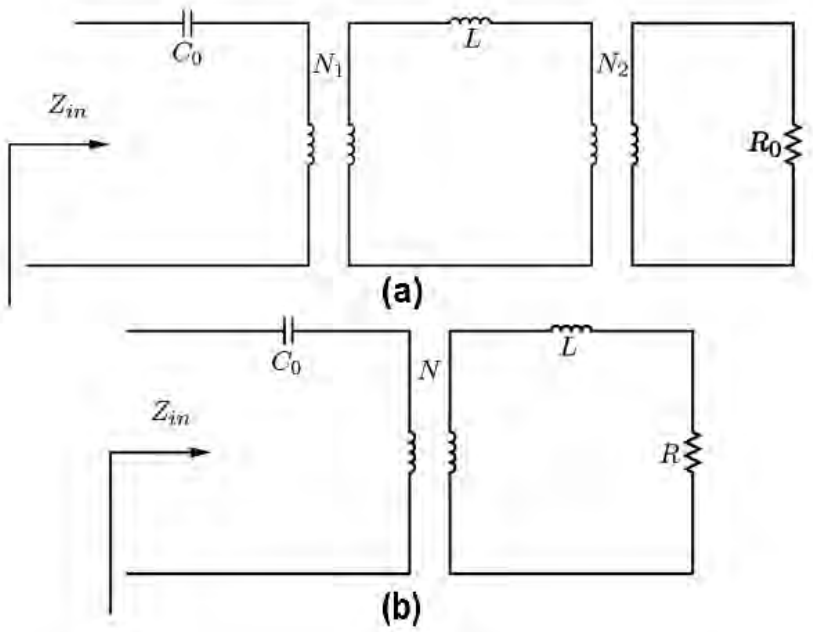

Figure 2.7: The equivalent circuits for an ESA operating with an ENG shell at its proximity [10]

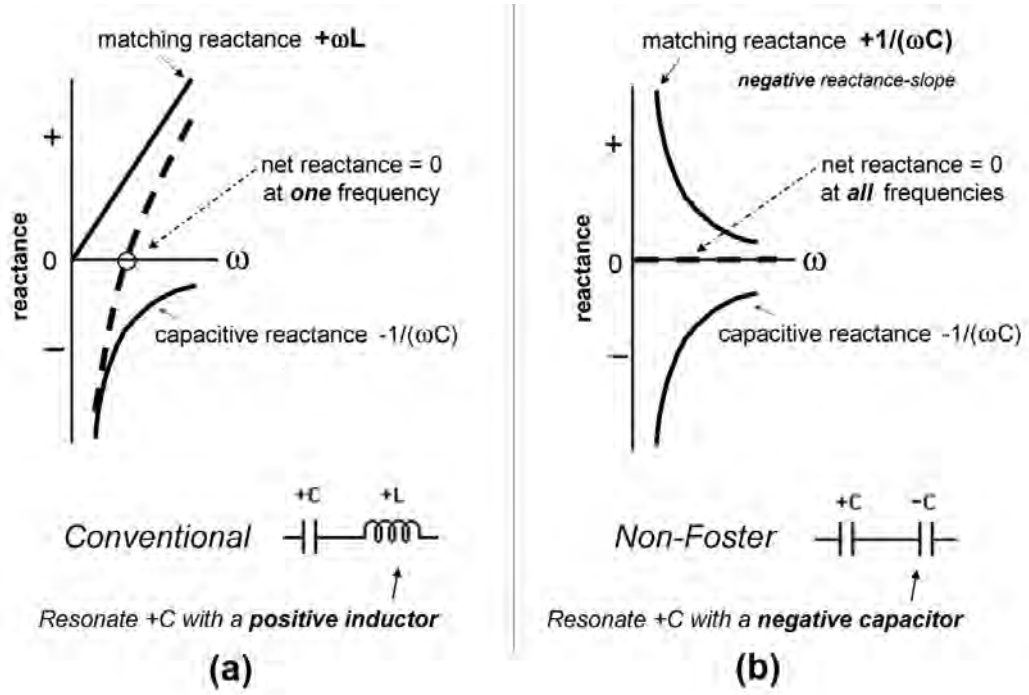

Figure 2.8: The theoretical difference between the passive and active matching [43].

reactance can be achieved at only one frequency as illustrated in Fig. 2.8 (a). However, this is in contrast to a Non-Foster matching technique in which the use of an element with negative reactance slope can result in zero reactance not just for a specific frequency but for a wide frequency band. This concept is illustrated in Fig. 2.8 (b). Numerous electrically small antennas with non-Foster matching networks have been introduced.

The negative Impedance Converter is a two port device presenting at its input port an impedance opposite of its load. In [45, 46] the matching for an electrically small dipole is improved by loading it with negative capacitance via an NIC. However in [47–50] the NIC circuit is introduced at the input terminal of the electrically small antenna to improve matching.

Generally, the use of non-Foster matching techniques can compensate for the reactive part of the small radiator. However, to compensate for the low radiation resistance of the small radiators, other approaches are used in parallel with the use of non-Foster (NIC) components.

Loading with NIC

One approach to keep the input impedance of an antenna constant and close to source impedance using the Non-Foster approach, is to control the current distribution on the radiating elements by introducing loads on it [51]. In accordance to the modal analysis presented in [52, 53], the required reactive loads which need to be introduced on the antenna structure (complex radiator) can be calculated. The required admittance behaviour for each load needs to be accomplished utilizing a number of active and/or passive matching networks. Whereas, the performance of this approach is investigated using simulation, it has not been validated throughout practical experiment due to the significant complexity [51, 54].

Metamaterial and NIC

The most recent trend in designing ESAs is to use the NIC circuit in parallel to meta material(NFRP) elements. This is important due to the following points. One is that the NFRP element as was discussed, can compensate for both reactance and the resistance of the ESAs. However, in fact any passive MTM have an inherent dispersive behaviour. This means desired values for electromagnetic parameters are normally achievable for a narrow band which will limit the operation band width of the MTM inspired network. To address these draw backs, an MTM based antenna can be loaded with an active circuit (NIC) to compensate for the unwanted reactance arisen from the dispersive nature of the MTM. To achieve such an antenna via this technique numerous designs have been suggested which can be summarized as the following steps [55, 55–63]:

- Antenna design with the use of NFRP element leading to an input resistance close to 50 Ω over as wide as a bandwidth as possible in the band of interest. This is an important step as the antenna with better initial matching will perform better under this technique [57].

- Finding the optimum position where the reactive element can be placed. This is important as it can significantly reduce sensitivity to errors and practical complexity and increases the band width of operation

- Passive loading of the antenna with inductor or capacitor (via simulation or calculation) to find the suitable reactance required for best matching versus frequency

- Replacing the passive loading with non-Foster loading to meet the required reactance behaviour derived in the previous item. The non-Foster circuit can be a single negative inductance, a series negative inductor and positive capacitor, and a parallel negative inductor and capacitor [50].

- Design of NIC circuit or using the available NIC architecture in the literature

The latter method which was defined in-depth, is the most recent and highly cited approach for designing ESAs. Following this approach, designing an antenna with electrically small size is feasible, $ka < 1$. Whereas this technique looks impressive and promising in theory, in practice it is not. Among all these antennas, very few of them have been designed and fabricated with measured data. The best practical achievement was presenting 3.8 times greater bandwidth compared with the initial matching which is still far from what is proposed in theory. This is mainly due to:

- Design complexity of the NIC circuits
- High sensitivity of the matching to the NIC circuit. A small error presented in the components of the NIC can significantly affect the overall matching
- The NIC network will have multiple resistors in its structure which will reduce the radiation efficiency of the small antennas.
- And the most important issue is the stability problem of the NIC which will limit the frequency bands that can be obtained using this technique (Not higher than 2 GHz).

2.3 State of the art in multi port antennas

To clarify the uniqueness of the proposed thesis, it is beneficial to investigate the literature for multi-port antennas. Herein, multi-port configuration used in antenna design is discussed and to clarify this some of the recent examples are illustrated. Apart from array application which is not the topic of the discussion here, the recent trend for the use of multi port antennas is mainly focused on MIMO and diversity applications [64–70]. Some of the recent papers presented in the literature are covered here to clarify and compare the uniqueness of the approach presented in this thesis. In [64, 65] an antenna is proposed which is suitable for the switched and combined diversity application. This is accomplished by merging two PIFA antennas such that they maintain very small coupling

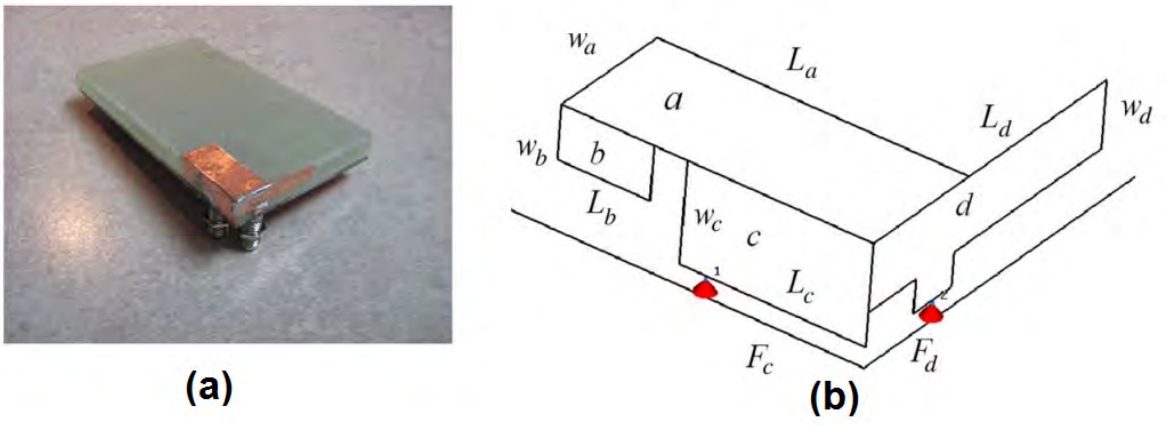

Figure 2.9: The geometry of a compact dual-Port diversity antenna for Long-Term Evolution (a)fabricated and (b) close schematic [64]

between the two feeding ports, while they are excited simultaneously or individually. This is achieved for a band width of 17 % at 2.6 GHz and with $ka > 1$ with -15dB of port isolation. The geometry of this antenna is illustrated in Fig. 2.9 (a) and (b).

In [67] one radiator is shared with three ports in which two ports are operating in the same frequency band (1-4 GHz), for diversity purposes, and a third port, at 2.4, 3.4 and 5.2 GHz to support WLAN/WiMAX. In this example to provide good isolation between the ports, a three layer structure is used. The radiator which is constructed of two fractal triangles is located at the top, two MIMO ports in the middle and a WLAN/WiMAX port at the back of the antenna. The fabricated antenna is depicted in Fig. 2.10.

In [68] a PIFA antenna is fed via two ports in which they are coupled to radiating elements via two perpendicular plates to provide polarization diversity. The schematic and the fabricated antenna is shown in Fig. 2.11. In [69] a radiation element including a patch ring and a monopole, in which two separated ports are used to feed the element, is constructed such that a coplanar waveguide port and a slotline port are shaped at the input of monopole and the patch ring, respectively. Via this configuration a dual-port MIMO antenna with -35 dB isolation is accomplished. The multiport feeding may also be used for pattern reconfiguration. The schematic of this antenna is illustrated in Fig. 2.12

As an example, in [70] a planar microstrip antenna with three feeding ports is pre-

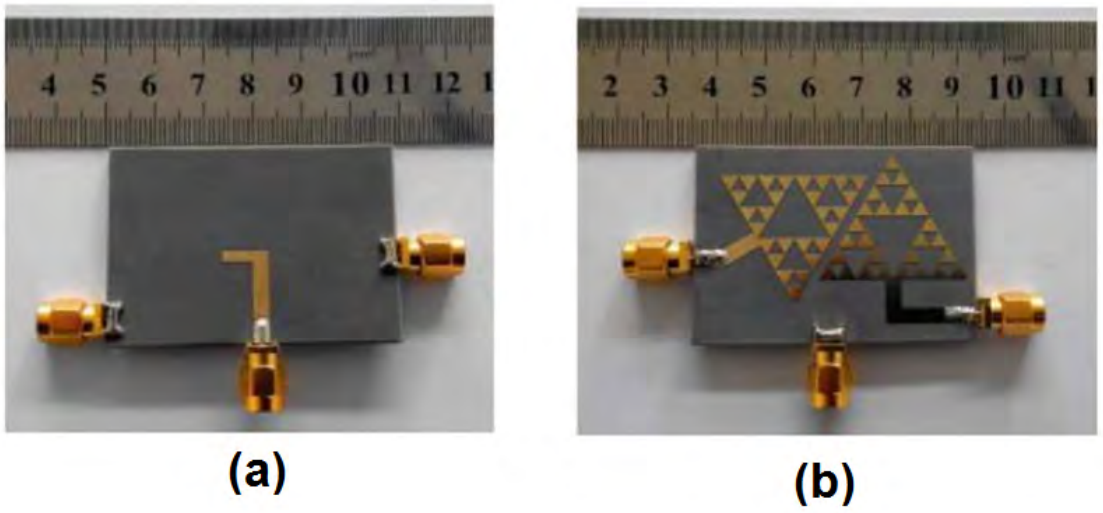

Figure 2.10: The front and back of the patch of a three port antenna (a) front and (b) back of the structure [67].

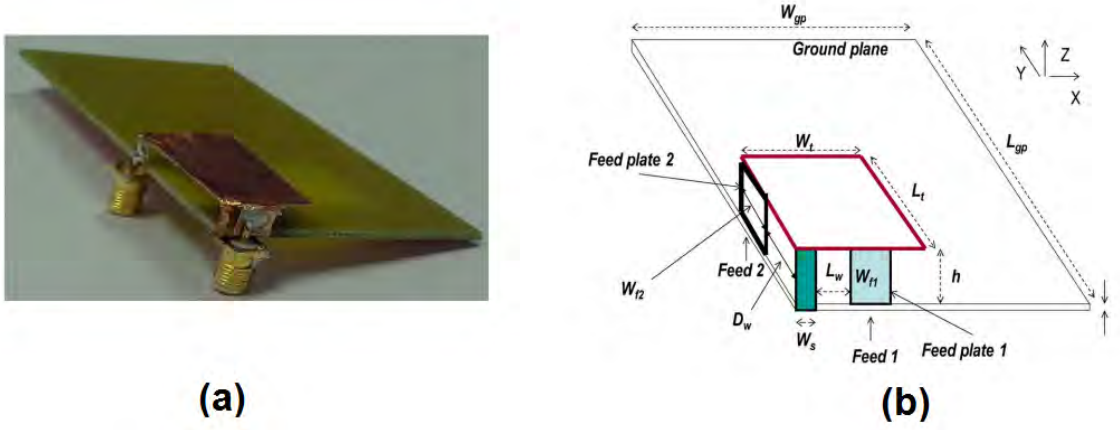

Figure 2.11: The geometry of a dual-Port antenna with polarization diversity (a)fabricated and (b) close schematic [68].

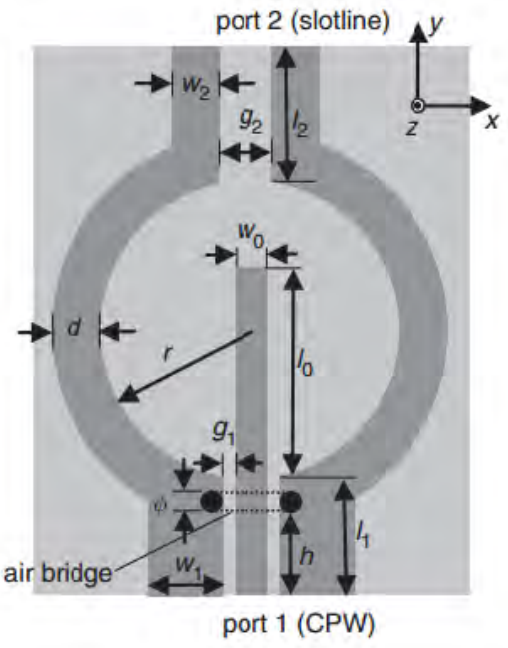

Figure 2.12: The schematic of the high isolation dual port MIMO antenna with waveguide and a slotline port [69].

sented. Excitation of each of these ports constructs a specific electric field distribution and therefore a specific radiation pattern. An isolation better than -10dB is achieved between the ports. This antenna is illustrated in 2.13

The common feature of all these examples and many other examples is that the ports, regardless of their application, are isolated. However, this is in contrast to what will be illustrated in this thesis. There is also power combiner/divider application proposed for two port configuration which is not directly related to this topic and examples on this are provided in Appendix A and B

2.4 State of the art in reconfigurable antenna

Future applications of reconfigurable antennas include rural area network systems which utilize separate search and communication antennas and the handheld radios in which the search and communication functions need to be performed with one antenna. In the

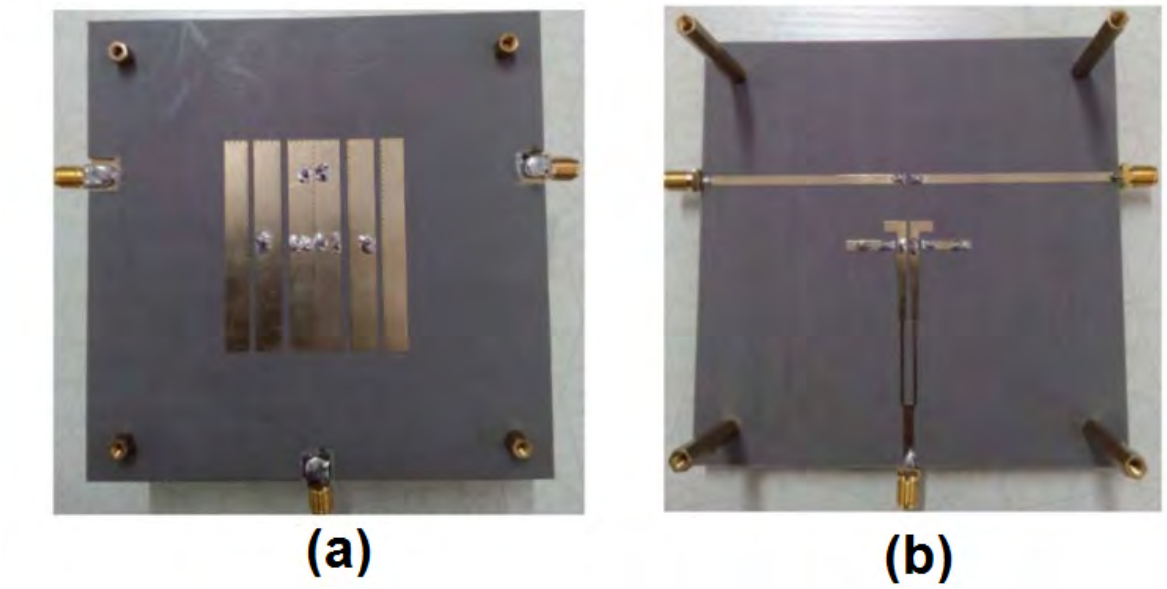

Figure 2.13: Photographs of the microstrip endfire antenna (a) top view; (b) back view [70].

first application, size is not a limiting factor, whilst hand held antennas should fit within the mobile phone. In this area the challenge is the Chu-Harington limit which relates the bandwidth to the size of the antenna. Therefore, to achieve broad bandwidth, matching circuits must be used. Interference is a big issue and the legacy and primary transmitter interference need to be filtered out for optimum action. Consequently, the filter should be inserted into the antenna, which in turn makes the antenna more complicated and less efficient. This is extremely challenging, and the mobile phone companies are currently seeking solutions [71].

The reconfiguration of an antenna can be achieved via either rearranging the current distribution or by reconfiguration of the antenna's radiating edges. The reconfigurable properties of an antenna are frequency, polarization, radiation pattern or any combination of these properties [72]. In the following some techniques for achieving reconfiguration capability, are illustrated. Recently various configurations for wideband to narrow band reconfigurable antennas have been proposed.

In [73] a band pass switchable filter is integrated with an UWB antenna. In narrow-

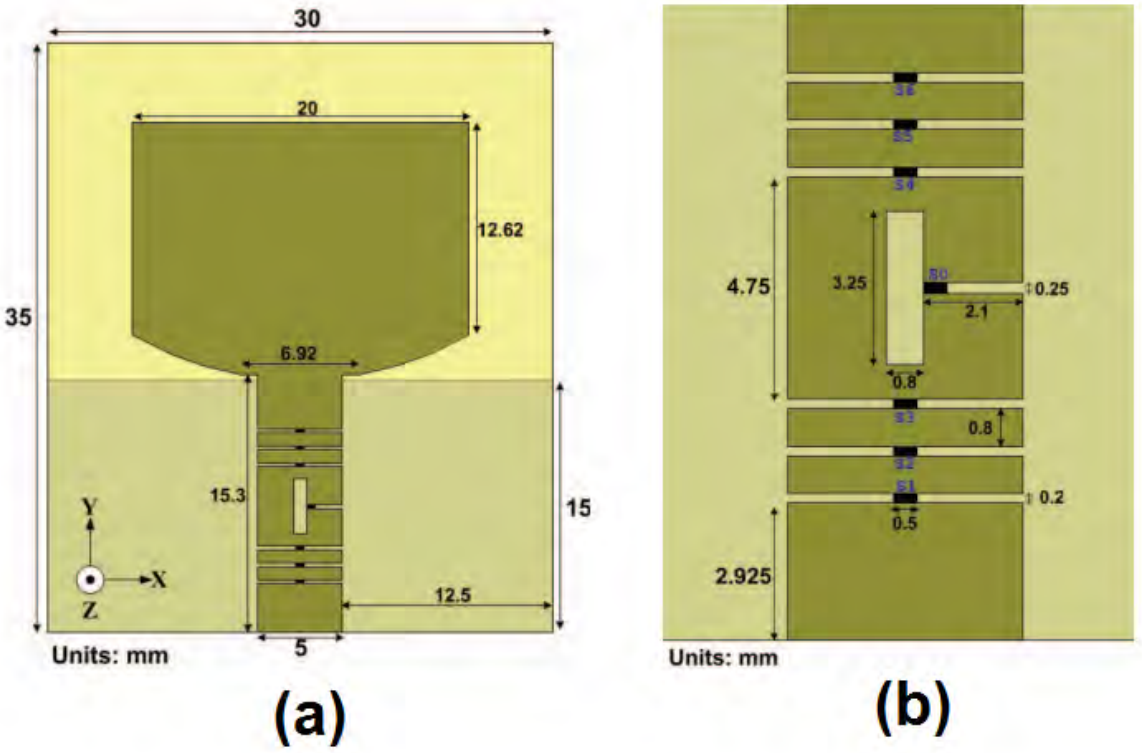

Figure 2.14: The configuration of the proposed antenna with filter at the feedline(a) top view; (b) back view [73].

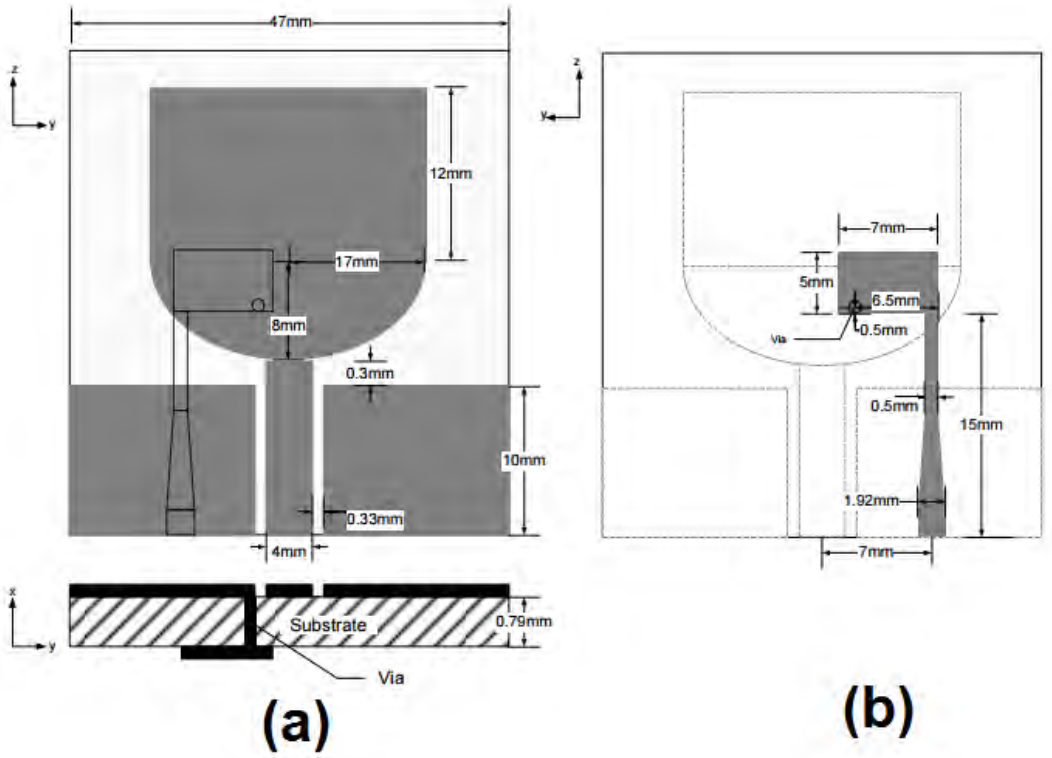

Figure 2.15: The configuration of the proposed wide to narrow band frequency reconfigurable antenna(a) top view; (b) back view [75]

band mode the operating frequency of the antenna can be reconfigured by tuning the centre frequency of the filter and when the filter is bypassed the antenna is operating as wideband. The geometry of this antenna is illustrated in Fig. 2.14. A similar technique is applied in [74] with the use of varactor diodes instead of switches. In this example miniaturization is also achieved via strategically matching the filter to the antenna. In [75] an antenna with wide-narrowband reconfigurable antenna is presented. In fact the design has two antennas at each side of the substrate. It has CPW fed monopole with partial ground and a varactor tuned microstrip patch at the back of the structure. The latter is provided to allow narrowband communication while the first is for wideband operation. The geometry of the design is illustrated in Fig. 2.15.

In [76–78] a Vivaldi antenna with additional switched band capability for operating over wide band (1-3.2 GHz) or narrow bands (three bands) is presented. Four pairs of switchable ring slots are integrated in the ground plane of the antenna to provide frequency

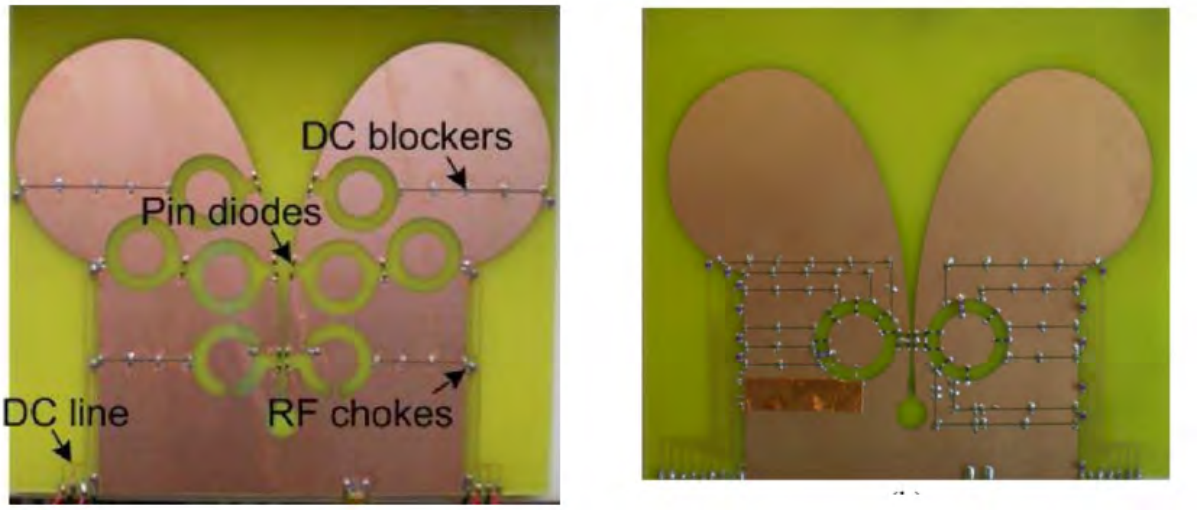

Figure 2.16: Two examples of fabricated Switched-Band Vivaldi Antenna, right figure taken from [76] and left figure from [77].

reconfiguration, by proper switching between them. The fabricated antenna and an earlier work from the same author which incorporate two ring slots are illustrated in Fig. 2.16.

To achieve radiation pattern and frequency reconfiguration capability for an antenna the approach in [79] is presented. The antenna configuration is constructed from two tilted monopoles by an angle of 30° and a printed reflector positioned between the two monopoles. Two switches are used to chose which monopole caries the current and the reflector between the monopoles will reflect the radiated field toward the excited monopole(right or left) to realize the pattern reconfiguration. For having tuning capability, two more switches are integrated on each monopole to change the radiating length of the monopoles. The top and back of the fabricated structure is illustrated in Fig. 2.17.

In [80] a two port reconfigurable circular patch antenna is presented with pattern and frequency reconfiguration capability. The frequency reconfiguration is achieved by varying the radius of the patch through 8 pin diode switches. The antenna consists of two coaxial ports which allow two different radiation patterns at each port. In order to provide proper isolation, the feed points are separated by 25°. The distance of the feed points from the centre of the patch have been chosen to match both operation frequencies. The schematic of this antenna is illustrated in Fig. 2.18.

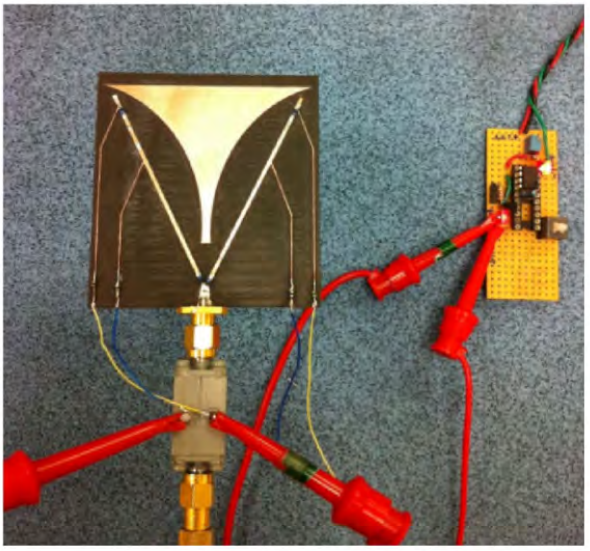

Figure 2.17: The fabricated structure of tiled monople pattern and frequency reconfigurable Antenna [79].

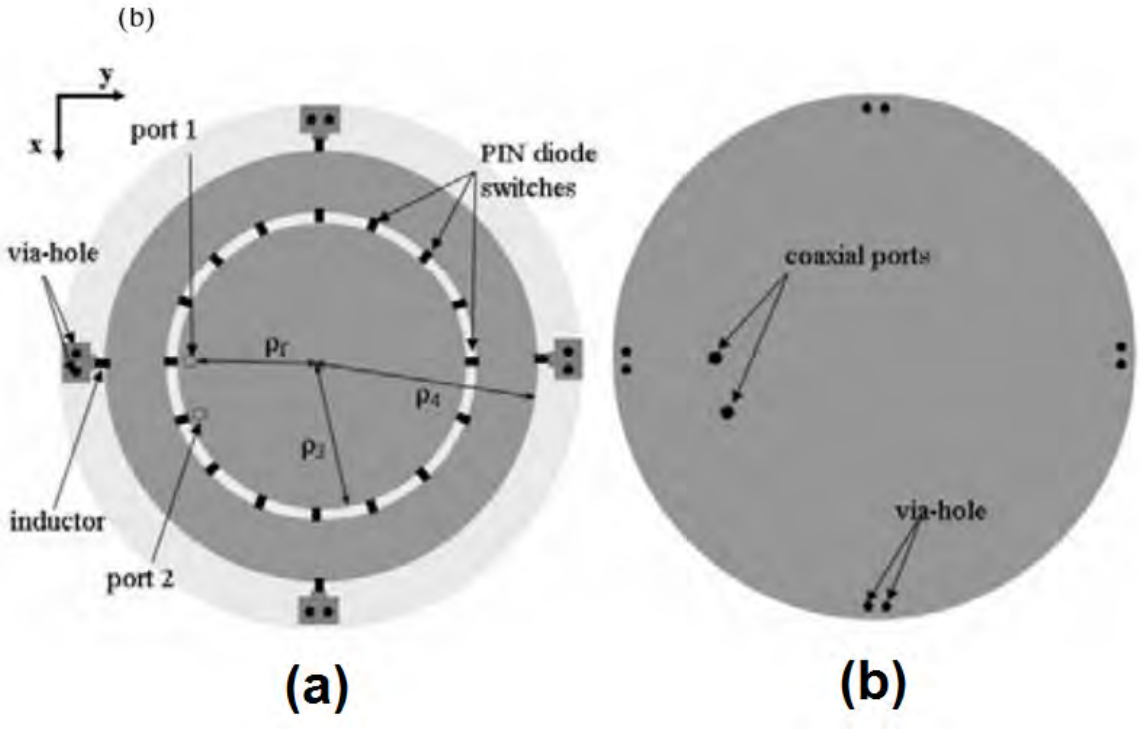

Figure 2.18: The configuration of the proposed frequency and pattern reconfigurable switchable circular patch antenna(a) top view; (b) back view [80].

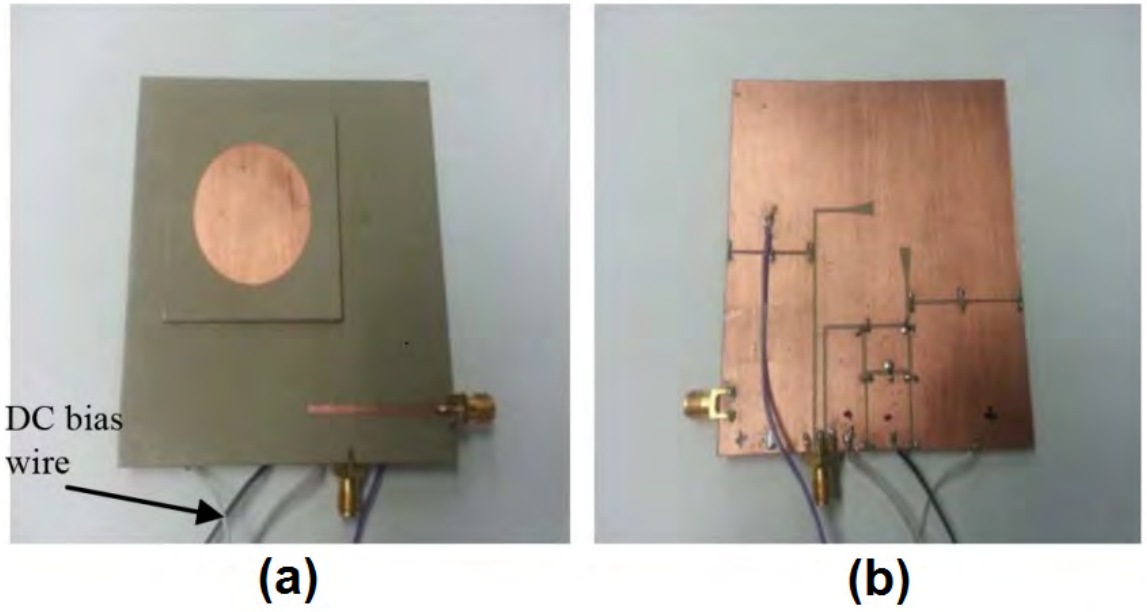

Figure 2.19: The configuration of the fabricated polarization reconfigurable antenna(a) top view; (b) back view [81].

In [81] a polarization reconfigurable antenna is proposed. This is achieved through feeding a circular patch at a small distance above two orthogonal feed lines including a co-planar-waveguide and a microstrip feed line. Having two different port types provides isolation between the ports. To improve matching, two impedance transformers are also integrated at the end of the feed lines. When the two ports are equal in magnitude and in phase quadrature circular polarization (CP) is achieved, left handed at one port and right handed on the other. The phase delay required for CP is provided via an extra transmission line controlled by switches. In contrast, linear simultaneous orthogonal polarization is achieved when there is no length difference between the feeding ports. Therefore depending on application any polarization can be achieved using this configuration. The fabricated antenna is illustrated in Fig. 2.19

2.5 Miniaturization techniques

An extensive literature review on various types of antenna extracted from large body of published designs is presented in [13]. To provide an understanding of all other minia-

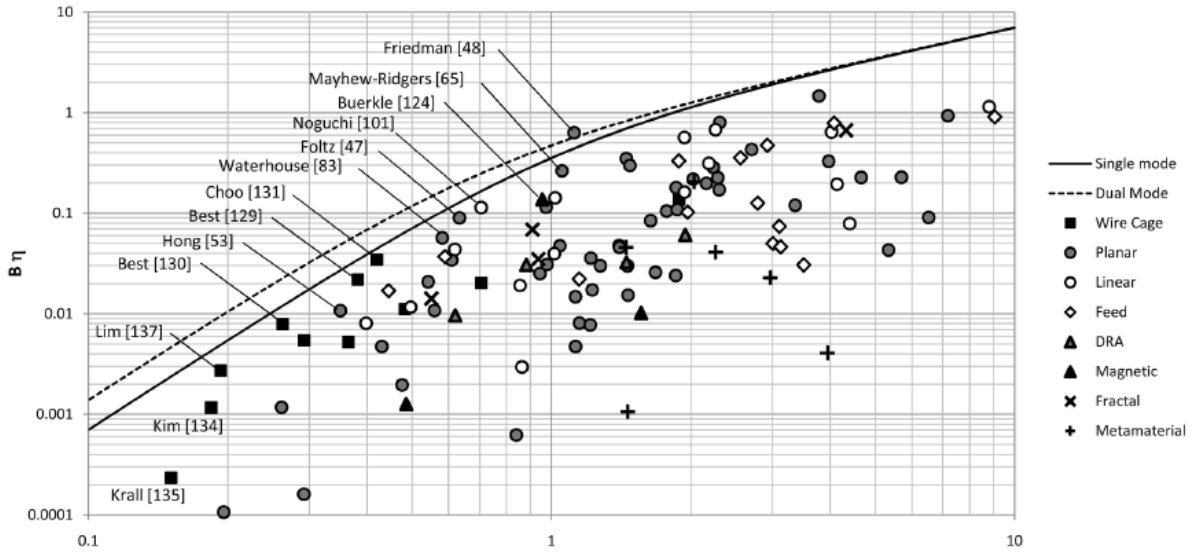

Figure 2.20: The measured bandwidth efficiency product for 110 antenna designs published in the IEEE transaction on antenna and propagation in comparison with the theoretical limit. Specific references which are available in the source, on the outer edge of the performance limit are noted [13].

turization approaches and how effective they are, Fig. 2.20 taken from [13] is presented. In this work the bandwidth efficiency product versus the electrical size for 110 relevant small antenna papers, published in the IEEE transaction on antenna and propagation are plotted and compared with the theoretical limit derived by 2.10 and 2.11 for the linear and circularly polarized antenna, respectively. The limits for linear and circularly polarized antennas are plotted with solid and dashed lines, respectively in Fig. 2.20.

In this reference all of the miniaturization techniques are classified as follows.

Antennas like planar inverted F antennas (PIFAs) and patches, and other designs which use a large ground plane, are considered as Planar.

Dipoles and other similar designs are grouped as Linear. This category also includes monopoles and designs similar to that.

Another category is the class of antenna, called Feed antennas herein which are antennas on small ground planes that are often constructed as a mobile phone, in which a small resonant structure behaves as an exciter or feed for a mode which uses the entire ground plane.

Dielectric resonator antennas (DRA) which consist of a block of ceramic material of various shapes, form another class. These antennas are denoted as DRA in the figure.

Antennas with relative permeability bigger than one, are denoted as magnetic antennas.

A promising miniaturization technique that performs particularly well is used to construct antennas that utilizes the entire volume of the sphere enclosing the maximum dimension of the antenna. Such antennas are called the Wire Cage in the figure.

The final two groups of antenna include designs which uses popular trends in antenna design, and attribute their performance to Fractal or Metamaterial features.

The conclusion from the reviewed papers are as followings. Wire cage designs are high-performance as they include low permittivity, low aspect ratio, and they have uniform distributed fields throughout their volume or surface. Moreover, as the dielectric resonator designs utilize high permittivity materials, their bandwidth is poor compare to their electrical size. The metamaterial and fractal designs normally involve highly resonant structures which they are exploited to concentrate the fields in those regions. Therefore, they can only use a subset of the available volume of the sphere encloses the antenna which limits their performance.

2.6 Contribution

The uniqueness of this thesis, becomes more clear by focusing on the reviewed papers and the literature.

The goal in non-Foster and NIC matching is to control the current on the radiating element, and force the current to resonate, coupling at the required wavelength on to the radiating element. This is achieved via numerical and mathematical techniques including theory of characteristic modes [51]. Then, to realize the calculated forced current distribution, internal ports are introduced on the antenna elements to support the required reactive behavior for the forced current excitation. In electrically small operation

these loads include negative reactances to release the unwanted stored energy at a specific points of the structure and force the current to resonate. This works well in theory, however in practice it is extremely challenging with the current technology. This is due the unavoidable losses present in the NIC circuits, the stability problem, and the design complexity.

In this thesis, a technique is introduced which enables the direct control of the current on the antenna structure. This is acheived by introducing a secondary port, on the antenna structure close to its extremities. With the introduction of the second port via the interaction between the ports, the end point restriction on the current distribution can be relaxed and therefore it can be controlled and forced to construct a wavelength that the antenna dimensions do not naturally permit. Moreover, having control on current can also be used to tune the frequency. Current control via this technique, is not suffering from the problems presented for the NIC and non-Foster matching.

On the other hand, the fundamental limitation arising from the size of the antenna (discussed in detail in 2.1) is due to the unavoidable stored energy within the radian sphere defined for an antenna with ***one-port*** excitation. However, when a second port, or a non-Foster circuit is used to accomplish forced resonance, the antenna size and the operating wavelength can be decoupled and therefore the unavoidable stored energy that is entangled with the antenna dimensions can be used. Consequently, antennas based on the theory introduced in this thesis are not limited by those constraints which were defined in 2.1. Therefore, this thesis opens up an unexplored field which could be used to address the current and future requirements in antenna design.

Chapter 3

3.1 An introduction to injection matching theory

In 1936, Doherty [82] introduced a theory which improves the efficiency of amplifiers. In this approach, the main or carrier amplifier is combined with a peaking or auxiliary amplifier and their output is connected via a quarter wavelength transmission line. In this arrangement the task of the auxiliary device is to inject current into the output load, when the input power of the main amplifier increases and the main amplifier operates close to saturation. This action modulates the impedance seen by the main carrier amplifier and its value becomes smaller. Consequently, through this load pulling effect, the main amplifier delivers more current to the load when it is close to saturation and therefore the efficiency of the main amplifier remains constant, while that of the peaking amplifier increases. Fig. 3.1 illustrates the schematic of the Doherty concept. The total current I_L delivered to the load R_L is the summation of the currents from the top (Main amplifier) and the bottom (Auxiliary amplifier) branches. These currents can be controlled by the gain of the corresponding amplifiers at the branches and by properly choosing their gains, load pulling effect can be accomplished.

The Doherty concept inspired the idea of utilizing two port antennas in a new set-up which is herein termed injection matching. Alteration of the impedance at one port by injecting a current from the other port is the main aspect of the Doherty approach which inspired the idea of employing two port antennas in a new arrangement (injection

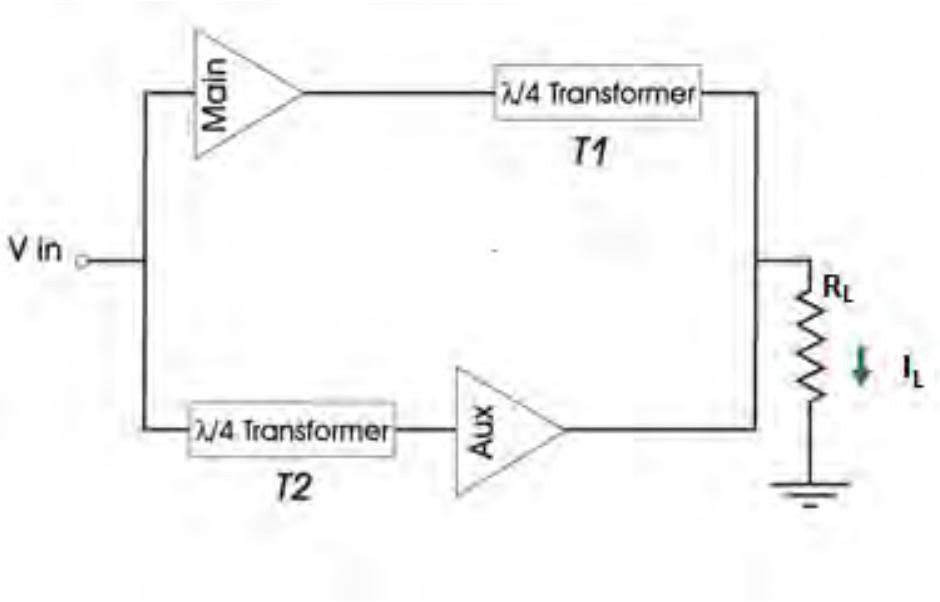

Figure 3.1: The schematic of the Doherty amplifier .

matching [83, 84].

In the simplest configuration of the injection matching concept, a two port antenna is considered as a two port network (apart from the radiation port) in which one of the ports (port 2) is used for the purpose of matching the other port (port 1) with the radiating structure. To illustrate this, Fig. 3.2 is provided.

To do so, the port 2 is injected with a current having amplitude and phase proportional to the current of port 1, to minimize the reflection coefficient at the port 1.

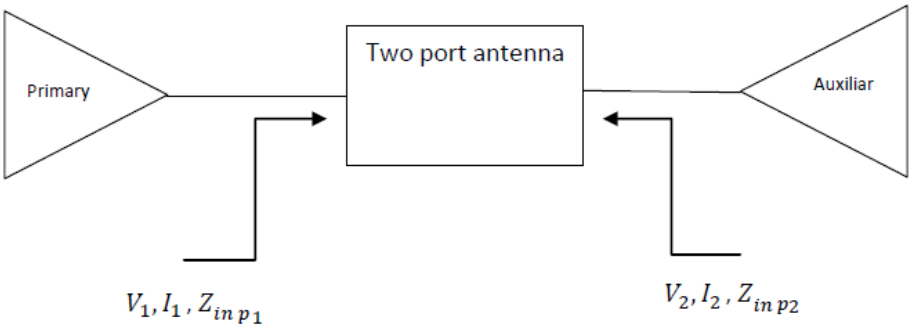

Figure 3.2: The schematic of the two port antenna design.

The ratio of the current at port 1 to that at port 2 can be described as:

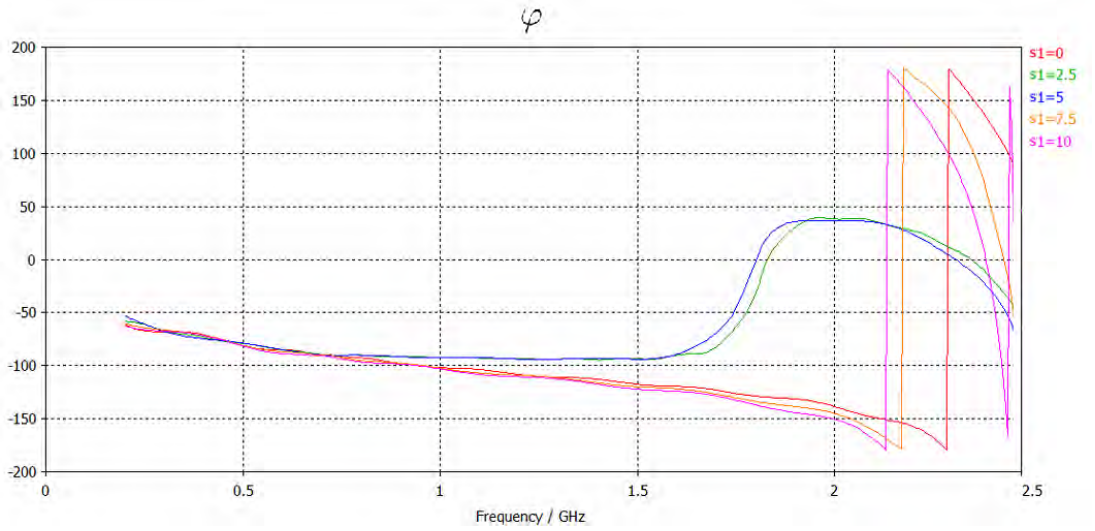

Figure 3.3: (a) Calculated φ in degrees over frequency for various port offsets value.

$$\frac{I_2}{I_1} = \gamma e^{j\varphi} \tag{3.1}$$

where I_1 and I_2 are the currents flowing in the port 1 and port 2 respectively, γ is the ratio of the amplitude of the currents, and φ is the relative phase shift between the currents.

The behaviour of any two port network, and here the antenna, can be described in terms of its Z matrix as a function of frequency. Generally, the Z matrix is complex and can be described as:

$$Z_{ij} = |Z_{ij}|e^{j\theta_{ij}} \tag{3.2}$$

where the Z_{ij} is the transfer impedance between ports i and j when other ports are open-circuited

The relation between the voltage and current for a two port network, can be expressed through the Z matrix as:

$$\begin{pmatrix} V_1 \\ V_2 \end{pmatrix} = \begin{pmatrix} Z_{11} & Z_{12} \\ Z_{21} & Z_{22} \end{pmatrix} . \begin{pmatrix} I_1 \\ I_2 \end{pmatrix} \tag{3.3}$$

where the $I_1$and V_1, and I_2 and V_2, are the current and the voltage at port 1 and port 2,

respectively [18]. The voltage at port 1 (V_1) can be calculated from (3.4) as:

$$V_1 = Z_{11}I_1 + Z_{12}I_2 \tag{3.4}$$

and consequently the input impedance at the port 1 $Z_{in_{p1}}$ can be obtained by dividing both sides by I_1,

$$Z_{in_{p1}} = Z_{11} + Z_{12}\gamma e^{j\varphi} \quad = R_{in_{p1}} + jX_{in_{p1}} \tag{3.5}$$

In order to minimise the reflected power at port 1 the effective reactance X_{in_p1} has to be zero and consequently,

$$X_{in_{p1}} = |Z_{11}|\sin\theta_{11} + \gamma|Z_{12}|\sin(\varphi + \theta_{12}) = 0 \tag{3.6}$$

On the other hand, for a specified value of input resistance $R_{in_{p1}}$ (normally 50Ω) at port 1 we have:

$$R_{in_{p1}} = |Z_{11}|\cos(\theta_{11}) + \gamma|Z_{12}|\cos(\varphi + \theta_{12}) \tag{3.7}$$

Dividing (3.6) by (3.7) and inverting, gives:

$$\varphi = \arctan\left(\frac{|Z_{11}|\sin\theta_{11}}{|Z_{11}|\cos\theta_{11} - R_{in_p}}\right) - \theta_{12} \tag{3.8}$$

The angle ambiguity in the arctan function is resolved by taking into consideration the sign of the sin and cos functions in (3.6) and (3.7).

The magnitude of γ in (3.1) can be obtained from (3.6) and (3.8), as:

$$\gamma = \frac{-|Z_{11}|\sin\theta_{11}}{|Z_{12}|\sin(\varphi + \theta_{12})} \tag{3.9}$$

Accordingly, for injection matching, realised through a specified Z matrix, the desirable θ and γ can be determined.

Likewise, the input impedance at the port 2 can also be determined. It can be calcu-

lated from the values of Z, θ and γ that are determined earlier:

$$R_{in_{p2}} = |Z_{22}| \cos\theta_{22} + \gamma^{-1}|Z_{21}| \cos(\theta_{21} - \varphi) \tag{3.10}$$

$$X_{in_{p2}} = |Z_{22}| \sin\theta_{22} + \gamma^{-1}|Z_{21}| \sin(\varphi + \theta_{21}) \tag{3.11}$$

It should be noted for any antenna under the injection matching condition we need to impose that, $R_{in_{p2}} > 0$, otherwise the incident power to port 1 will flow out from port 2 instead of being radiated [83, 84]. In the next section it is demonstrated that, properly specifying φ and γ can be utilized to:

- Match the radiating elements which are not inherently well matched with the source, or in other words, match small antennas
- Facilitate reconfiguration of the operating frequency by changing the φ and γ values
- Achieve pattern reconfiguration of the antenna by altering the current distribution on the patch

3.2 Simulation results and discussion

3.2.1 Description and simulated results

From an injection matching point of view, the optimum antenna geometry is one which leads to constant values for φ and γ for a wide range of frequencies. It should be noted that due to the dispersive nature of any practical circuit, an absolutely constant value for φ and γ over an appreciable bandwidth is impossible to achieve. However, it is determined through simulation that a fairly constant φ (10° variation) and γ (15% variation) satisfy the required operation condition.

For investigating the validation of the proposed theory a rectangular microstrip patch antenna with $\varepsilon_r = 2.2$ and resonating length of 20 mm, is chosen. The intrinsic resonance

frequency of the chosen structure occurs at 4.6 GHz where the length of the rectangular patch antenna is almost equal to $\lambda/2$. Throughout this experiment, it is intended to investigate the possibility of the resonance at a frequency much lower than the intrinsic resonance frequency of the chosen antenna under the injection matching condition.

In injection matching theory, the position of port 2 on the patch antenna was empirically observed to be important. Through a number of trial and error simulations, it was concluded that when port 2 is located on the opposite edge of the patch relative to port 1, the most constant φ over a broad range of frequencies can be achieved.

To find the optimum position and to understand how sensitive the relative position of the ports are, Fig. 3.3 is provided. It shows the calculated optimum φ required for injection matching from (3.8) for variant relative position of the port from the line of symmetry (parameter S1 in Fig 3.4(b)). Fig. 3.3 illustrates that the calculated optimum φ for various values of parameter S1 are fairly constant in the band of interest $0-2.5$ GHz. Therefore for the ease of fabrication the S1=0 can be chosen.

Fig. 3.4(a) demonstrates the calculated φ in degrees over a frequency range $0-2.5$ GHz when the positions of the ports are optimized in the simulation.

The position of the ports has been optimized so that the calculated φ becomes fairly constant over a wide frequency range ($0.45-1.7$ GHz) and is about $-80°$. Fig. 3.4(b) and (c) depict the geometry of the proposed antenna after optimizing the port positions. CST simulations have been used to simulate and optimize the proposed antenna [85]. More information about the software is provided in appendix C

In order to excite the antenna in simulation with the relative shift and amplification between the ports, a Current Control Current Source is used (CCCS) in AWR simulation [86]. The S-parameter file of the simulated two port antenna was exported from CST and imported in AWR as the CCCS component with phase shifting and amplification capability was not available in CST. Therefore, the S-parameter calculation of the whole antenna with the existence of the CCCS is accomplished in the AWR design environment. For this purpose, the schematic illustrated in Fig. 3.5 is used which includes the CCCS

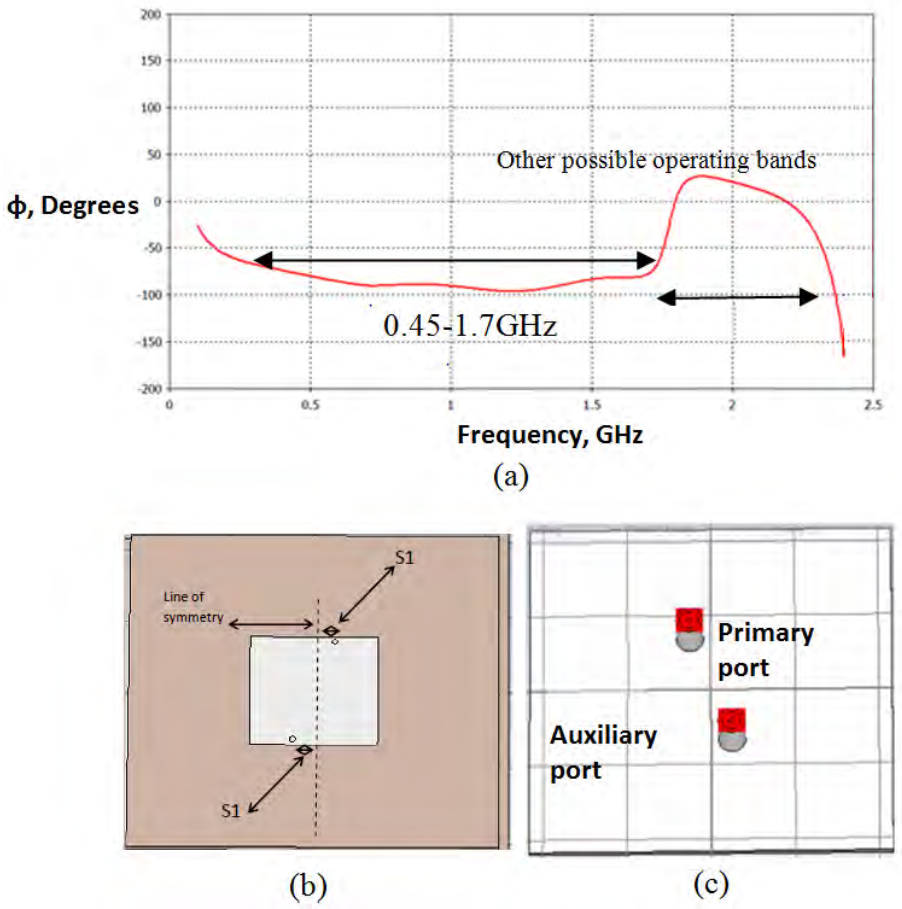

Figure 3.4: (a) Calculated φ in degrees over frequency (b) the front (C) back of the proposed structure [83] .

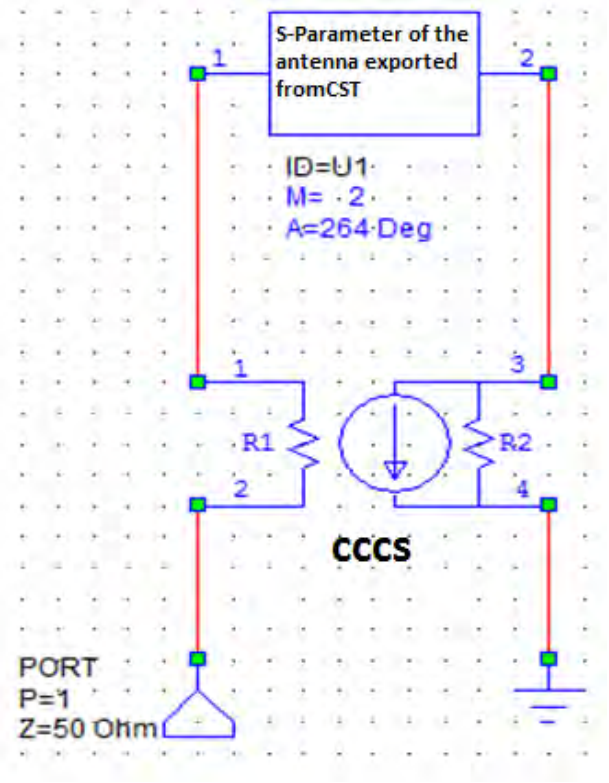

Figure 3.5: The the CCCS in AWR design environment.

and the S-parameter file exported from CST. The calculated values for φ and γ in CST are close to $-84°$ and 3 from $0.3 - 1.8$ GHz. Consequently, the values of φ and γ are set to $-84°$ and 3, respectively, in the CCCS.

Fig. 3.6 shows the S_{11} (see appendix D for definition) of the injection matching antenna when $\varphi = -84°$ and $\gamma = 3$. It illustrates that good matching is obtained where the φ is fairly constant ($0.45 - 1.7$ GHz) and equal to $-84°$ as depicted in Fig. 3.4(a).

Moreover, this graph validates the proposed theory in the simulation environment as the antenna which was intrinsically resonating at 4.6 GHz, is now resonating at about 0.9 GHz under the injection matching condition. The resulting antenna can be considered as an ESA with $ka = 0.6$ at 0.9 GHz. Fig. 3.4 (a) shows the value of the φ that is required at every single frequency for perfect matching. As the phase shifter can only realize a specific phase shift value, only at a single frequency perfect matching is achievable. This is the reason for a single resonance in Fig. 3.6 at 0.9 GHz. For the rest of the adjacent frequencies where the φ is fairly constant, acceptable matching is achieved.

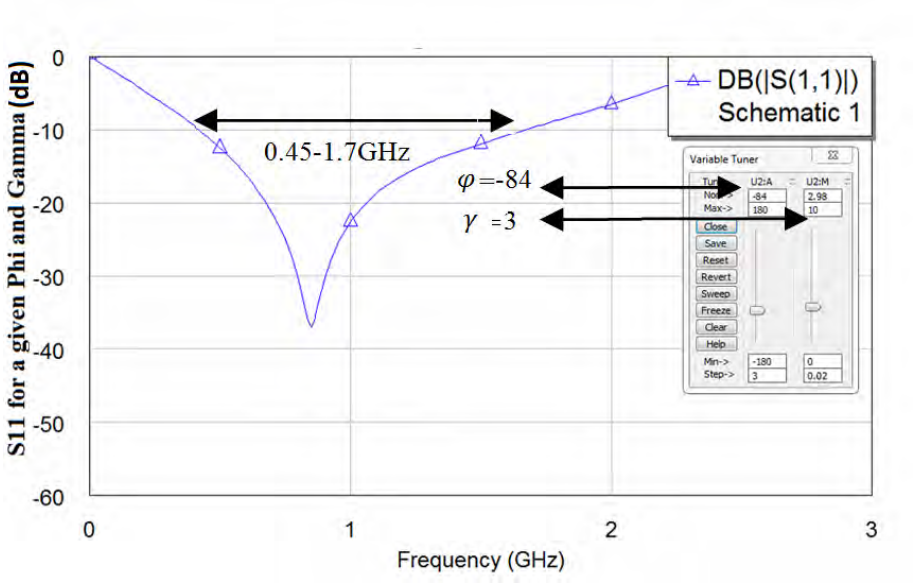

Figure 3.6: The return loss of the antenna at port 1 under injection matching condition with φ=-84.

In the literature, antennas with $ka < 1$ are designated as ESAs. Previously it was discussed that one of the advantages of this theory is the enabling of a frequency reconfiguration capability. This can be realized by having different combinations of φ and γ. Fig. 3.7 demonstrates the return loss of the proposed antenna for different combinations of φ and γ. A wide range of frequency reconfiguration is achieved utilizing the proposed approach.

3.2.2 Assumptions and challenges

It is assumed that the optimum phase shifts and amplification between port 1 and port 2, can be realized accurately using a CCCS over a wide bandwidth. In practice such a component does not exist and needs to be realized using a number of components (which may contain losses) which is discussed in detail in a later section.

3.2.3 Current and radiation pattern

For monitoring the radiation pattern and current distribution of the proposed antenna, the "combined result" feature in CST is utilized. It allows to combine the current from

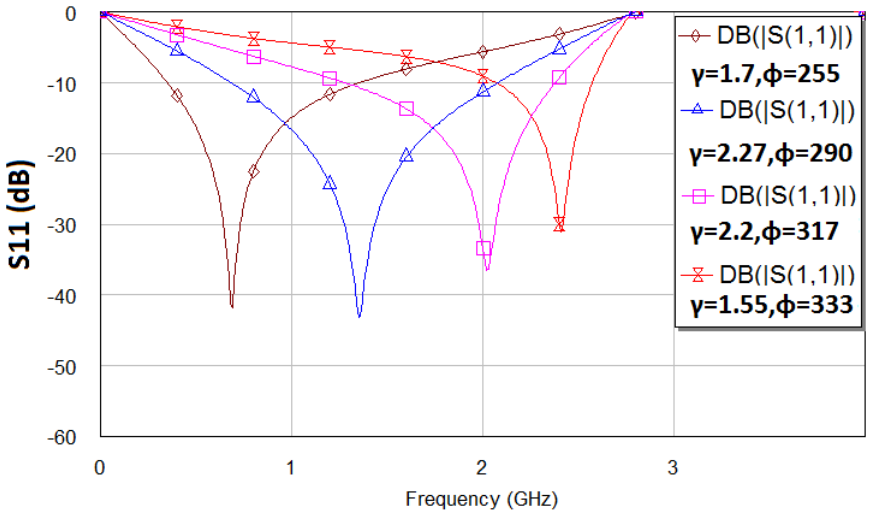

Figure 3.7: Tuning capability of the proposed approach with S11 for different values of φ and γ [83] .

excitation ports with any amplitude and phase and the resultant radiation pattern can be monitored. The simulation results show that the peak current, directivity and power pattern of the antenna, are improved under the injection matching condition, compared with when the ports are fed with in-phase currents with the same magnitudes and when the antenna is fed from just one port. Fig. 3.8(a) and (b) show the radiation pattern and the current distribution of the microstrip patch antenna at its intrinsic resonance before injection matching.

In order to verify how the injection matching affects the characteristics of the conventional patch (see Fig. 3.8) the current distribution and the radiation pattern of the same antenna but under the injection matching condition are illustrated in Fig. 3.9 at 1.4 GHz and 2 GHz (i.e. at the two middle resonances in Fig. 3.7). By comparing the field distribution at the intrinsic resonance and the resonance under the injection matching condition (Fig. 3.8(b) and Fig. 3.9(a) and (b)), it is concluded that the field distribution node locations are altered. Further investigation of the field distribution also shows that the observed node's position can be changed by changing the φ. These effects can be utilized for altering the electrical resonance length (or current distribution) of the patch antenna and, therefore, the resonance frequency.

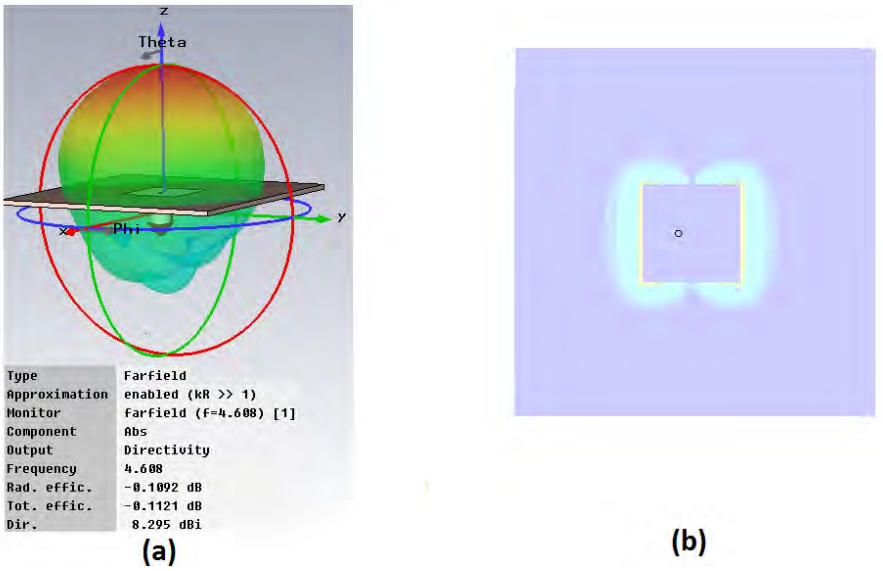

Figure 3.8: The radiation pattern and field distribution of normal patch before injection matching at 4.6 GHz [83]

The radiation patterns of the antenna show a small degree of degradation in the main lobe under the injection matching compared with the intrinsic case. This is caused by the change in current density or (field distribution) on the patch. Moreover, at 1.4 GHz (the frequency of the injection matching), the radiation pattern of the antenna is shown in Fig. 3.10 under normal condition (single feed). The directivity is much smaller than that of the antenna under the injection matching (Fig. 3.9(c)). This suggests that injection matching improves not only the matching, but also the radiation characteristics of the antenna.

In order to investigate how the IMT affects the radiation of the antenna, experiments are designed and discussed in the further subsections.

3.3 Fabrication and measurement

In order to validate the proposed theory, the injection matched antenna described above is fabricated and its properties are experimentally investigated. In the following subsections the practical work carried out is discussed. Fig. 3.11 shows the configuration of the practical implementation of an injection matched antenna which allows the antenna to be

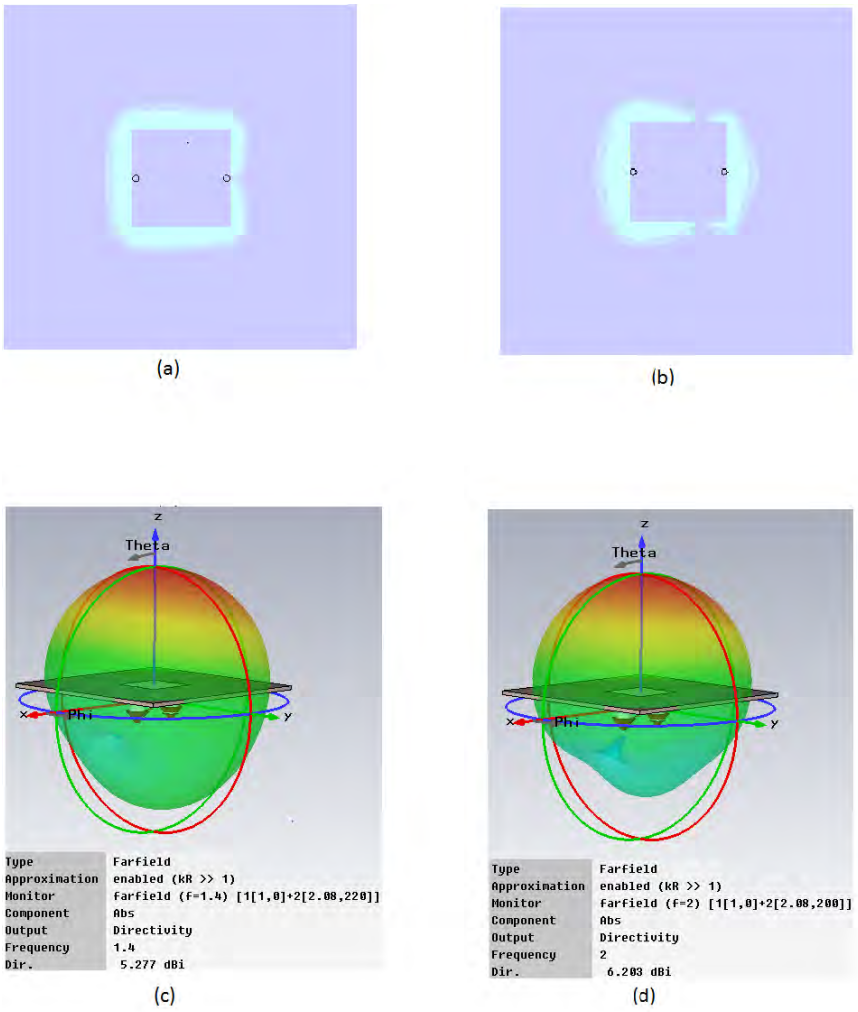

Figure 3.9: The radiation pattern and field distribution under the injection matching condition at 1.4 GHz((a) and (c)) and 2 GHz ((b) and (d)) [83]

fed from two branches with the required φ and γ . Each of these elements is discussed in the following section.

3.3.1 The vector modulator

In order to realize the required phase shift φ, Analogue Devices AD8341 vector modulator is used. The input signal of the vector modulator is modulated with baseband signals, I and Q and by properly choosing d.c. values for I and Q the required phase and amplitude modulation can be achieved. In other words, the vector modulator can operate as a variable attenuator and phase shifter. For this purpose, a PIC has been programmed such

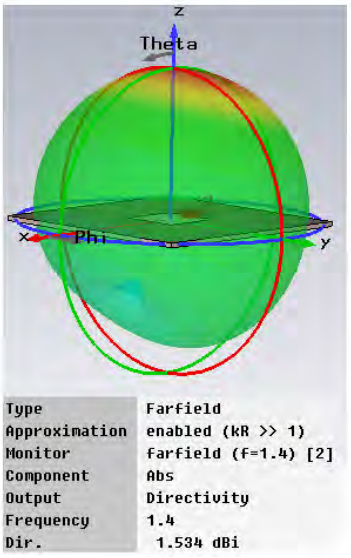

Figure 3.10: The radiation pattern of the antenna in normal condition (single feed) at 1.4 GHz

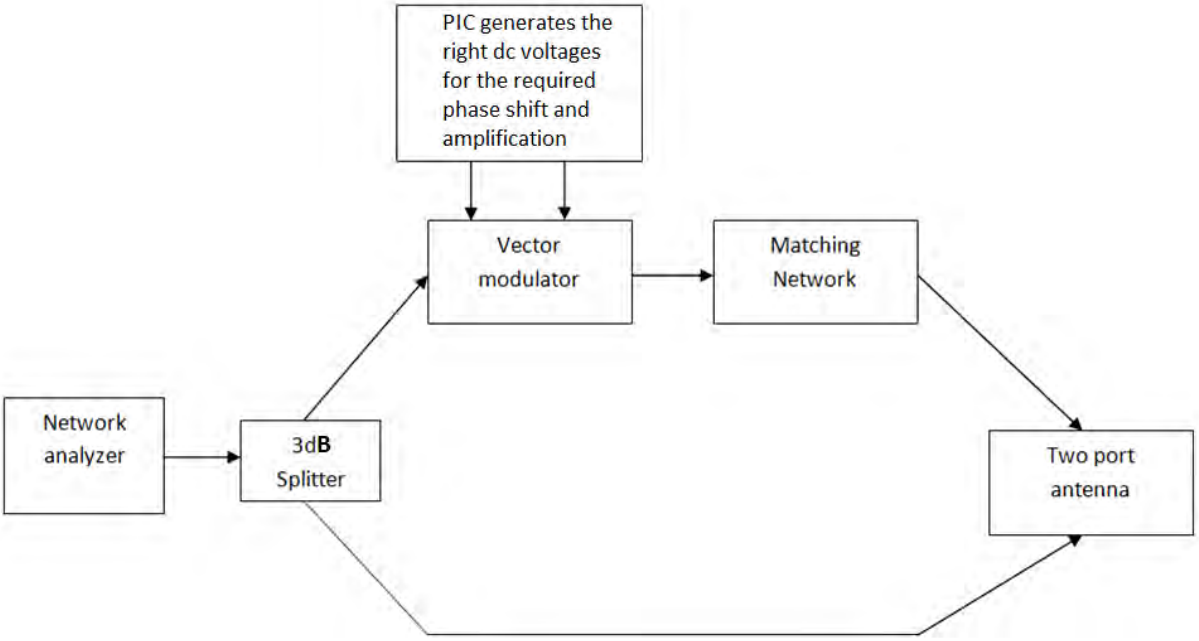

Figure 3.11: The overview of the practical implementation of the injection matched antenna

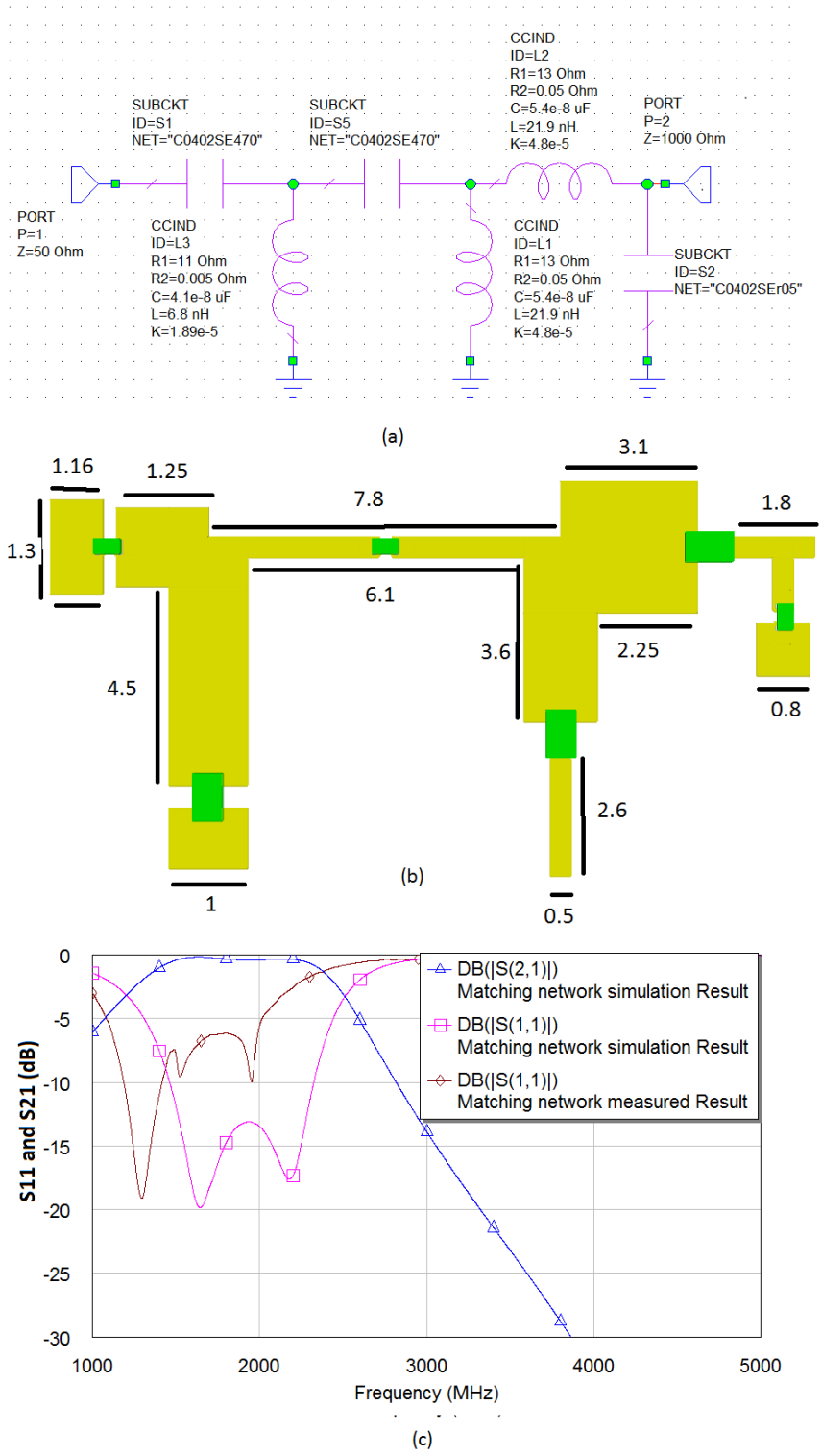

Figure 3.12: (a) The lumped element realization and (b) the layout of the matching network with the transmission lines after optimization and (c) the measured and simulated result of the matching network

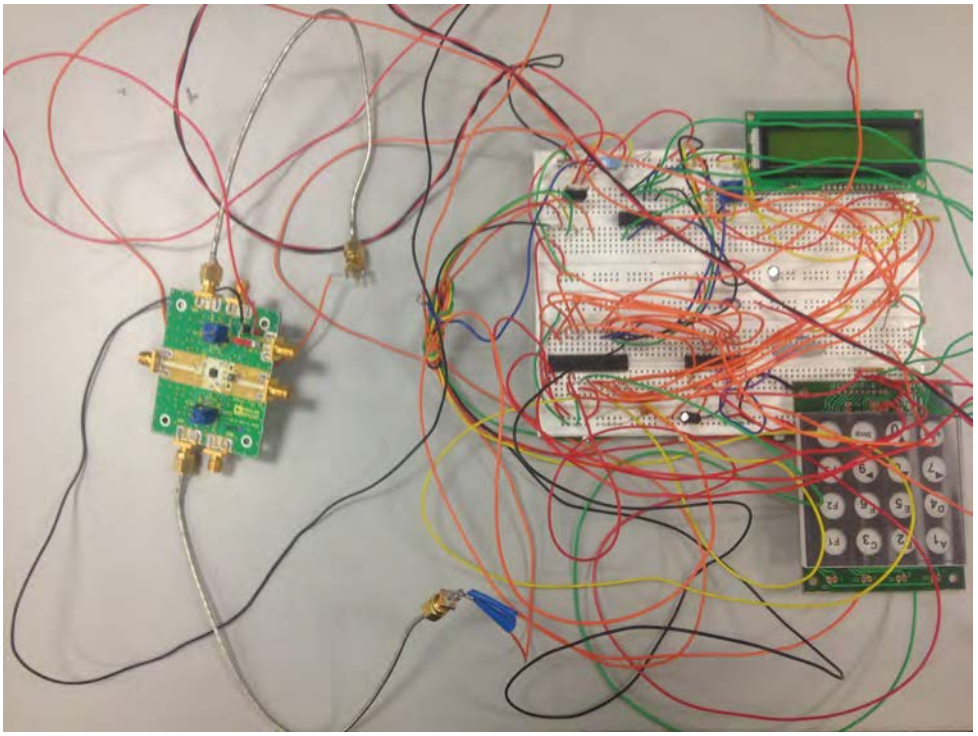

Figure 3.13: The vector modulator (on the left) and the developed circuit for providing the required voltage(on the right)

that it accurately generates the I and Q signals for the intended phase and amplitude modulation. Moreover, the programed PIC, has a feature which can sweep the phase shift of the vector modulator with a specified step, while keeping its amplitude constant and vice versa. The operating frequency of the vector modulator which is used here is $1 - 2.4$ GHz and its output impedance is 50 Ω. The practical realization of this is illustrated in Fig. 3.13. More information regarding the vector modulator and how to drive it is provided in appendix E.

3.3.2 Impedance converter

As was discussed earlier, in the simulation the CCCS component, which has considerably high output impedance, has been used to inject the current in to port 2. On the other hand, a high degree of isolation between the ports guarantees that the incident power into port 1 is radiated via the patch antenna and does not flow back out of port 2. To achieve the optimum impedance at port 2, the matching at port one is monitored while

the impedance of the second port is changed under the injection matching condition. This can be simply realized in the simulation by using an ideal transformer with variable turn ratio. The required phase shift for the injection matching is also realized by exploiting a phase shifter in the simulation. The simulation procedure is explained in detail in section 4.2.1. It is established through simulation that when the impedance of port 2 is 1000 Ω, a similar port 1 matching behaviour is achieved as when the CCCS was being used. Consequently an impedance converter is designed (instead of an ideal transformer) so that it converts the 50 Ω output impedance of the vector modulator to 1000 Ω

For these purposes, utilizing the AWR simulation, initially a bandpass filter which behaves as a matching network in the operating frequency of the vector modulator has been designed using lumped elements.

To achieve the required bandwidth, a three section band pass matching network is designed. A matching network with more sections, will lead to a wider bandwidth but more complexity. Herein for the purpose of proof of concept 3 sections would be adequate. After adding the transmission lines to the lumped element realization, the AWR optimizer is used to achieve the optimum values for inductances, capacitances and transmission lines sizes. The transmission lines are added to the design, to simplify the fabrication process and provide extra space for the soldering.

Fig. 3.12(a) and 3.12 (b) illustrate the values of the lumped elements and the layout of the matching network after optimization, respectively. In Fig. 3.12(a) the impedance of port 1 and port 2 are 50 Ω and 1000 Ω, respectively. Once the matching network was fabricated, in order to measure the practical result, the high impedance end of the matching network, was terminated in a 1000 Ω resistance. Therefore, in this way the return loss at 50 Ω termination (port 1) can be compared with the simulation result. Fig. 3.12(c) shows the simulation result (return loss and transmission loss) and the measured result (return loss). By comparing the measured and simulated return loss, a shift of 300 MHz is visible. Moreover, the return loss of the second resonance is reduced by 15 dB. These faults arise from the fabrication imperfections and the tolerances in the values of the

lumped elements which can be reduced by more accurate design and using more accurate components. It should be noted that the first resonance of the measured result occurred at about 1.2 GHz which is in the operating band of the vector modulator.

3.3.3 Antenna and matching network integration

In the practical realization of the injection matched antenna, a 50 Ω coaxial feed is considered as port 1. The feeding position of port 1 is found such that it leads to the best matching at the intrinsic resonance of the rectangular patch, in the absence of port 2. At port 2, the 50 Ω termination of the matching network is connected to the output of the vector modulator while the high impedance termination of the matching network, is connected to the patch. Therefore, the impedance of the modulated signal source is transformed to 1000 Ω and is fed to the patch to approximate the CCCS component in the AWR simulation. Using simulation, it is concluded that when the port 1 and port 2 are located on the symmetry line of the patch, the best matching is achievable. Consequently, the 1000 Ω termination of the matching network is connected to the centre point of the edge of the patch. Fig.3.14 (a) and (b) illustrate the front and back of the antenna and the matching network after integration, respectively.

3.3.4 Measurement procedure

In order to generate two stimulus signals for exciting the ports and measuring the return loss simultaneously, the ZVA network analyser from Rohde and Schwarz is used. For this purpose, port 1 and 2 of the network analyser are set to a generator mode simultaneously. Then the signal from port 2 of the network analyser is fed in to the Vector modulator, and the shifted version, is fed in to the port 2 of the antenna. As was discussed in section III, under the injection matching condition the amplitude of the signals at port 2 and port 1 are different. By trial and error it was concluded that when the signal at the port 1 is 6 dB weaker than that of port 2, the best matching is achieved. Therefore, the port 1 of the network analyser is connected to the port 1 of the antenna via a 6 dB attenuator.

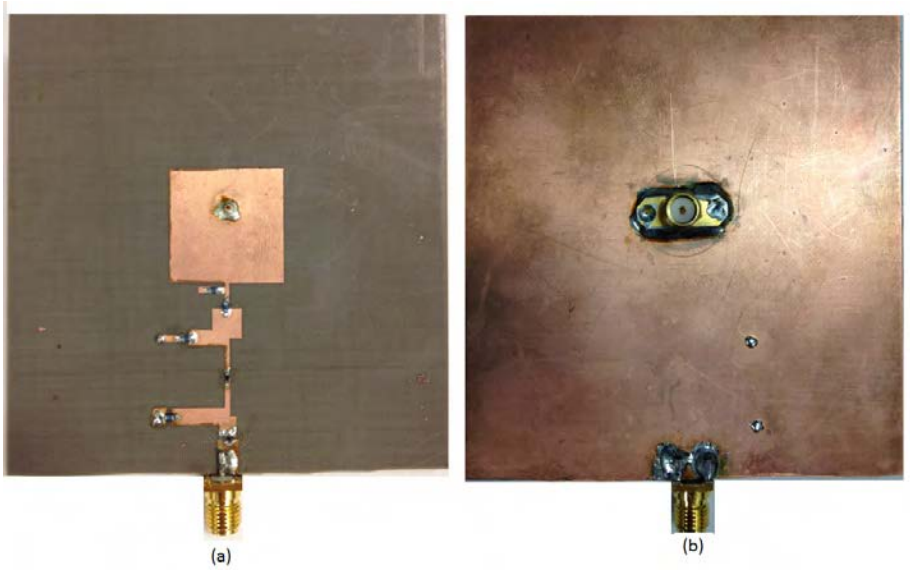

Figure 3.14: The front and back of the antenna after integration with the matching network [87]

Afterwards, in order to find the optimum value of φ for the injection matching condition and the frequency reconfiguration capability, the phase shift of the vector modulator is swept from 0 to 360° utilizing the programmed PIC. The complete measurement set-up is illustrated in Fig. 3.15.

Fig. 3.16 demonstrates the intrinsic resonance and the simulated and measured resonance under the injection matching condition when the phase shift between the ports is 60°. The $20mm \times 20mm$ patch antenna is resonating at 4.6 GHz, while under the injection matching, the resonance frequency is reduced to 1.3 GHz and a better matching in wider bandwidth is achieved. It also illustrates that the return loss of the antenna under the injection matching condition is below -10 dB in the optimum operating frequency of the matching network.

By comparing the measured and simulated S_{11} results for port 1 of the IM antenna, a slight resonance frequency shift as well as small S_{11} fluctuations in the experimental curve are observed . These are attributable to imperfections in the fabrication process for the 6 dB attenuator, impedance matching network and the vector modulator.

In order to investigate the tuning capability of the proposed approach, the phase shift of the vector modulator is swept while an attenuator of 6 dB is connected to the

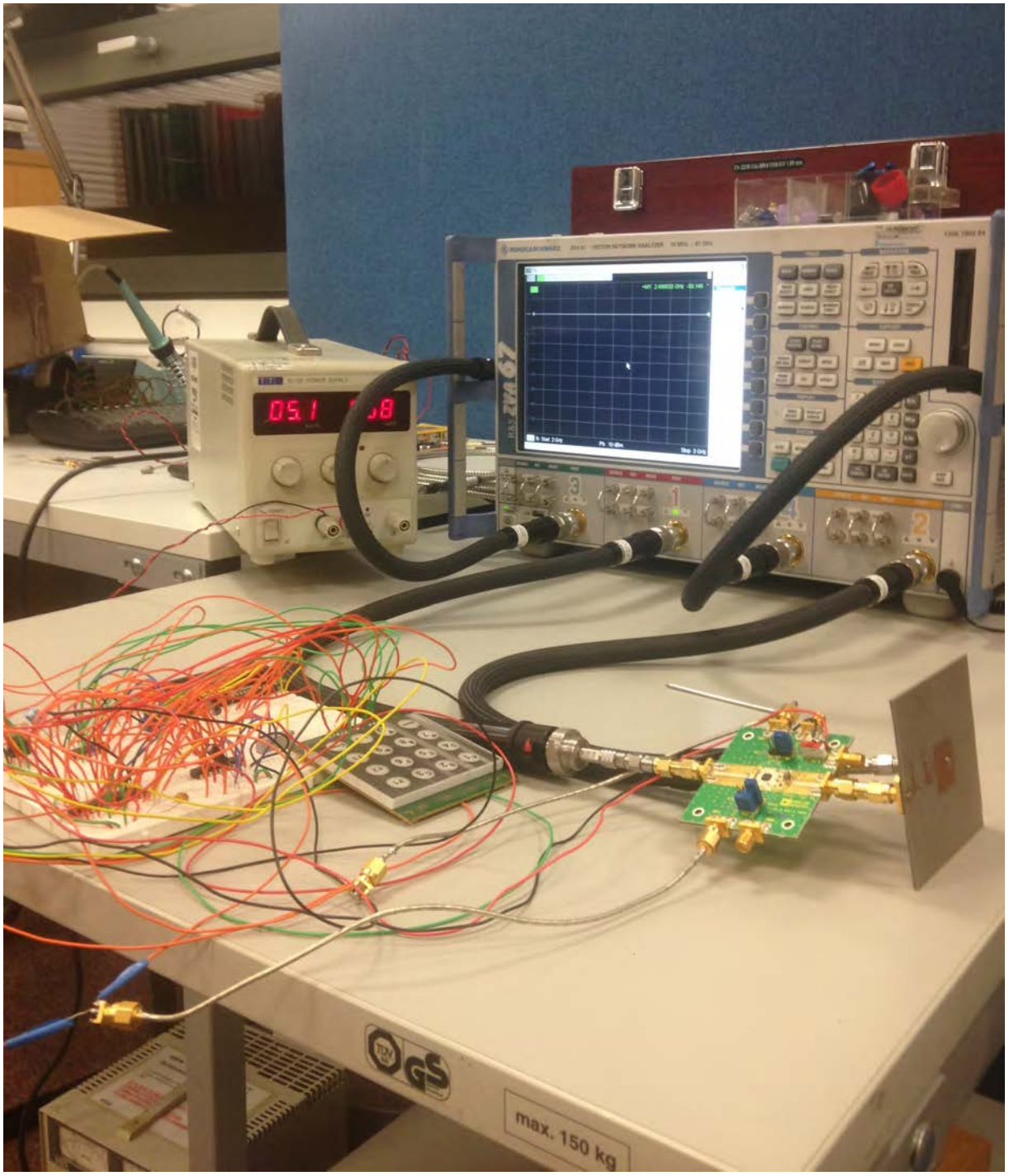

Figure 3.15: The complete measurement set-up for the IMT patch antenna The ZVA67, antenna, vector modulator and the developed circuit for providing the required voltage

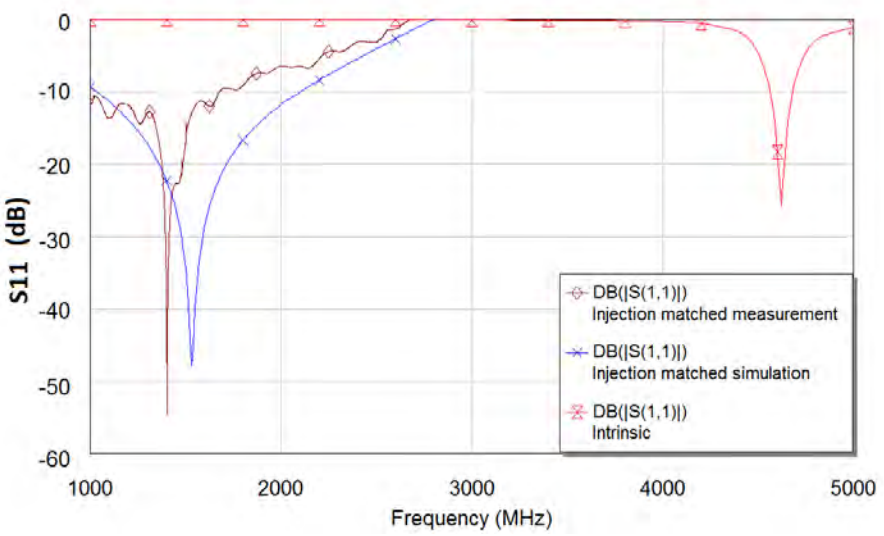

Figure 3.16: The measured return loss of the normal rectangular patch antenna $20mm \times 20mm$ and under the injection matching condition

port 1. Fig. 3.17 illustrates the return loss of the antenna at port 1 for different values of the phase shift of the vector modulator. The operating frequency of the antenna is reconfigured by the phase shift between the stimulus signals. A good frequency tuning range is experimentally achieved where the loss of the matching network is negligible. Therefore, the tuning range can also improved by using a matching network with smaller losses.

3.3.5 Improving the bandwidth and the tuning range

For improving the bandwidth of the practical work the following items can be undertaken for a future work

- Utilizing a vector modulator with wider operational bandwidth.
- Designing a matching network with wider bandwidth that is less sensitive to the fabrication errors and components tolerances.
- Utilizing bipolar transistors for directly injecting the current.

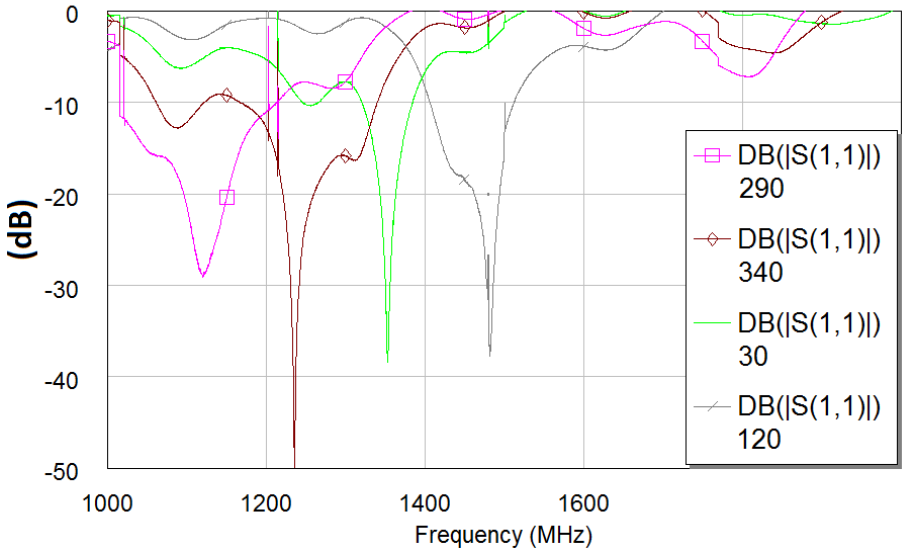

Figure 3.17: The measured result of the antenna under the injection matching for different values of φ in degrees

3.3.6 Receive mode

The presented antenna is not reciprocal due to the non-reciprocal nature of the vector modulator, here the proposed theory is utilized to design an antenna in the transmit mode. For the reciprocal operation passive implementation of the antenna can be accomplished. This can be accomplished by having a branch from the main feed line and then feeding that line to the radiating element. The width and the length of the line can be used to adjust the ratio and the relative phase of the input signal to the radiating element. Following these guidelines, a reciprocal example of IMT is developed in [88].

In accordance to IMT, in chapters 5 and 6 antennas are designed which can also be used for receive mode operation.

3.4 The radiation measurement of the Injection Matched Antennas

In order to validate the IMT, it is vital to investigate how the injection matching can influence the radiation of an antenna under the injection matching. To excite the antenna with the optimum relative amplitude and phase shift between the ports, two approaches are discussed herein [87].

3.4.1 Conventional VNA

In the case of a conventional two-port network analyser, only one port of the analyser can be used for transmitting. Using a 3-dB splitter, the output signal of the network analyser port is divided into two phased locked signals with equal amplitudes. Then one branch of the signal is fed into one port of the antenna and the other branch is fed to the vector modulator (Described in 3.3.1). The vector modulator is used to create the desired phase shift and amplification. Therefore, the output signal of the vector modulator will be a phased shifted and amplified version of the signal in the other branch. By strategically choosing the values for the phase shift and amplification, the injection matching operation can be accomplished [87].

3.4.2 Multi port VNA with true differential mode

The next approach is to use a modern four-port vector network analyser (VNA) such as a ZVA-67 from Rohde and Schwarz. Using the true differential mode option of this analyser the signals at two ports can be locked with the required phase shift, and the power level at each port can also be controlled. Consequently, via this option, the required phase shift and amplification between the ports can be realized directly. This approach is found to be more precise than the first approach, as the vector modulator introduces losses and inaccuracies in the measurement. Fig. 3.18 illustrates the configuration of the

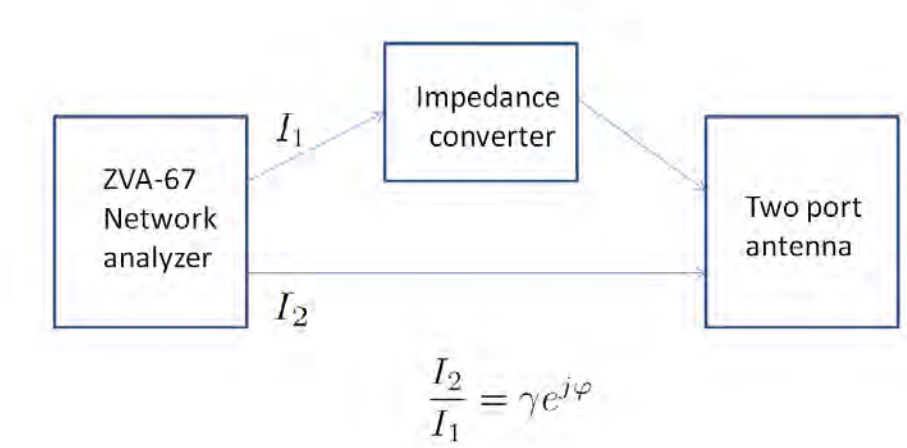

Figure 3.18: The configuration of the measurement using ZVA-67 [87]

measurement using the ZVA-67 [87].

3.4.3 Procedure and measurement

In accordance to the second approach for providing the required signals, in order to investigate how the radiation of an electrically small patch antenna is affected by the IMT, the following two experiments are designed and accomplished.

Two ports of the VNA are utilized to excite the two-port antenna and a third port is connected to a reference antenna for receiving the radiated power from the two-port IMT antenna.

Fig. 3.19 illustrates the schematic of the first and the second experiment and their summarised results.

In the first experiment the antenna is fed with equal amplitudes (0 dBm or 1 mW) but not the suitable phase shift for the injection matching operation from two ports. The total input power into the antenna is therefore 2 mW. In this situation the maximum measured received power was −68 dBm (curve with cross symbols in Fig. 3.20) [87].

In the second experiment the antenna is excited under the injection matching (optimum values for γ=0.5 and φ=220). Hence, one port is fed with 0 dBm (1 mW) signal and

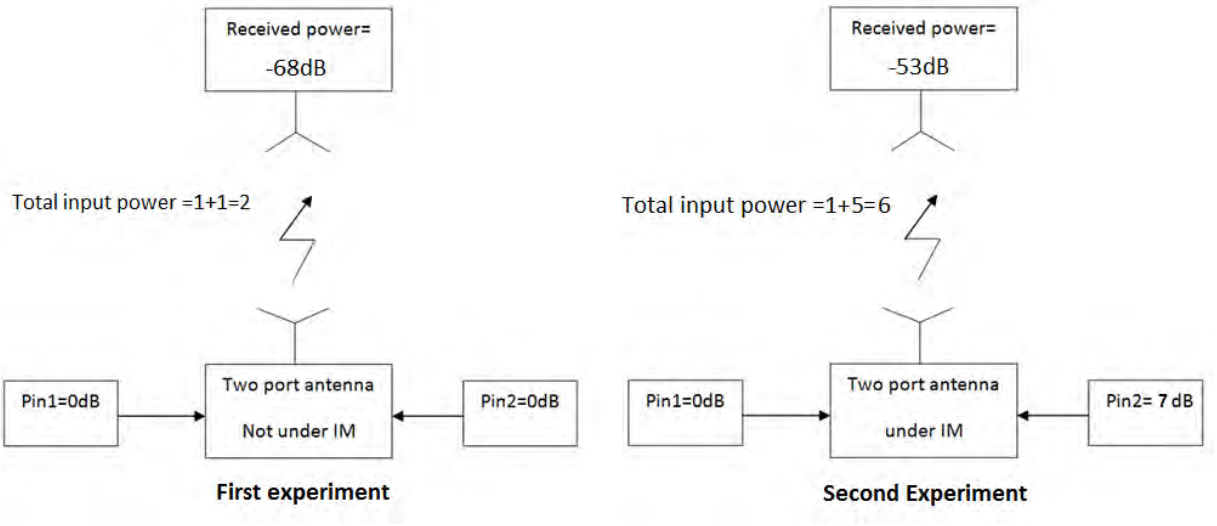

Figure 3.19: The summary of the first and second experiment for radiation measurement [87]

the other port is fed with 7 dBm (5 mW) which led to the total input power of 6 mW. Under this condition the measured received power at the receiver side was −53 dBm (curve with circle symbols in Fig. 3.20). Fig. 3.20 shows the measured received power of the

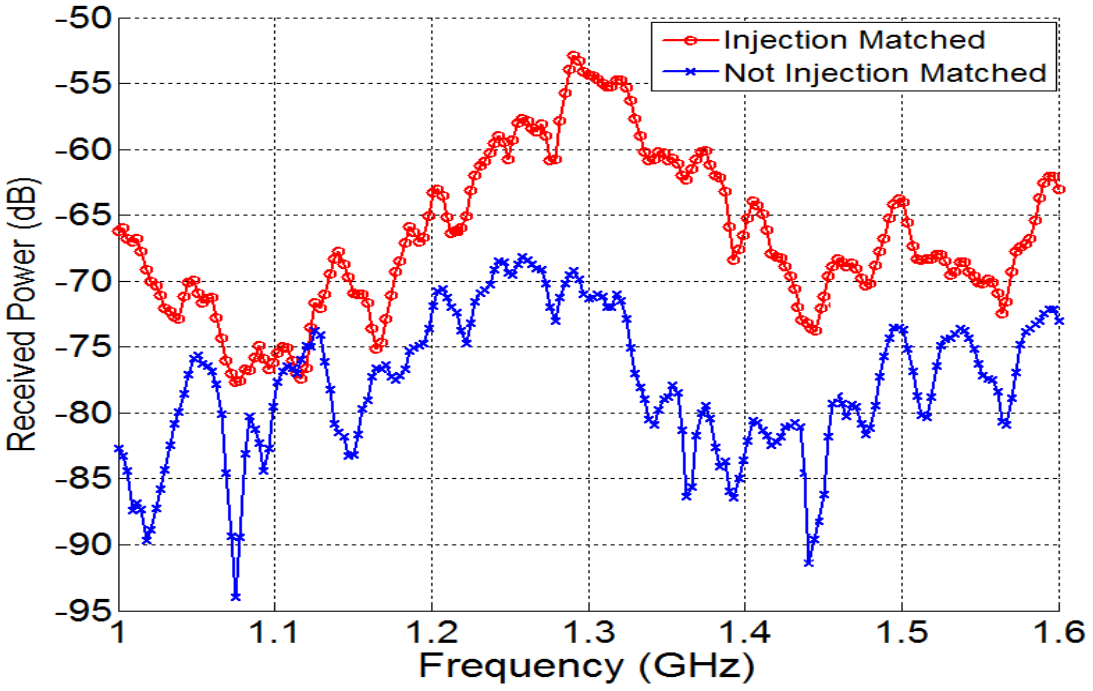

Figure 3.20: The received power at the receiver side under the injection matched condition and normal condition [87]

antenna under the injection matching and unforced resonance conditions [87].

By comparing the two experiments, it is concluded that the input power of the antenna in the second experiment is increased by the factor of 3 while the received power (radiated power from the antenna) is increased by the factor of 32 (15 dB) under the IM. Consequently, the IMT not only improves the matching of an ESA, but also improves the radiation of an antenna dramatically. The fact that the improvement in the received signal is improved for not very wide bandwidth is due to the limited bandwidth of the matching network.

3.5 Conclusion

In conclusion, electrically small antennas with multifunctional capabilities are highly desirable in current communication technology. For the purpose of making them more functional and useful, one solution might be to produce frequency and pattern reconfigurable ESAs. However, owing to the compact size and small radiation resistance, frequency tuning and pattern reconfiguration in small antennas is considerably challenging and therefore there are very few designs with severely limited functionality presented in the literature. In this chapter, an approach which is called "injection matching" is presented which can be utilized for making multi-functional small antennas. The injection matching theory has been outlined and validated through simulation and experiment. The proposed theory stipulates the possibility of matching an antenna over the frequencies where it is not inherently matched with the source, by injecting current with proper phase shift and amplitude proportional to the source current. The inherent resonance was reduced from 4.6 GHz to about 1 GHz under the injection matching. The wide bandwidth and frequency reconfiguration capability of the proposed approach, make it suitable for ESAs where the realization of the mentioned features are extremely challenging.

Chapter 4

Simultaneous Injection Matching Theory

In chapter 3 the IMT was introduced and discussed. In that approach one port was exploited to match the other port to the source, and single port matching via this technique was discussed. Injecting current to one port, only for the purpose of matching the other, consumes power and may not represent the best overall efficiency, if the injected power is relatively high. This can be solved by investigation of simultaneous matching at both ports.

By performing the right phase shift and relative amplitude ratio between the incoming signals at the ports, matching at both ports can be achieved at the same time. Consequently, the incoming power from both ports will lead to radiation and together can be used for transferring data. Intuitively, the total efficiency will increase. In this chapter the concept of SIMT is developed and described via a physical description of the current distribution on a two port antenna under the Simultaneous Injection Matching condition. Then, the SIMT is also discussed from a circuit point of view and the essentials for accomplishing this approach in practice, are defined and described.

4.1 The physics of the simultaneous injection matching

The physics of electromagnetic wave radiation dictates that the current distribution on an antenna is the source term of the wave equation derived from Maxwell's equations. The forced source current distribution is a standing or travelling wave with wavenumber $k = \omega/c$ in the absence of dielectrics in the immediate vicinity of the antenna conductor(s). In deriving the fundamental limits of electrically small antennas, $ka < 1$, where a is the radius of the smallest circumscribed sphere to the antenna structure, the forced source current distribution is not examined explicitly, but the spherical harmonic expansion of the electromagnetic field outside the sphere of radius a is instead considered, with all modes being evanescent [11, 12]. A universally adopted implicit assumption is that the sphere of radius a *contains completely* the forced source current distribution, which typically has a node at the antenna extremities. The consequences of this assumption are that only a small fraction of a cycle of the spatial oscillation of the current distribution is excited along the antenna, and the boundary condition is that the current goes to 0 at the ends of the antenna structure. A complete electromagnetic field analysis of the radiating current distribution yields the same conclusion as the more general evanescent spherical harmonic field decomposition analysis, namely that the electrically small radiator is inefficient as it has a very large terminal reactance and a very small resistance.

However, the above assumptions are predicated on the implicitly imposed condition that the forced source current distribution falls to zero at the antenna extremities. This assumption can be relaxed by considering an antenna structure that is driven by two coherent sources at near its extremities. Focusing on the current viewpoint, it is instructive to think in terms of an analogy with waves on elastic strings: An antenna driven at one port corresponds to the forced oscillation of one end of the string, with its other end held fixed. For slow oscillations (i.e. long wavelengths compared to the string length)

the string tension presents considerable resistance to the driving force and the maximum oscillation amplitude achieved is small. On the other hand, if both ends of the elastic string are driven at the same frequency, but with carefully arranged relative magnitude and phase, large amplitude excitation is achievable (the mechanical wave can be either a standing or travelling wave), provided that the two sources do not do work against each other.

4.1.1 Current analysis of SIMT

The goal of simultaneous injection matching theory (SIMT) is to excite a current distribution having a wavelength significantly larger than the natural resonant wavelength corresponding to the antenna dimensions, by having two driven ports near the extremities of the antenna structure. To illustrate the operating principle, a perfectly conducting metallic strip is excited via a capacitive coupling element. The reason for choosing a conducting strip is that, an electrically short linear antenna has a mutual impedance between two ports at its two ends that cannot satisfy the simultaneous injection matched condition presented later. Whereas, the small but finite strip width can be chosen to satisfy this condition, and at the same time minimize the transverse component of the surface current and maximize the longitudinal component. In this way a structure can be arrived at that can be directly discussed with reference to the vibrating elastic string analogy.

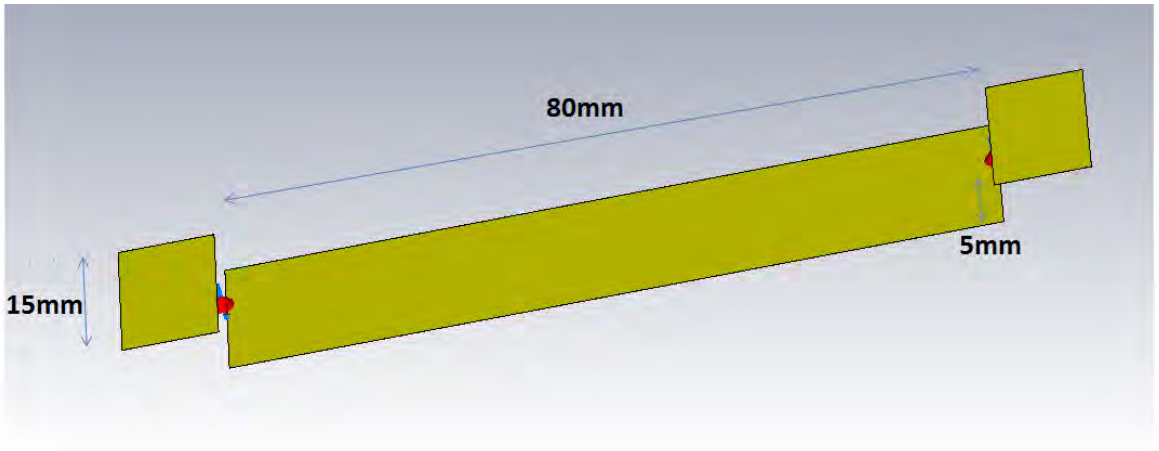

Figure 4.1: The 3D view and the dimensions of the strip

The strip dimensions are illustrated in Fig. 4.1. The two point sources are connected to the strip using two small ground planes at each end, in series with 10 pF capacitors to improve matching to the 50 Ω source impedance. At a spot frequency (of 1 GHz), well below the natural resonance achieved through one-port excitation (at 3.2 GHz), the surface current and radiation from the strip are investigated under the SIMT condition, and compared to those observed when it is excited at one end only.

Fig. 4.2(a) and (b) depict the transverse and longitudinal current magnitude distribution on the antenna when it is excited at one end, with the second port being open-circuited. The total surface current vector distribution is illustrated in Fig. 4.2(c). It is observed that the transverse current is negligible compared to the longitudinal current on

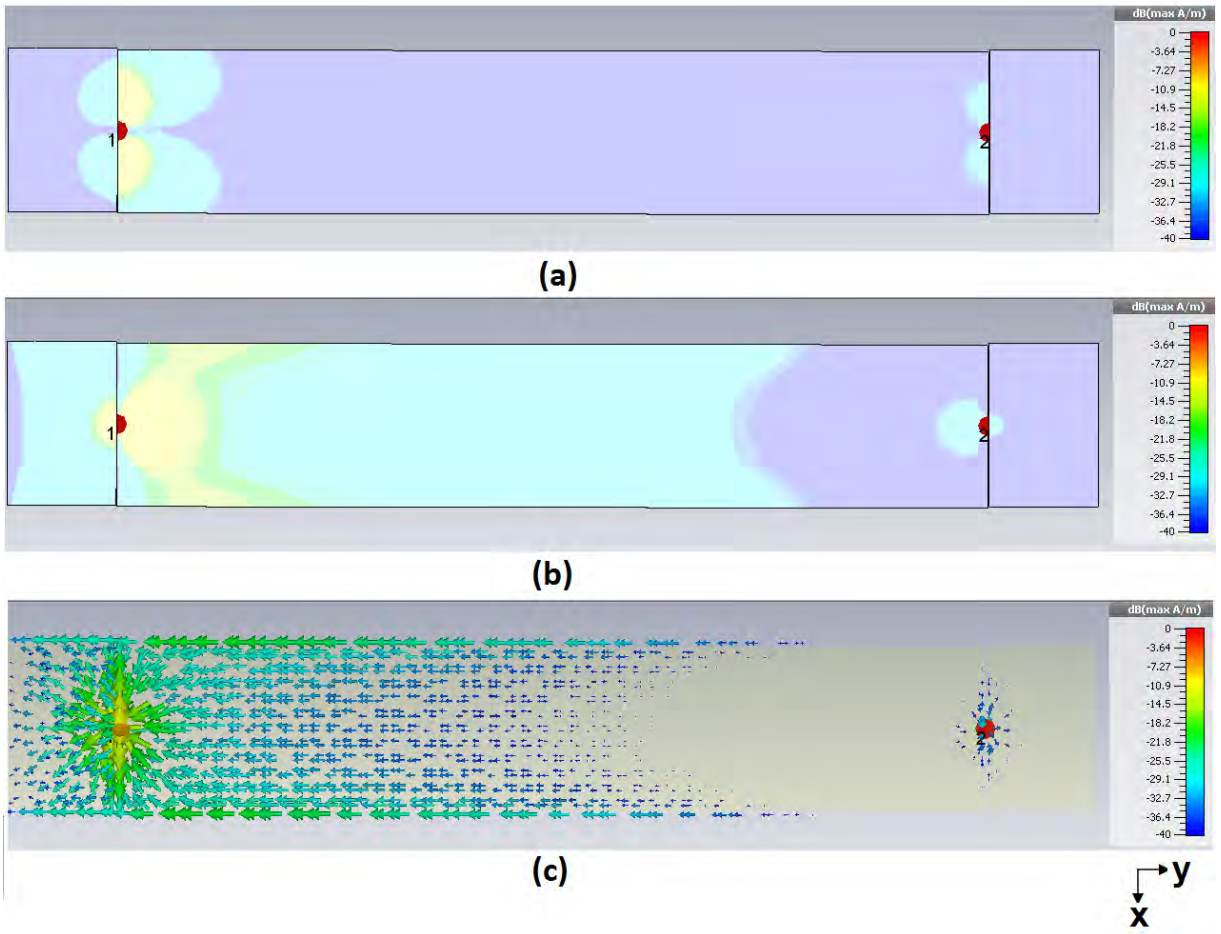

Figure 4.2: The surface current (a) X-component (b) Y-component (c) total current for normal excitation

the strip, as was expected.

Fig. 4.3(a) and (b) depict the transverse and longitudinal current magnitude distribution on the antenna under the SIMT condition. The corresponding total surface current vector distribution is shown in Fig. 4.3(c). It can be seen clearly that the y-component of the current remains dominant. For ease of understanding, the structure and the position of the ports are designed such that they are symmetrical. Therefore, in this example the optimum relative excitation phase for the two sources under the SIMT condition is found to be close to 180° (it can be varied from 170° to 190°). The 180° of phase shift between the excitation sources at the antenna terminals under the SIMT condition illustrates that by having a push-pull excitation at the antenna terminals it is possible to excite a current of a wavelength much bigger than the antenna structure. This can seen in Fig. 4.3(c)

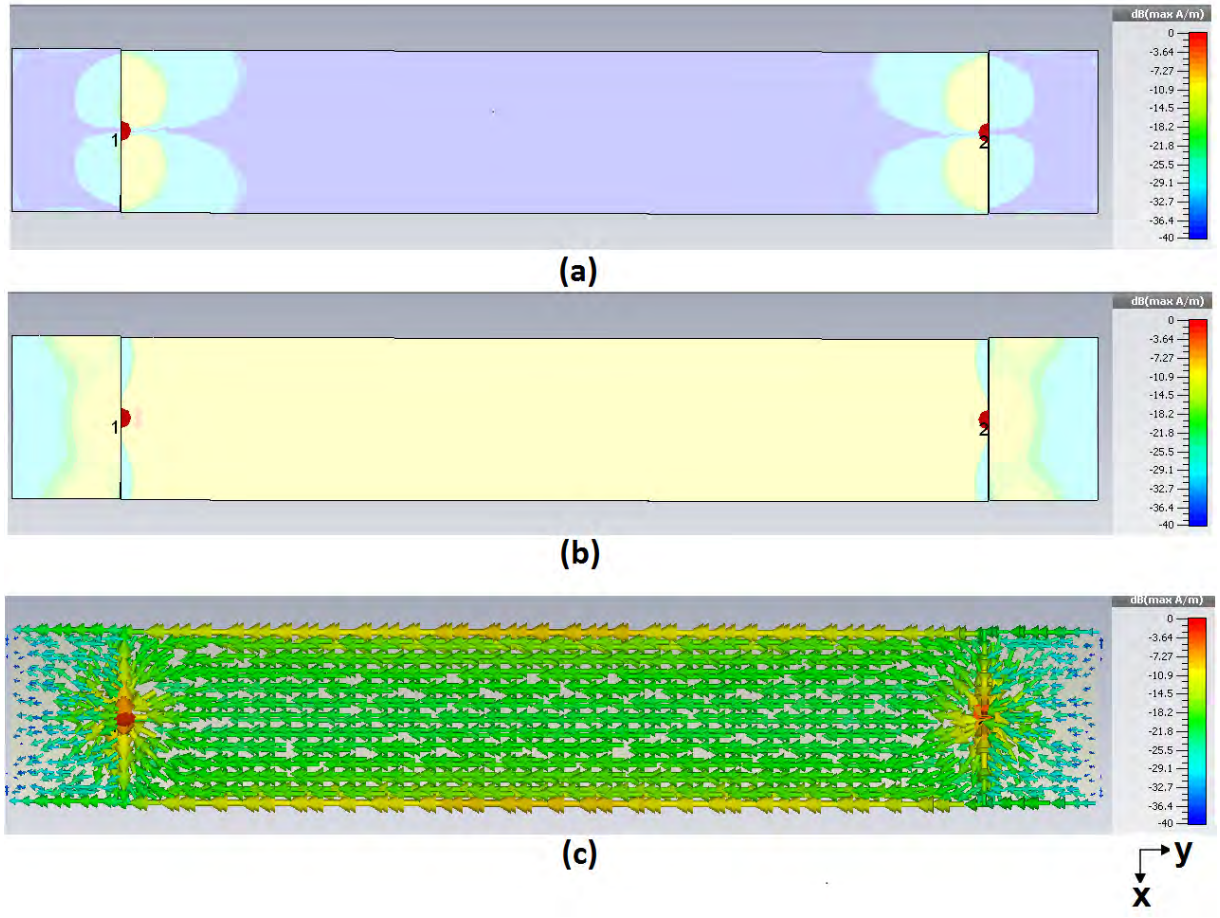

Figure 4.3: The surface current (a) X-component (b) Y-component (c) total current under SIMT condition excitation

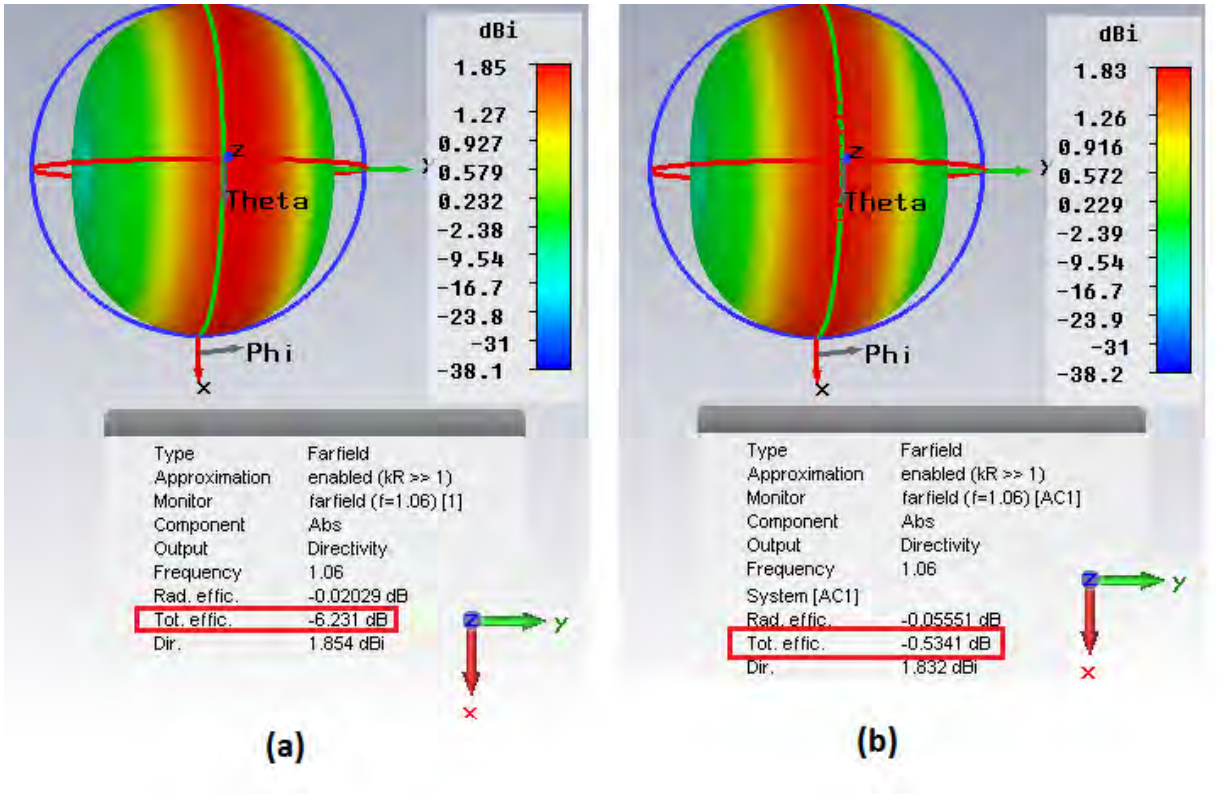

Figure 4.4: The radiation pattern and the total efficiency (a) normal excitation (b) under SIMT

by observing the direction of the arrows (phase of the current). Although the excitation sources are out of phase, the surface current under the SIMT has a near uniform direction along the string. Moreover, the amplitude of the excited standing wave is maximum at the centre of the string along the y-direction. On the other hand, by directly comparing the current density of the natural resonance (Fig. 4.2(c)) and under the SIMT condition (Fig. 4.3(c)), a significant increase in the amplitude of the current standing wave is achieved.

To go beyond the elastic string analogy, the radiation pattern and the total radiation efficiency of the antenna are monitored under the SIMT and normal excitation. This is shown in Fig. 4.4. Although the radiation pattern and directivity do not change in any significant way, the total efficiency of the antenna is improved by 5.7 dB under the SIMT condition.

The lower frequency limit of this approach can be explained using Fig. 4.5 where the

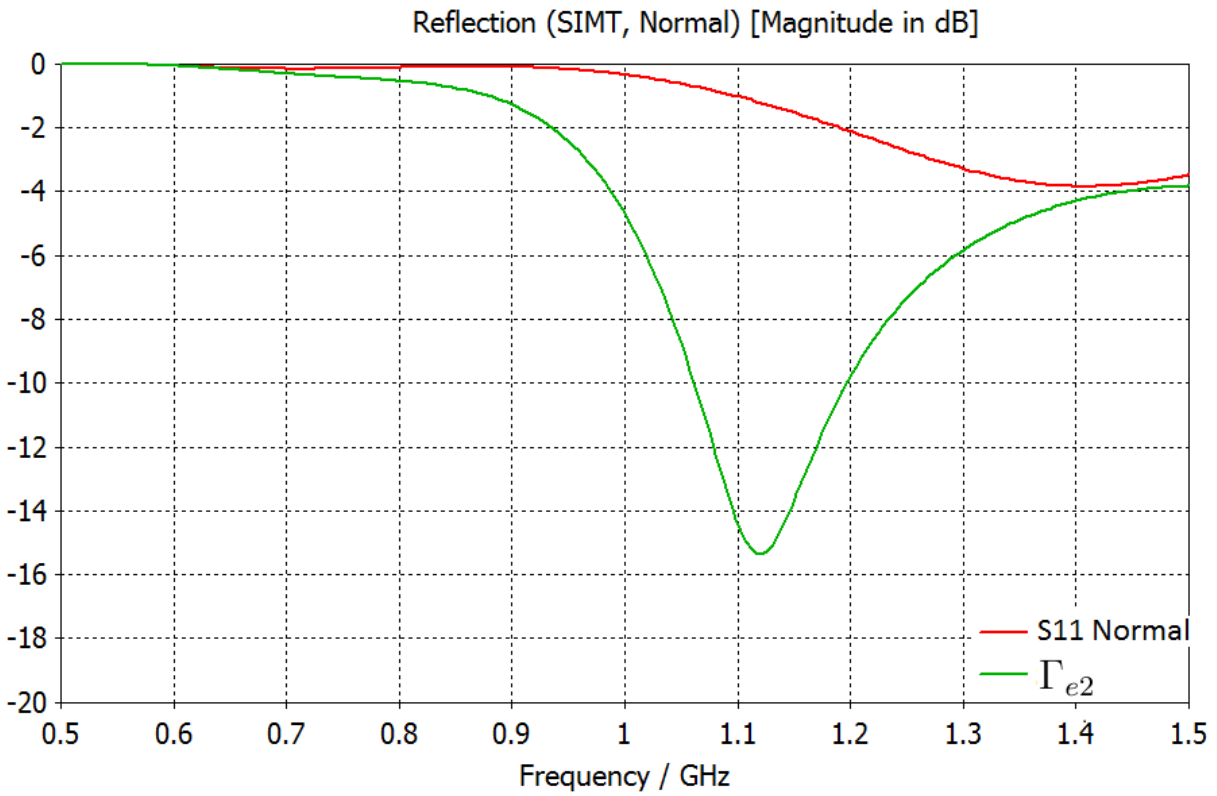

Figure 4.5: The reflection coefficient for normal excitation and under SIMT

reflection coefficient at the antenna terminal for one-port excitation and the two port equivalent coefficient for SIMT antenna called Γ_{e2}, defined later in equation (4.4) (i.e. the square root of the ratio of the total reflected power to the total incident power at the two ports) are illustrated.

To have the opportunity to excite an electrically large wavelength on an antenna structure, some current has to be injected in to the antenna structure. Therefore, in the frequency range where the one-port match is 0 dB in the S_{11} curve, virtually no current (or energy) can be injected to the structure and consequently even the SIMT condition excitation (in this case the push-pull operation) can not be achieved.

By comparing the SIM matching (Γ_{e2} curve) and single feed matching (S11 curve) in Fig. 4.5, it can be seen that the SIMT matching is achievable when the “initial” S_{11} curve (normal excitation) starts to deviate even by a small amount (e.g. -0.5 dB) from zero. All frequencies at which this criterion is satisfied can be an operating band for a SIMT antenna. Moreover, this small “initial" level of port matching required for SIMT

operation can be accomplished artificially using conventional techniques such as 1-section LC circuit, negative impedance converters (NICs) circuits or meta-materials.

4.2 The circuit description of the simultaneous injection matching

In the case of a one port injection matched antenna as demonstrated in Chapter 3 the second port is replaced with a high output impedance current source. The optimum values for γ and φ which guarantee the injection matching ($X_{in_{p1}} = 0, R_{in_{p2}} = 50\Omega$), were derived also in chapter 3. It should be noted that, at the matched port, apart from reactance compensation, the real part of the impedance can also be changed by properly choosing γ and φ.

Herein, the goal is to investigate the possibility of simultaneous matching at both ports using IMT. For this purpose for a given structure, the calculated $X_{in_{p1}}$ and $X_{in_{p2}}$, from (3.6) and (3.11) have to be close to zero simultaneously for the frequency of operation. Moreover, for balanced operation, calculated values for $R_{in_{p1}}$ and $R_{in_{p2}}$ from (3.7) and (3.10) of the same order are preferred. To shed light on this, the impedances Z_1 and Z_2 at the primary and secondary ports respectively in a two-port injection matched antenna can be considered in the complex domain can be expressed as:

$$Z_1 = Z_{11} + \gamma e^{j\varphi} Z_{12} \tag{4.1}$$

$$Z_2 = Z_{22} + \gamma^{-1} e^{-j\varphi} Z_{21} \tag{4.2}$$

According to (4.1) and (4.2), for simultaneous injection matching of both ports of a given antenna, Z_1, Z_2, φ and γ are the parameters which need to be chosen. A systematic

search for feeding points with values of Z_1, Z_2 is constructed to ensure that

$$|\Gamma_i|^2 = |(Z_i - Z_0)/(Z_i + Z_0)| << 1 \tag{4.3}$$

can be found for a range of values of φ and γ where $|\Gamma_i|$ is the reflection coefficient at port i . The search and matching procedure is performed through a geometrical matching criterion for $|\Gamma_i| << 1$ on the complex Z-plane.

Due to the complexity and number of variables which need to be calculated for SIM, using numerical approaches (via Matlab or Matematica) is unsuited for finding the unknowns over the frequency band of interest. Therefore, (4.1) and (4.2) are translated to the circuit schematic which can be analysed by EM packages which reduces the calculation time and complexity significantly. Moreover, tuning and optimization features of the EM packages are strongly helpful to find the optimum solutions more readily. For meeting the $|\Gamma_i| << 1$ condition at both ports of a given two port network (antenna here), an equivalent reflection coefficient for two port antennas called the Equivalent Two Port Reflection Coefficient (Γ_{e2}) is defined as:

$$\Gamma_{e2} = \sqrt{\frac{\text{total reflected power at two ports}}{\text{total incident power at two ports}}} \tag{4.4}$$

In a two port network, a small value of $|\Gamma_{e2}|$ (smaller than -10dB in logarithmic unit) can only be achieved when both ports are simultaneously well matched with the sources. This also indicates a good overall matching efficiency. Therefore, the goal is to achieve $|\Gamma_{e2}| << 1$ under the SIM condition. This will guarantee isolation between the ports, under the SIM condition, as lack of isolation between the ports will increase the total apparent reflected power and consequently Γ_{e2} becomes greater.

4.2.1 Circuit schematic solution

For performing the simultaneous injection matched condition the values of Z_1, Z_2, φ and γ have to be chosen such that they satisfy $|\Gamma_{e2}| << 1$. This will guarantee matching at both ports and express high overall matching efficiency for the two-port antenna system. In order to translate (4.1) and (4.2) to a circuit schematic, the system illustrated in Fig. 4.6 is proposed.

To perform the phase shift between the signals at the primary and secondary ports of the antenna, a single excitation source is used via an ideal 3dB splitter, so the signals are divided into two branches. Therefore, the outputs of the splitter are phase coherent and by exploiting a phase shifter at one branch, the required phase shift (φ) between the signals at the ports can be implemented. The outputs of the splitter have also the same amplitude and therefore γ is found by introducing an attenuator in one branch. To enable the designed system to analyse (4.1) and (4.2) for various values of impedances

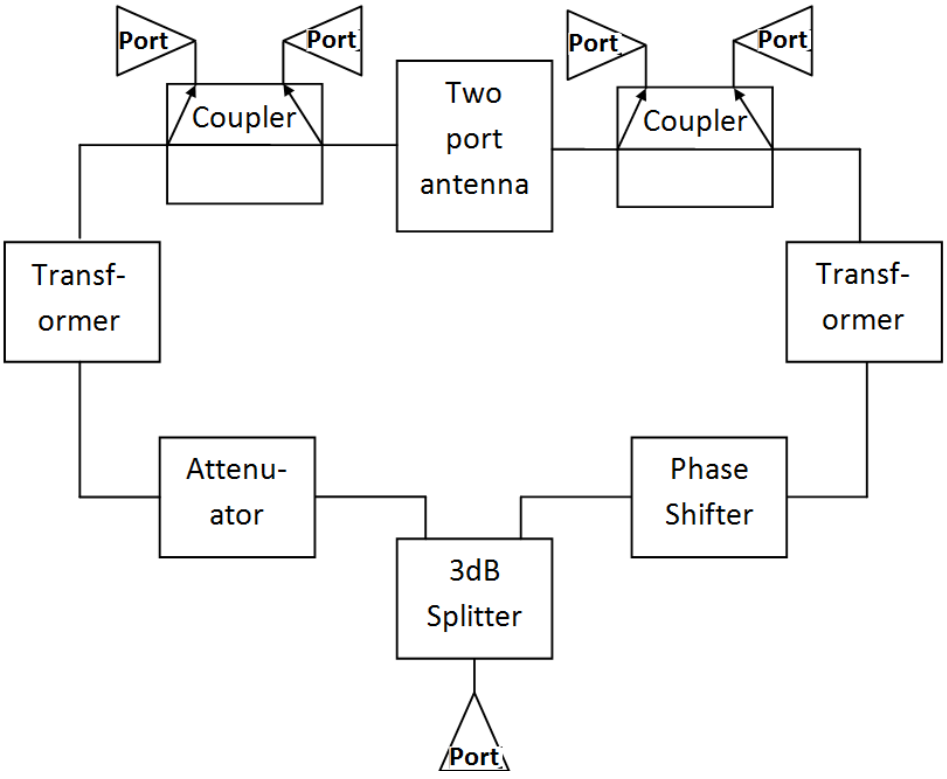

Figure 4.6: The proposed system for solving equation (4.3)

at the ports, an impedance transformers is used in each branch. The outputs of the transformers realize Z_1, Z_2 in (4.1) and (4.2). These values can be controlled by properly choosing the turn ratios of the transformers.

To allow the system to determine Γ_{e2} in (4.4) for a given two-port antenna, the main target of the design, bidirectional couplers are exploited at each port at the outputs of the transformer. Their impedances are set to be equal to the impedances at the outputs of the transformers. Therefore, the reflection coefficient at each port of the antenna can be calculated by dividing the reflected and the incident power at the bidirectional couplers corresponding to that port. Intuitively, the total reflected and incident power of a two port antenna can be calculated.

4.2.2 Design methodology

The simultaneous injection match technique can be used for any antenna structures which suffer from poor matching with the source at the frequency of interest. To have a systematic design the following steps can be taken when the design criterion is bandwidth. The second step can be varied in accordance to the design criteria which will be discussed in detail in a later chapter.

1. Choose the antenna structure which suffers from poor matching(single port)
2. Find the feed point position for the single port antenna which leads to wider matching even it is not perfectly matched.
3. Introduce the second port of the antenna.
4. Find the position of the second port of the antenna such that the coupling between the ports becomes as small as possible but not zero.
5. Set the circuit schematic goal ($|\Gamma_{e2}| << -10$ dB) for the frequency of interest.
6. Set the turn ratios of the transformers to 1 (set Z_1, Z_2 to 50 Ω).

7. Set $\gamma = 1$.

8. Solve the designed system via optimization/sweeping for φ.

9. If the criterion is met, finish

10. Otherwise, set a range for the turn ratios of the transformer (calculating the equations for more values of Z_1, Z_2) and/or set a range for γ.

11. Go to step 8

4.3 Conclusion

A technique called injection matching was newly proposed which was initially used for making an electrically small antenna in which a secondary port was introduced to the antenna structure to match the primary port. In this chapter the potential of simultaneous matching at both ports is investigated. The physical description of the IMT is developed based on the current distribution under the SIMT. A systematic approach for making a simultaneous injection matched antenna is presented and a design methodology is developed. Various antenna types with the desired design criterion can be designed by following the introduced methodology which will be discussed in the later chapters.

Chapter 5

A Wide Bandwidth Injection Matched Patch Antenna

5.1 An example of wideband simultaneous injection match antenna

In the previous chapters the Single feed injection matching theory was introduced and the theory was validated through practical and simulation results from a fabricated injection matched patch antenna. Afterwards, the simultaneous injection matching theory was introduced and discussed. To show the importance and the benefits of this approach, the potential applications of this approach are discussed in the rest of this thesis and it is validated through the measured and simulated data.

In this chapter one potential application of this approach, which is bandwidth improvement capability, is discussed. In order to validate the developed technique and illustrate how well matching and bandwidth of an antenna with inherent poor matching can be amended, a proximity patch antenna with length of 25 mm and width of 20 mm is designed. It consists of 3 copper layers and two dielectric layers of thickness 0.78 mm with dielectric constant of 2.2 having a natural resonance of 4 GHz. It is intended to investigate the potential of using a miniaturized wideband patch antenna to operate in the S

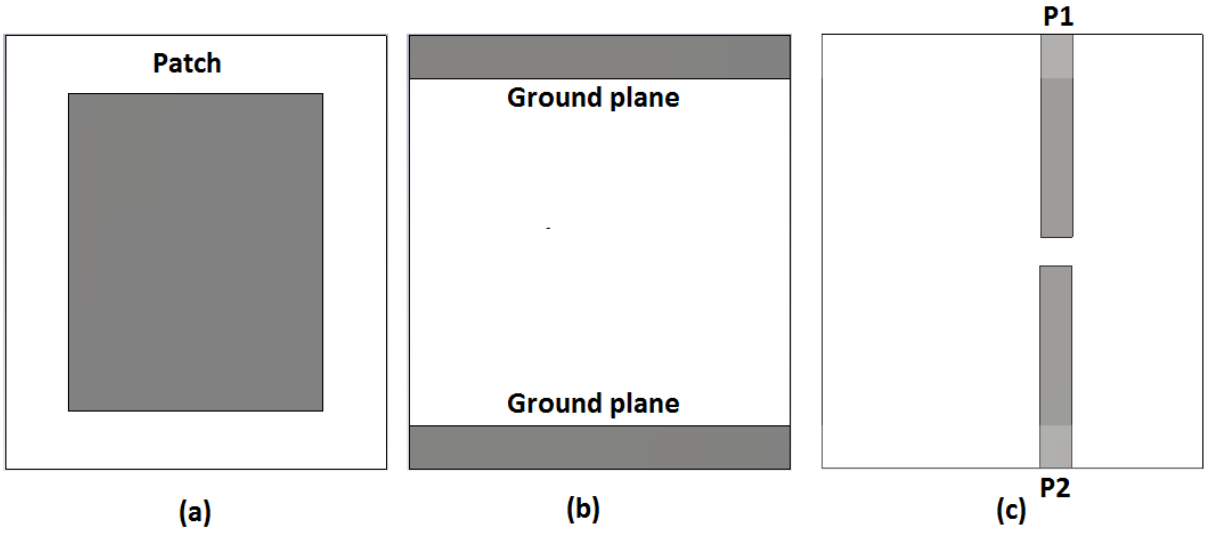

Figure 5.1: The fabricated two port simultaneous injection matched antenna (a) front and (b) back of the structure (c) the feed lines

and C bands (2.5-7 GHz). Therefore, as a method to allow wideband operation for the patch antenna, the partial ground plane is used [89].More information on this is provide in appendix G.

Due to size reduction, initially poor matching is achieved for the single feed antenna. In order to improve the matching and the bandwidth, the simultaneous injection matched approach is used. Therefore, the steps provided in section (4.2.2) are followed. Among the other feeding methods (as described in appendix F) the proximity feed is chosen to provide a better initial isolation between the ports (step 4 of the design methodology provided in 4.2.2).

Fig. 5.1 illustrates the geometry of the SIM antenna after following the provided steps. The bandwidth criterion is met in the first iteration. Fig. 5.1(a) illustrates the front of the antenna where the radiating element is located. Fig. 5.1(b) shows the back of the structure where the partial grounds are located. Fig. 5.1(c) demonstrates the proximity feed lines which are located in between the radiating element and the ground. The single feed antenna only has one feed line and a partial ground (top or bottom) in Fig. 5.1(b) and Fig. 5.1(c).

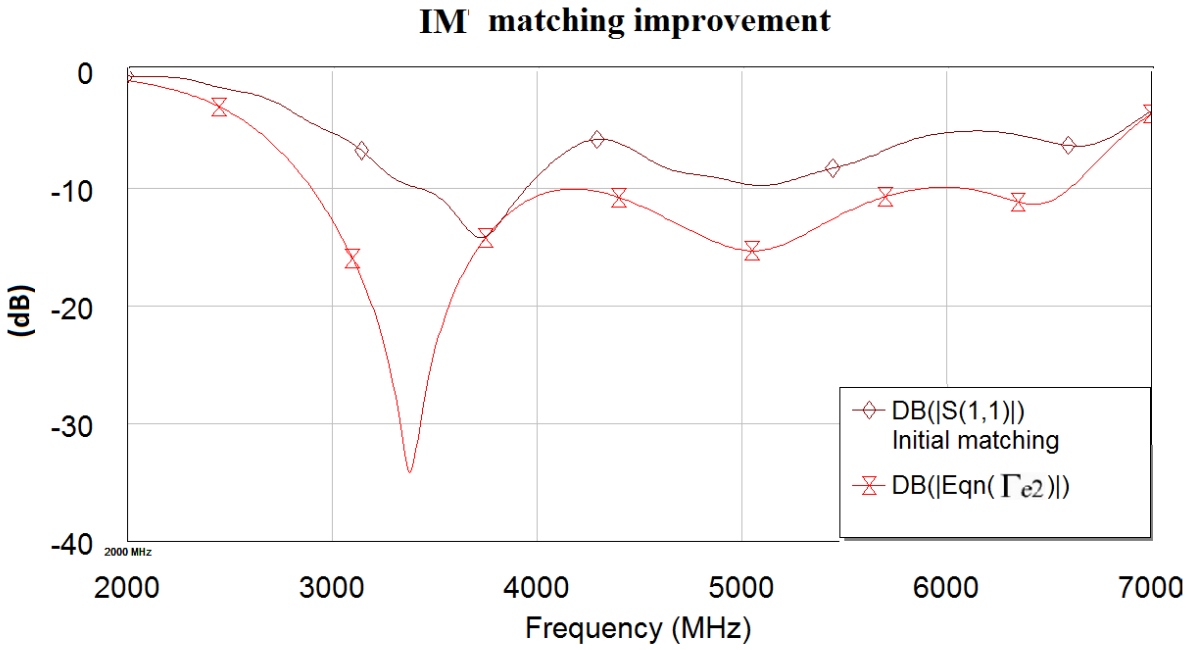

Figure 5.2: The simulated Γ_{e2} for two port simultaneous injection matched antenna and S11 for the single feed antenna

5.2 Simulation result

The simulation results from the packages are in a good agreement. In order to monitor the required parameters like Γ_{e2} and total efficiency of the system under the SIM, the configuration presented in Fig. 4.6 is developed within the software packages. Fig. 5.2 illustrates the S11 for the single feed antenna and its equivalent for a two port antenna Γ_{e2} under the SIM. The curve with square symbols illustrates the initial matching for the single feed antenna and a -10dB bandwidth of 0.45 GHz. The curve with triangles shows matching under the SIM condition and a -10dB bandwidth of 3.8 GHz. Therefore it illustrates that the SIMT can significantly improve the bandwidth of an antenna with poor matching.

In order to check that the achieved improvement in matching is due to the radiation resistance and not losses, the total efficiency curves are provided in Fig. 5.3 for the single feed antenna (for both ports one and two) and SIM antenna. For this purpose the AC

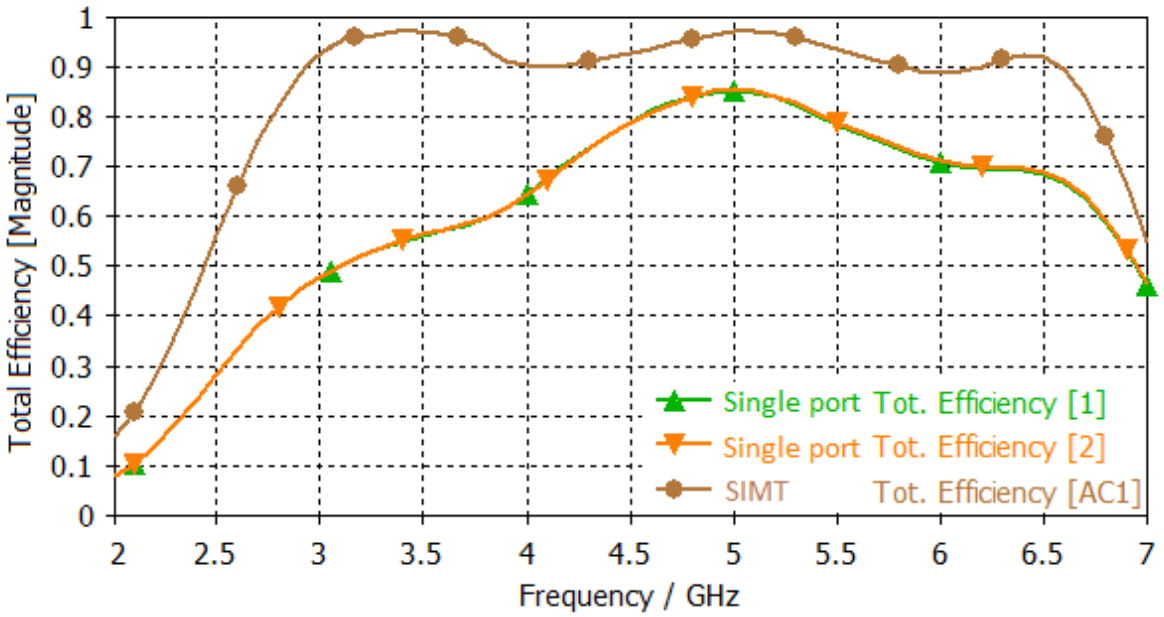

Figure 5.3: The total effieciency of the antenna under the SIM and single feed at port 1 and port2

combined feature of the CST software is used which allows monitoring of the desired antenna parameters with the existence of external components [85] as presented in Fig.4.6. As Fig. 5.3 illustrates, in the whole range of operation the AC combined result curve (the efficiency of the SIM antenna) stands well above the single feed antennas (port1 and port2) and the efficiency increases from 50 to 97 percent at some frequencies. Therefore, it shows that the improvement in the matching leads to radiation and not losses.

In order to have an insight into how well the SIMT can improve matching compared with the common approaches, a four section matching network is designed to match the same single feed antenna over the band of interest with the source. Then, it is optimized in order to guarantee that the best values for its elements, which leads to the widest possible bandwidth, are chosen [90]. Fig. 5.4(a) and (b) illustrate the matching network elements and the matching of the single feed antenna with the existence of an external matching network. Using a 4-section matching network, a -10dB bandwidth of 1.3 GHz is achieved. This shows that for a similar bandwidth improvement as SIMT, a minimum of three, 4-section matching networks are required which will make the antenna much bigger

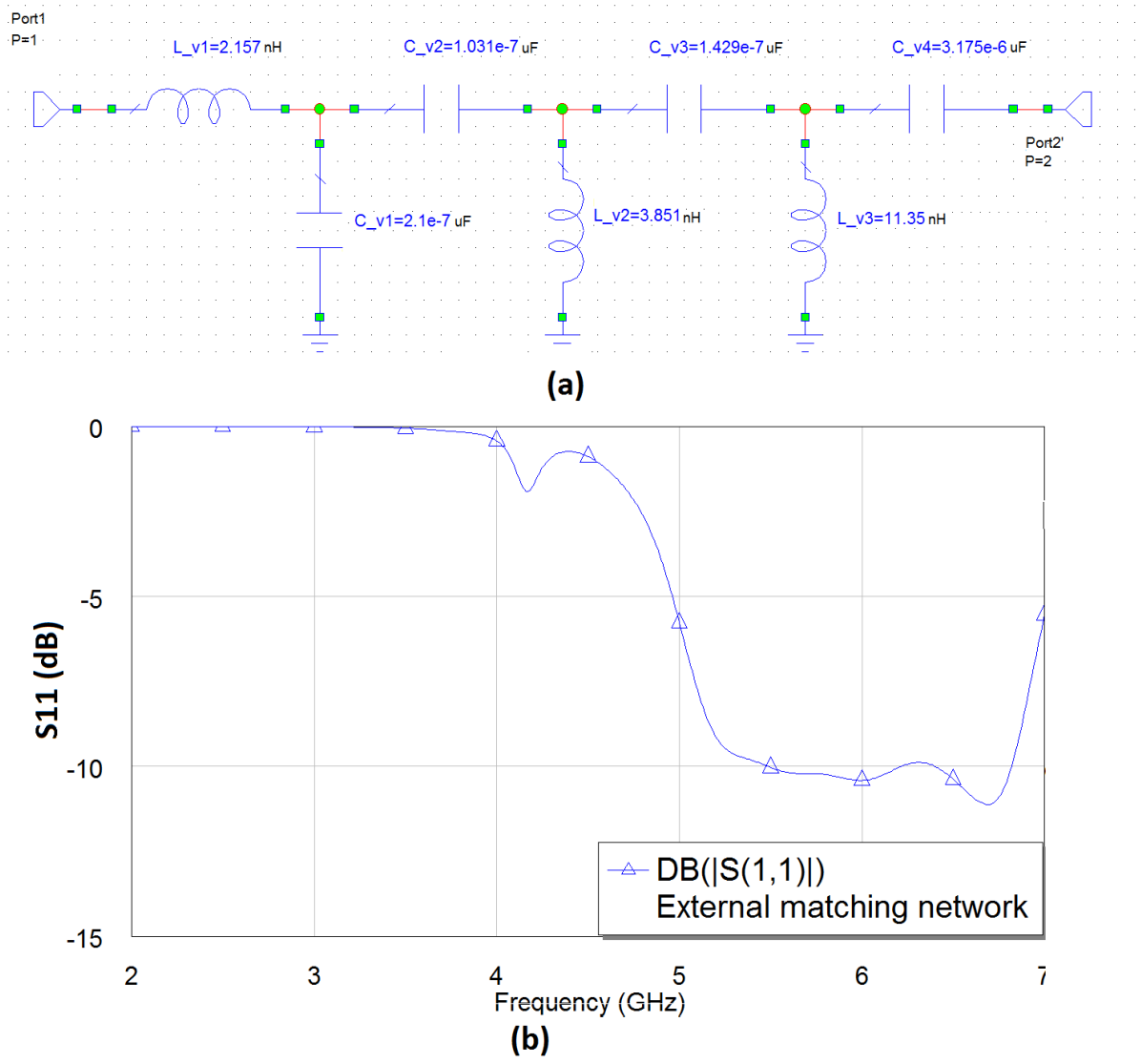

Figure 5.4: (a) Four section external matching network and its elements after optimization (b) the S11 curve for the single feed antenna with existence of the external matching network

and lossy with a total of 19 lumped element components.

To determine how the radiation pattern is affected in a SIM antenna, two frequencies in which the initial single feed antenna shows acceptable omnidirectional patterns, are monitored. Fig. 5.5 (a) and (b) illustrate the radiation patterns of the single feed antenna at 2.7 and 3.7 GHz, respectively. Fig. 5.5 (c) and (d) show the radiation pattern of the SIM antenna for these frequencies. By comparing Fig. 5.5 (a) and (c) at 2.7 GHz and (b) and (d) at 3.7 GHz, it is concluded that herein using SIMT has not changed radiation

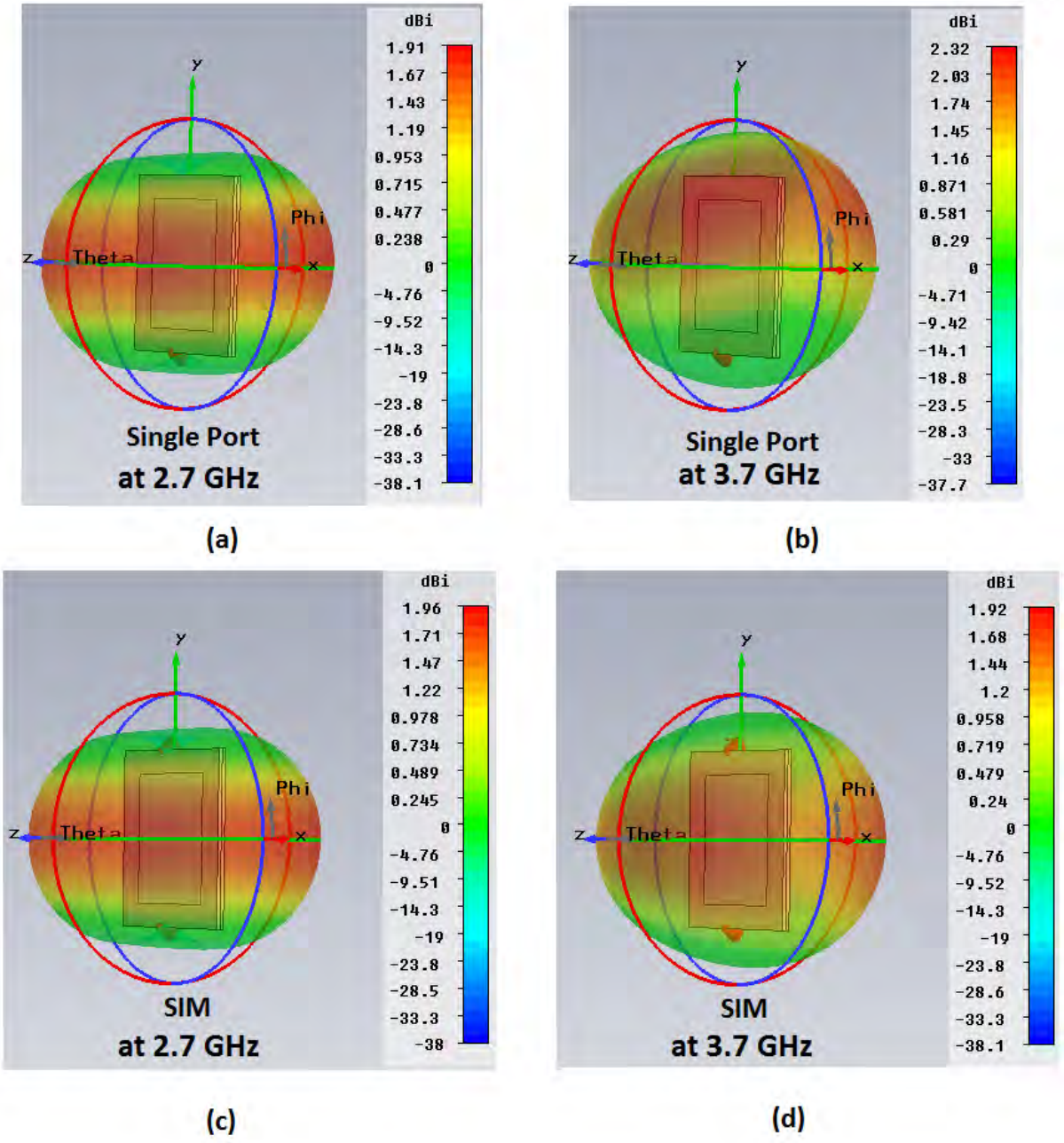

Figure 5.5: The radiation pattern of the single feed antenna (a) at 2.7 GHz and (b) at 3.7 GHz and the radiation of the SIM antenna (c) at 2.7 GHz and (d) at 3.7 GHz

pattern significantly for these frequencies.

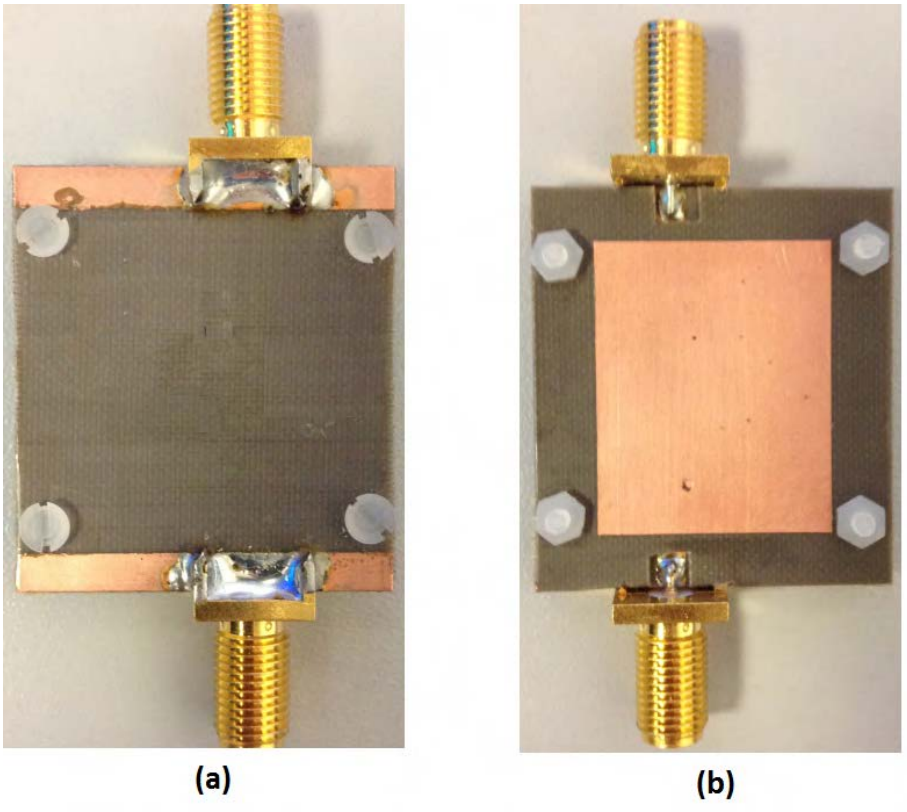

Figure 5.6: (a) front and (b) bottom of the fabricated SIM antenna

5.3 Practical measurements

To validate the proposed theory, the simultaneous injection matched patch antenna, described above, is fabricated and its properties are experimentally investigated. In this subsection, the practical work carried out is discussed and is followed by the experimental results.

Fig. 5.6 (a) and (b) show the top and bottom of the fabricated SIM antenna. The two layers are attached via 4 plastic screws. Herein, in order to feed the antenna with the required relative amplitude and phase between the ports the Rohde and Schwarz ZVA67 network analyser is used. The true differential mode of the analyser allows the definition of coherent excitations between the ports. Therefore, initially two ports of the analyser are locked together and the required relative phase shift and amplitude between the ports can be accomplished via this option [91]. In practice the required relative phase shift and

amplification can be realized by using a 3-dB splitter to generate two locked signals and a vector modulator to perform the desired phase shift and amplification [84].

In order to measure the Γ_{e2} for the fabricated two port antenna using the network analyser, wave quantities are used. The Γ_{e2} can be defined based on the wave quantities as:

$$\Gamma_{e2} = \sqrt{\frac{|b_1|^2 + |b_2|^2}{|a_1|^2 + |a_2|^2}}, \tag{5.1}$$

where a_1 and a_2 are the input normalised voltage waves at port1 and 2 while b_1 and b_2 are the output normalised voltage waves at port1 and 2. Therefore, (5.1) would be equivalent to (4.4). Fig. 5.7 illustrates measured S11 and S22 for the single port antenna and the measured Γ_{e2} under SIM condition. The measured -10 dB bandwidth of the single feed antenna is 1.3 GHz while that of SIM antenna is 4.8 GHz. This can validate the SIMT as experimentally the bandwidth of an antenna with poor matching over the band of interest is improved significantly using the SIMT.

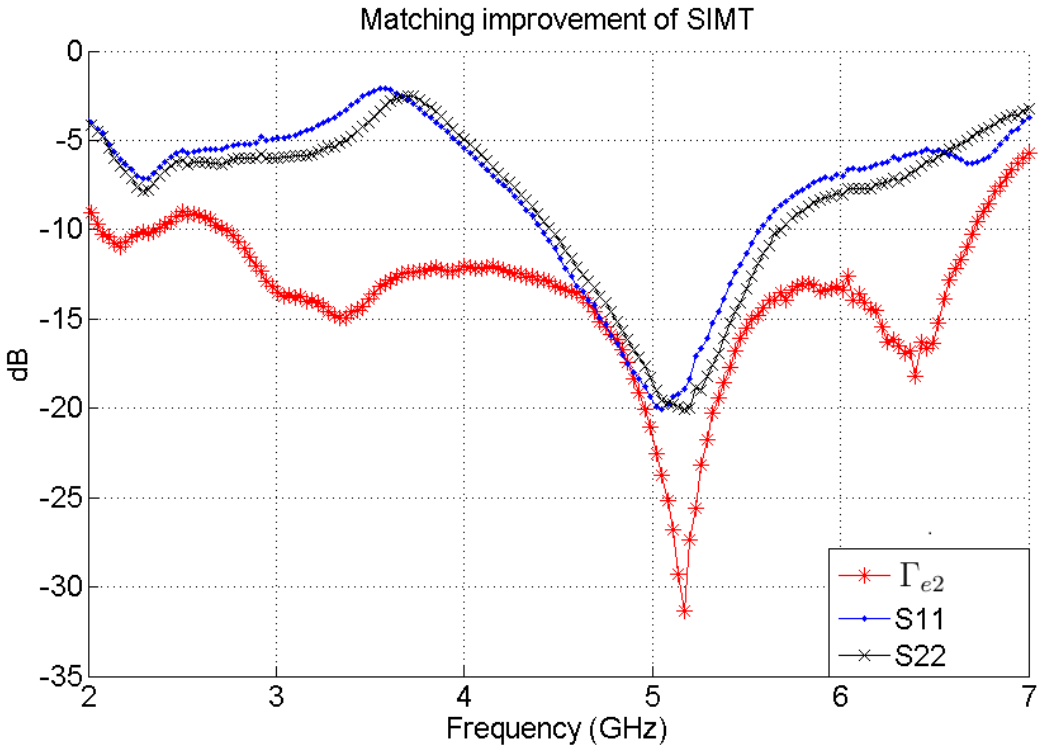

Figure 5.7: The measured S11 and S22 for the single port antenna and the measured Γ_{e2} under the SIM condition

It is very important to confirm that the matching improvement in the experimental results will lead to radiation and not losses. Therefore, the following experiment is performed. For single feed antenna radiation measurement, two ports of the network analyser are activated and a wide band horn antenna is connected to port 1 as a reference antenna. The single feed antenna is then connected to port 2 and the ratio of $|b_1|^2$ and $|a_2|^2$ is measured (equivalent to S12). This is illustrated in the dotted curve in Fig. 5.8. In order to measure the radiation of the SIM antenna three ports of the analyser are activated in which port 1 is connected to the reference horn antenna and ports 2 and 3 are used to feed the SIM antenna using the true differential mode option. The ratio of $|b_1|^2$ and $|a_2|^2+|a_3|^2$ is measured. This is shown in solid curve in Fig. 5.8. The total input power levels in both experiments are set to be equal. Therefore, by comparing the doted and solid curve in Fig. 5.8 it is concluded that the SIM antenna is radiating more efficiently than the single feed antenna and this proves that the SIMT improves not only the matching but also the radiation.

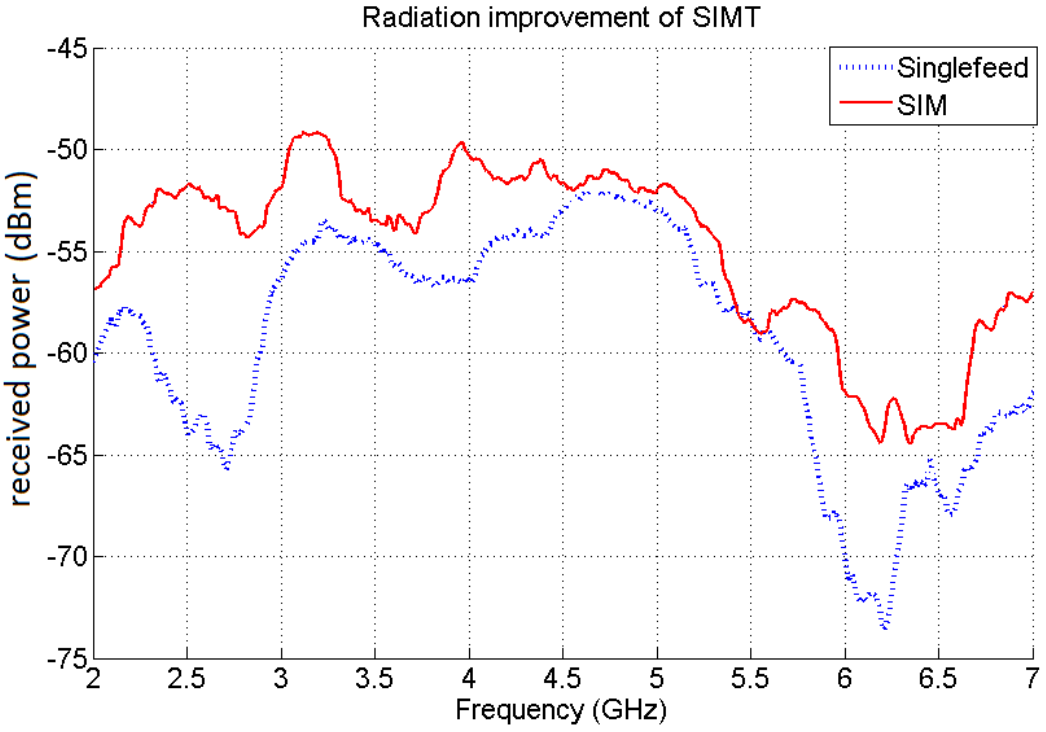

Figure 5.8: The radiation of the antenna under the SIM and single feed

5.4 Conclusion

This chapter investigates the possibility of simultaneous matching and proposes a simultaneous injection matching patch antenna. The SIMT is used to achieve wide bandwidth operation for an intrinsically narrowband antenna. This technique is investigated via simulation for a miniaturized, proximity-fed patch antenna of -10 dB bandwidth of approximately 16%, which is simultaneously injection matched at two ports to a 50 Ω source over a 2.4:1 -10 dB bandwidth. Then the proposed theory is validated through the experimental results. Therefore, it is concluded that using injection matching, simultaneous matching at both ports can be achieved leading to a significant improvement of the overall antenna efficiency and bandwidth.

Chapter 6

Electrically Small Injection Matched Antenna

6.1 Introduction

In chapter 5 one potential application of the SIMT, the bandwidth improvement, was discussed and validated through simulation and measured data from an antenna with poor inherent matching. Potential applications of Electrically Small antennas (ESA) in the field of wireless applications, such as personal communication and wireless sensor networks, make them highly desirable among antenna designers. Consequently, the potential of the SIMT for making electrically small antennas is investigated in this chapter. Based on this method, a two port electrically small chassis antenna is produced which benefits from a wide bandwidth as well as high efficiency.

6.2 Injection matched electrically small chassis antennas

According to (4.1) and (4.2), for a given antenna structure, Z_1, Z_2, φ and γ are the parameters which can lead to simultaneous matching provided that their optimum values

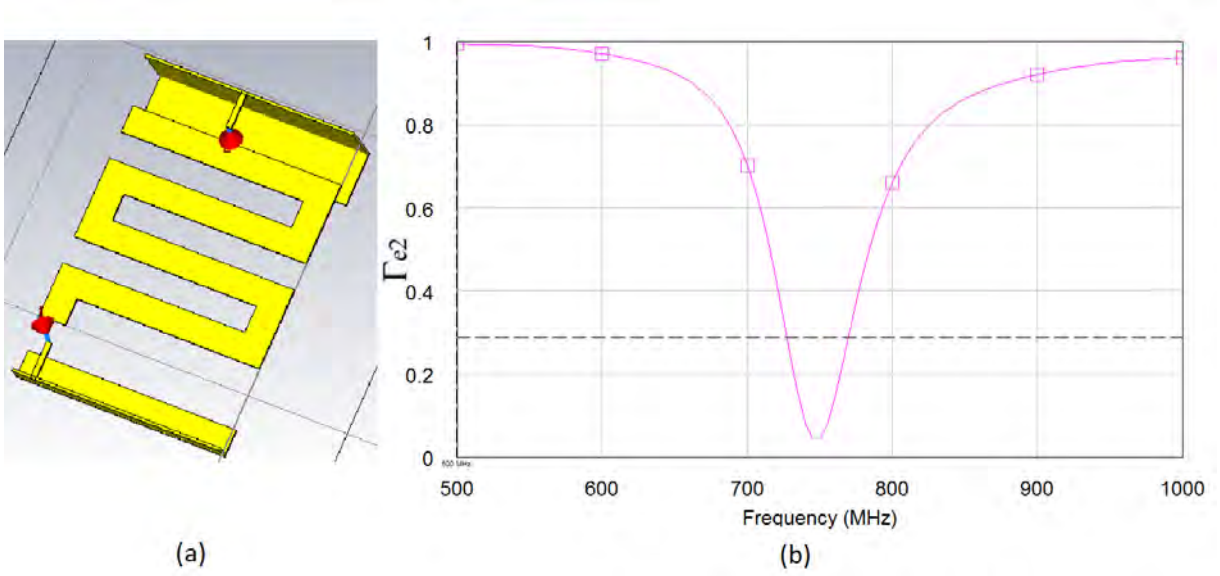

Figure 6.1: (a) The two port injection matched electrically small chassis antenna (b) The equivalent two port reflection coefficient of the injection matched chassis antenna

are chosen. Naturally for having a two port operation, values of the same order for Z_1 and Z_2 are preferred. In order to validate the proposed theory (simultaneous matching at both ports) and its potential for making electrically small antennas, a chassis antenna is chosen. The dimensions of the antenna are reduced to 32 mm $\times$ 32 mm, a 60% size reduction compared to the structure designed in [92]. Moreover, in order to make ka even smaller, four slots are introduced to shape a meander current path on the radiating element.

The geometry of the two port injection matched chassis antenna is depicted in Fig. 6.1(a). Peripheral components such as the matching networks and phase shifter are not shown. Two matching networks are used to convert standard 50 Ω lines to the two ports, both having a terminal impedance of 20 Ω. They can be readily designed using an L-section of lumped elements including a parallel 5.2 pF capacitor and a 5.2 nH series inductor. The port impedances and the phase shift between the excitation sources, have been calculated via the design methodology presented in 4.2.2 and the system for solving equation (4.3) in Fig. 4.6, such that they lead to a forced excitation. It should be noted that, one port excitation via the same matching network which is used for SIM operation (50 Ω to 20 Ω

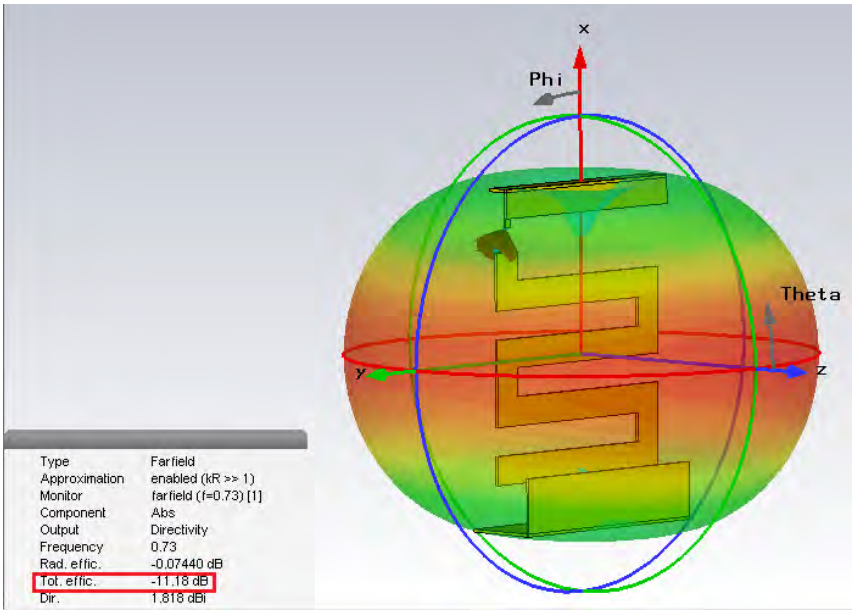

Figure 6.2: The radiation pattern and the total efficiency for one port excited chassis antenna

impedance converter), will not lead to any resonance at the frequency of interest.

The matching networks can be placed in the chassis volume and they will not increase the overall size of the antenna.

In order to have an insight into how well this antenna is radiating and to show the operating frequency of the proposed two port antenna, the equivalent to reflection coefficient for two port antennas (Γ_{e2}) as defined in 4.4 is used.

The operating frequency of this antenna can be considered where $\Gamma_{e2} < 0.25$ This can only occur when good matching at both ports is achieved, simultaneously.

The resonant frequency occurs at 750 MHz while the intrinsic resonance of the single feed chassis occurs at 4.5 GHz (see Fig. 6.1(b)) which leads to $ka \simeq 0.67$ with $Q \simeq 1.6Q_{\text{Chu}}$. Therefore, this antenna can be considered as an ESA. The Γ_{e2} shown in Fig. 6.1(b), illustrates a bandwidth of 45 MHz and it reaches 0.05 at the centre frequency indicating that the majority of the input power is radiated (this will be discussed in section 6.4.1).

The antenna here is just to show the potential capability of the SIMT for electrically small operation. However, with better initial miniaturization, operation closer or even beyond the fundamental limits would have been achievable.

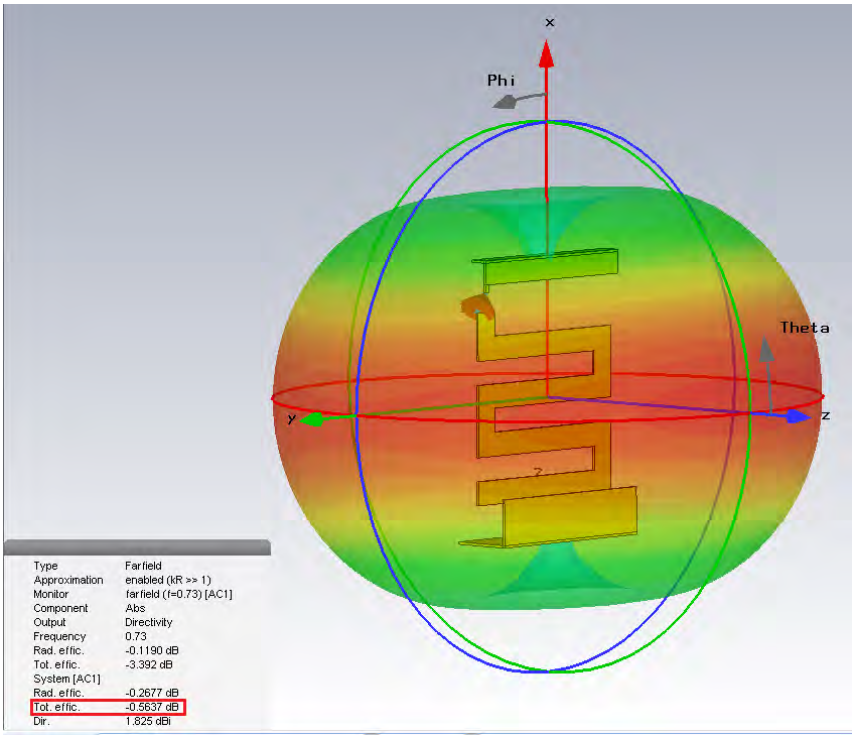

Figure 6.3: The radiation pattern and the total efficiency for the two port injection matched electrically small chassis antenna

6.3 Results and discussion

In order to validate the proposed theory and its application to the presented antenna, it is essential to investigate how injection matching can affect the radiation of an antenna. For this purpose, the radiation and the total efficiency of the proposed chassis antenna are investigated under forced excitation (injection matched) and normal excitation.

Fig. 6.2 illustrates the radiation pattern and the total efficiency of the chassis antenna when only one port is excited at 0.73 GHz (The operating frequency under SIM condition). The simulated result shows the total efficiency of -11dB. This experiment (one port excitation) was repeated for the other port and the measured total efficiency was -12dB. Fig. 6.3 shows the radiation pattern and the total efficiency of the chassis antenna under forced excitation (SIM) at 0.73 GHz. The simulated result shows that the total efficiency reaches -0.5dB. By comparing these figures it can be concluded that while the radiation pattern of the antenna is almost unchanged, the total efficiency is improved by 10.5dB.

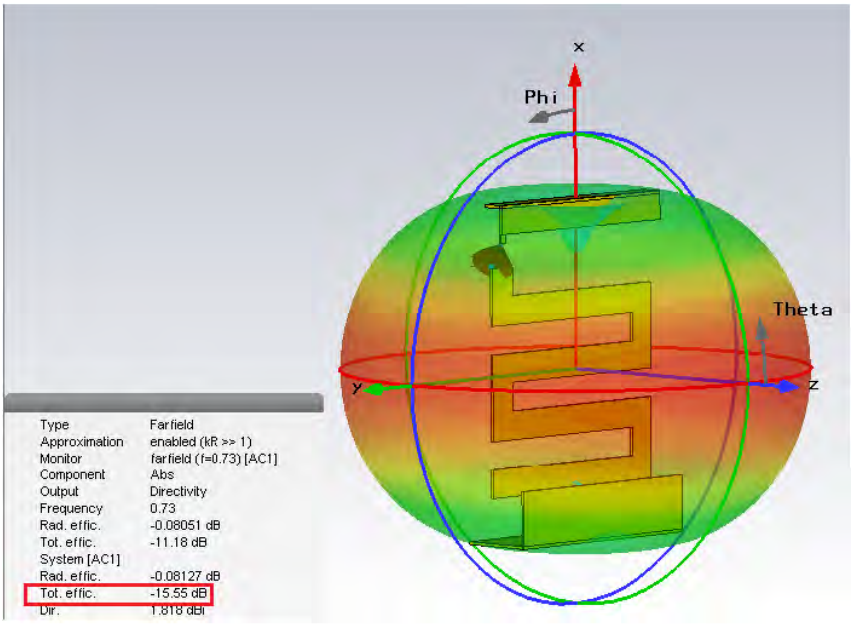

Figure 6.4: The radiation pattern and the total efficiency for one port excited chassis antenna in presence of the utilized matching network

Therefore, it can be concluded that injection matching not only improves the matching of an ESA, but also improves the radiation significantly and can be used for designing electrically small antennas with high radiation efficiency.

In order to guarantee that the significant improvement in the total efficiency is due to the forced excitation (SIM) and not the matching network, the total efficiency is investigated at 0.73 GHz for one port excitation when the same matching network (50 Ω to 20 Ω impedance converter) is used at the excitation port (this is different from Figure 6.2 in which there was no matching network present in the measurement). As Fig. 6.4 illustrates, the total efficiency is reduced to -15dB which validates that the efficiency improvement of 14.5 dB is due to the injection matching at 0.73 GHz.

6.4 Circuit analysis

The key challenge for making small antennas is to compensate for their inherent low radiation resistance and high reactance at their input ports. For a highly efficient small antenna, the real part of its input impedance has to be close to the source impedance

(50Ω) while the imaginary part of its input impedance should be close to zero. Therefore, an effective design methodology has to have the capability of increasing the radiation resistance while keeping the reactance close to zero.

One advantage of the SIMT compared with other approaches for making small antennas (such as NIC circuits and meta materials) is that not only reactance compensation can be achieved in a wider bandwidth, but also it is possible to modulate and increase the real part (radiation resistance) of the input impedance. To make this concept more clear and show this capability of SIMT, the input impedance (real and imaginary parts) of the ESA described in the previous section (with a small change) is investigated under the SIMT and normal condition (the single feed antenna). This antenna is then fabricated which is depicted in Fig. 6.9.

For calculating the real and imaginary parts of the port impedances under the SIM condition, equations 3.6, 3.7, 3.10 and 3.11 described in section 3 are used. To illustrate the effect of the SIMT on the impedances of the ports, the intrinsic impedance of the single feed antenna is also illustrated. For this purpose two separated figures are provided to investigate reactance compensation and resistance modulation. The φ are set to their optimum values so that the SIM antenna is well matched close to 0.75 GHz.

Fig. 6.5 illustrates the real part of the impedances for the single feed antenna and for both ports of the SIM antenna. The blue curve (square marked) is the resistance of the single feed antenna at its input port and it is relativley small compared with the source impedance (50Ω). This behaviour is expected as the illustrated frequency band is much lower than the intrinsic resonance of the single feed antenna. The small resistance of the single feed antenna at its input port is one of the main reasons for small total efficiency of this antenna as depicted in Fig 6.2.

The green (triangle marked) and the red (circle marked) in Fig. 6.5 are the real parts of the impedances of the two port simultaneous injection matched antenna. It shows that under the injection matching the real part of the impedances are significantly increased and it reaches to the source impedance 50Ω at 0.75 GHz, the centre frequency of the SIM

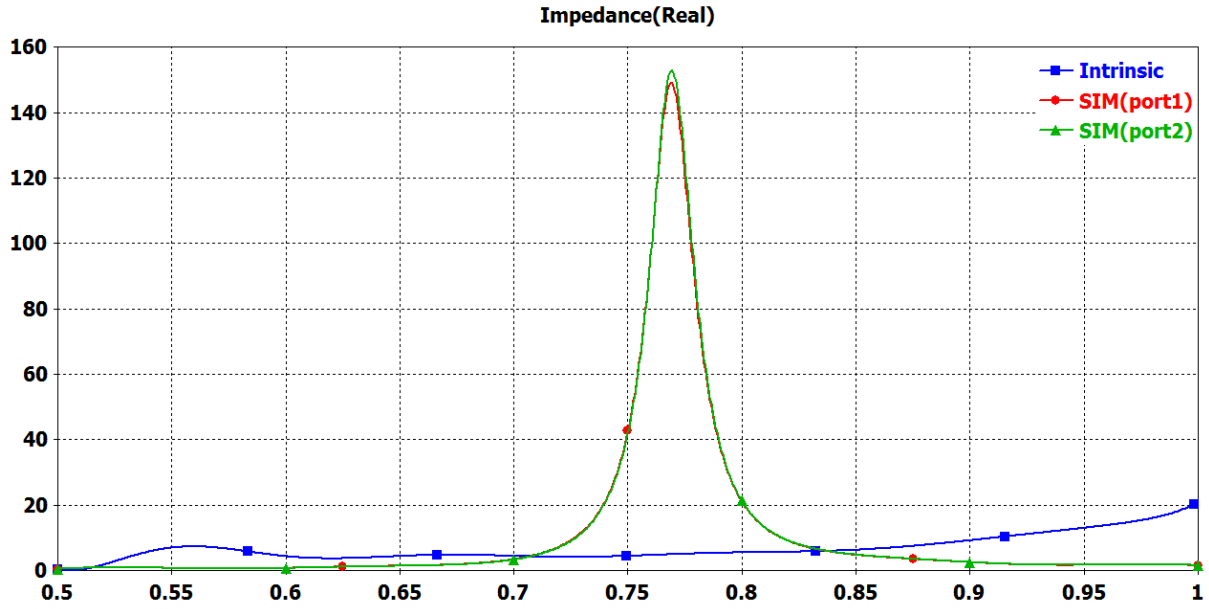

Figure 6.5: The real part of the impedance for the both ports of the SIM antenna and for the single feed antenna

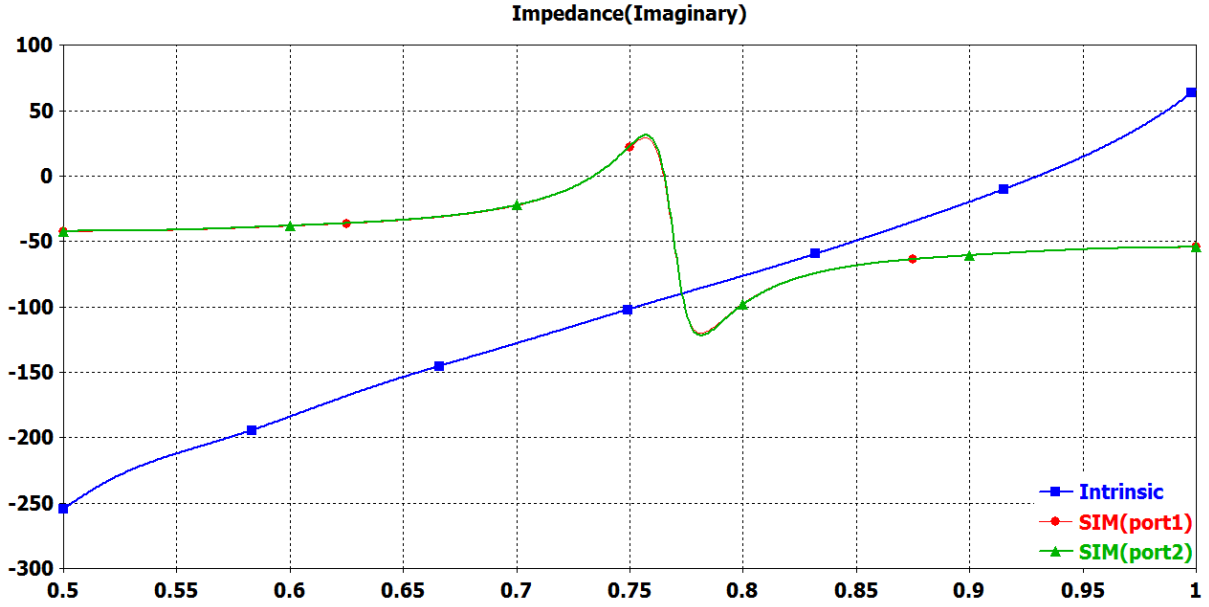

Figure 6.6: The imaginary part of the impedance for the both ports of the SIM antenna and for the single feed antenna

antenna (see Fig.6.1 (b)).

Fig. 6.6 shows the reactances for the single feed antenna and for both ports of the SIM antenna. The blue curve (square marked) is the reactance of the single feed antenna at its input port. At the centre frequency of the SIM antenna (at 0.75 GHz) the reactance

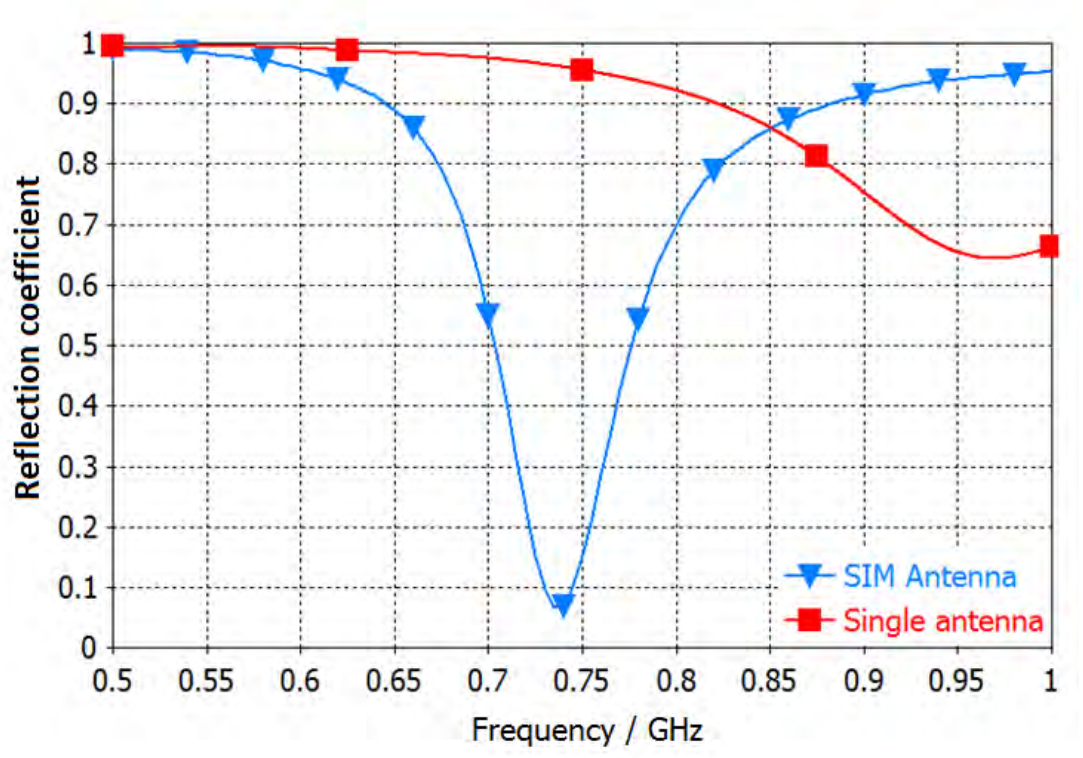

Figure 6.7: Reflection coefficient single port and equivalent reflection coefficient

of the single port is much smaller than zero (-100Ω) which is a reason for the small total efficiency of this antenna as depicted in Fig. 6.2.

The green (triangle marked) and the red (circle marked) in Fig. 6.6 are the reactance of the two port simultaneous injection matched antenna. It shows that under the injection matching the reactances of both ports, are significantly reduced and it reaches zero close to the centre frequency of the SIM antenna (at 0.75 GHz) (see Fig.6.1 (b)).

Consequently, as the SIM antenna has much larger radiation resistance compared with the single feed antenna, and a reactance close to zero, the efficiency reaches almost 90 % as illustrated in Fig. 6.3.

6.4.1 Matching and efficiency

In order to have a better insight into how the SIM works for the chassis antenna and what is the minimum achievable ka (reducing the operating frequency while keeping the size unchanged), the matching and the efficiency of the single feed and SIM chassis are

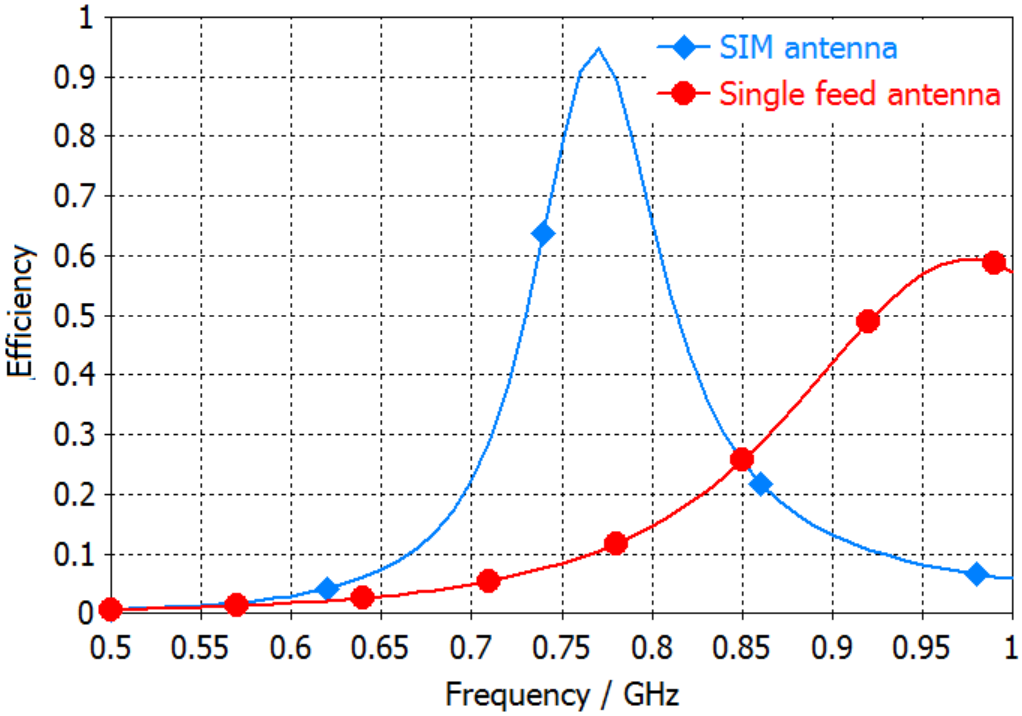

Figure 6.8: The total efficiency of the SIM and single feed antenna over frequency

illustrated over the band of interest in Figs. 6.7 and 6.8, respectively. To be able to perform SIM operation on the chassis antenna, some current has to be injected into the antenna structure. This cannot be achieved in the frequency range where the single feed antenna is purely reactive. This is the case at frequencies where the single port antenna's reflection coefficient is 1 in Fig. 6.7. The SIM operation can be achieved for the frequencies where the single feed antenna matching curve (initial matching), starts to deviate form 1. An example of a possible SIM operating band for the described chassis antenna is shown in Fig. 6.7 via the triangle marked curve.

By comparing these two curves it is clear that the SIM operation is achieved where the red curve is slightly deviated from 1.

On the other hand, this fact can be investigated via the efficiencies of the single feed and SIM antenna as illustrated in Fig. 6.8. In this figure the red curve (circle marked) and the blue curve (square marked) illustrate the total efficiency for the single feed and SIM chassis antenna, respectively. The efficiency of the SIM antenna is raised dramatically and

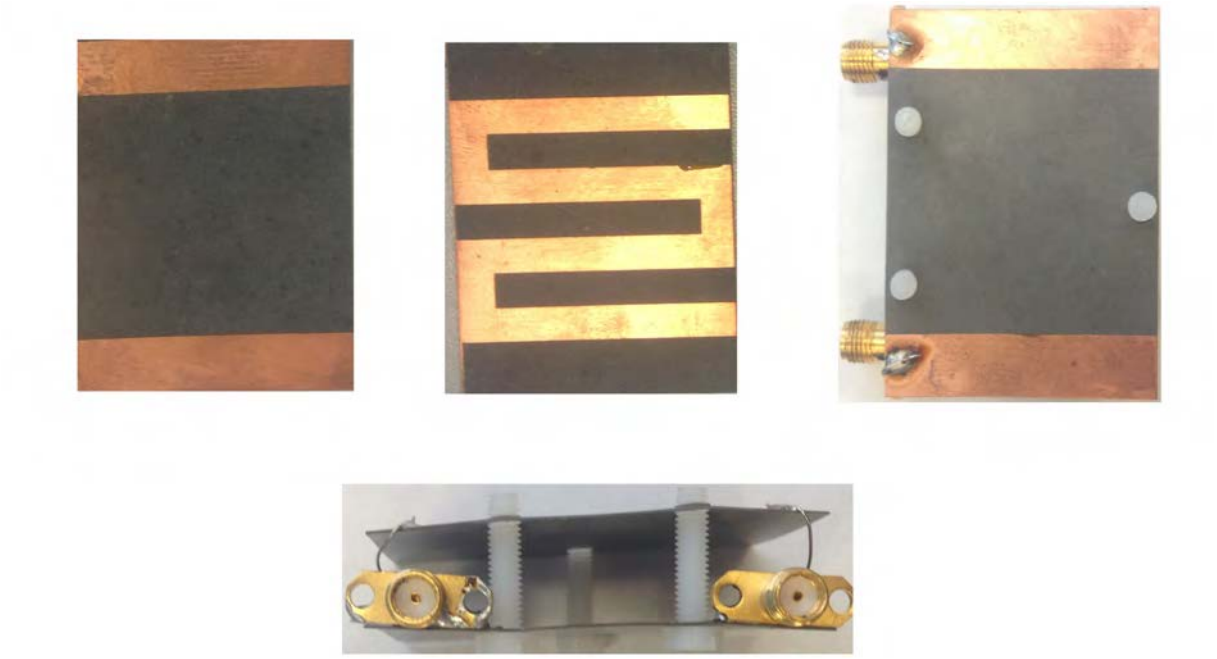

Figure 6.9: The practical implementation of the SIM antenna

reaches more than 90 percent, when the single feed efficiency starts to become greater than zero. Therefore, the efficiency of the single feed antenna is improved by almost 80 percent under the SIM while the size is maintained the same.

6.5 Practical measurement

To validate the potential of the proposed theory for making ESAs, the simultaneous injection matched electrically small chassis antenna is fabricated and its properties are experimentally investigated. For the measurements, the true differential mode of the ZVA67 is used as described in Chapter 5. Herein, the matching and the radiation characteristics of the SIM small antenna is practically measured and discussed.

6.5.1 Fabrication process

In order to fabricate the chassis antenna and to ease this process, the antenna elements (made from copper) are printed on two 35mmx40mm substrate sheets. These sheets are

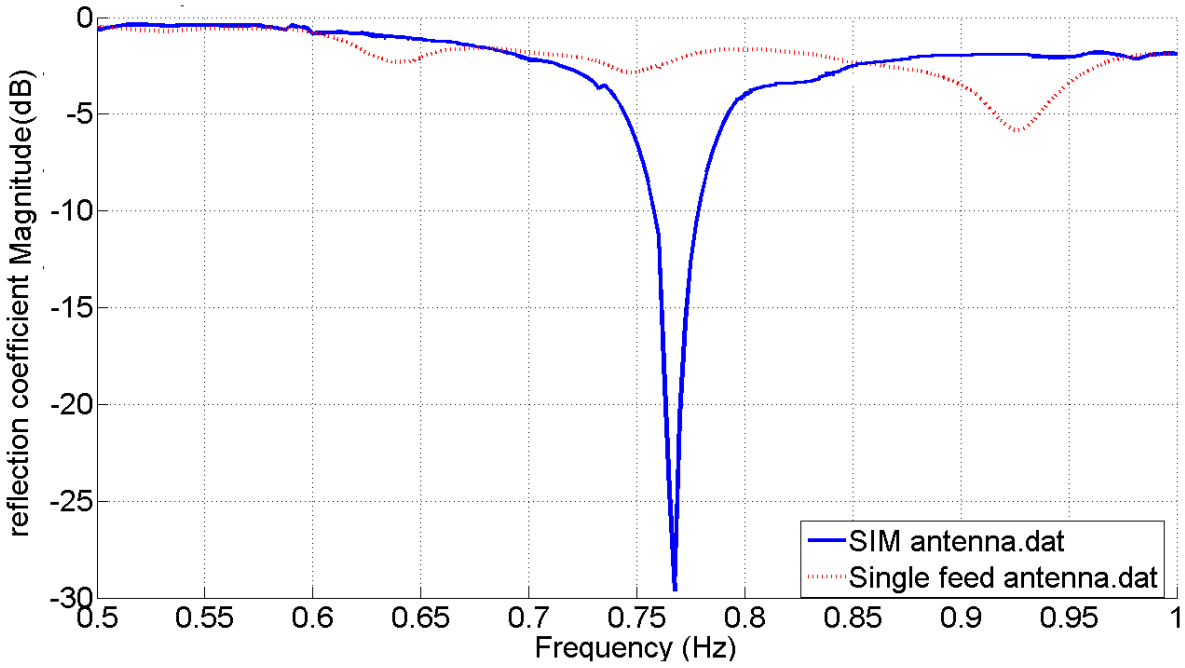

Figure 6.10: The reflection measurement for the single feed and SIM antenna

separated from each other via three nylon screws. The top layer consists of two coupling elements which couples the signal coming out of the SMA pins. The other layer consists of the meander line which is connected to the ground at both ends via the copper mesh of the SMA feeds. Then the two SMA terminations are connected to the ZVA67 ports. Fig. 6.9 illustrates the fabricated antenna.

6.5.2 Matching

To investigate the effect of SIMT on the ESA chassis, the matching is measured when only one port is excited and also when both ports are excited under the SIM condition. For this purpose the true differential mode of the ZVA is used. The measured reflection coefficients are illustrated in Fig. 6.10. The dotted curve illustrates the single feed matching which suffers from poor matching at the considered frequency range. The solid blue curve illustrates the Γ_{e2} for the SIM antenna which shows a resonance close to 0.75 GHz as was expected from the simulation results. The simulation and measurement results for the SIM antenna are in good agreement and both illustrate a resonance close to 0.75 GHz

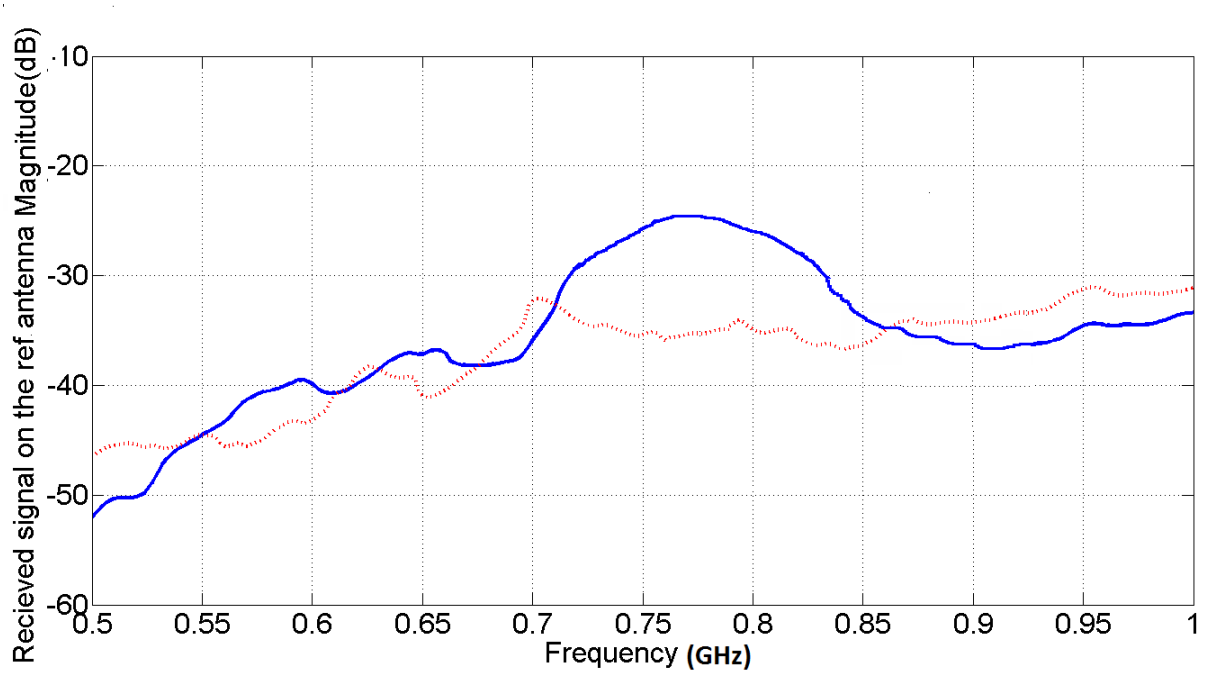

Figure 6.11: The radiation measurement for the single feed and SIM antenna

which can validate the theory.

6.5.3 Radiation

It is very important to confirm that the matching improvement in the experimental results will lead to radiation and not losses. Therefore, following the procedure presented in chapter 5 section 5.3 the following experiment is performed. For single feed antenna radiation measurement, two ports of the network analyser are activated and a wide band horn antenna is connected to the port 1 as a reference antenna. The single feed antenna is then connected to the port 2 and the the received signal is measured at the reference antenna while port two is in transmit mode (equivalent to S12). This is illustrated in the dotted curve in Fig. 6.11. In order to measure the radiation of the SIM antenna three ports of the analyser are activated in which port 1 is connected to the reference horn antenna and port 2 and 3 are used to feed the SIM antenna using true differential mode option. The total input power at both ports of the SIM antenna, are set to be equivalent to the input power of the single feed antenna. Then the recieved power from the SIM

antenna is illustrated via the solid line in Fig. 6.11. Therefore, by comparing the dotted and solid curve in Fig. 6.11 it is concluded that the SIM antenna is radiating 8dB more efficiently that the single feed antenna and this proves that the SIMT improves not only the matching but also the radiation.

6.6 Conclusion

Numerous approaches have been proposed for miniaturizing the size of the antennas. A typical method is to utilize active matching so that the antenna efficiency and bandwidth are no longer subjected to the Chu limit. However, the active components such as NICs suffer from instability at high frequencies. In this Chapter an electrically small chassis antenna is produced based on a two port configuration in which simultaneous matching can be achieved at both ports. This can lead to highly efficient and wide bandwidth electrically small antennas without stability limitations. The theory is then verified based on the circuit point of view. It was illustrated that the SIM not only can compensate for the reactive part of the input impedance but also it can increase the real part of the input impedance.

Chapter 7

Reconfigurable Chassis Simultaneous injection matched Antenna

7.1 Introduction

Reconfigurable antennas can add significant degrees of freedom and functionality to current communication systems. As an example, in mobile systems in which the demand for new frequency bands are growing fast, an antenna with frequency reconfiguration capability would be a great candidate to adapt the transmit and receive operation to this demand. In this chapter, the SIMT is investigated as a potential design methodology for frequency reconfigurable antennas for handset devices or other applications. The uniqueness of this design is that it offers wide tuning range and bandwidth of operation.

7.2 Reconfigurable SIM antenna

A common approach for making frequency reconfigurable antennas is to use a matching network with a varactor diode, at the feed point or on the structure of an antenna. Voltage alteration across the varactor diode results in a change in the value of the capacitance of the diode to tune the operating frequency of an antenna. One of the limiting factors

in this type of antennas is the tuning range, as it is limited by the available capacitance range of the varactor. A range of varactor diodes suitable for RF tuning is provided in appendix H

Various approaches, such as using multiple matching networks, have been suggested to increase the tuning range. The operational bandwidth is also limited for these antennas as tuning a wide bandwidth (multiple resonance) is challenging in practice as they need a number of varactors with their associated biasing circuits. To validate and investigate the potential of the SIMT for making reconfigurable antennas, a common design platform used in the handset antenna is chosen with minor modifications, and then the SIMT is used to improve its performance. Moreover, a chassis design is also developed and the SIMT is applied. To validate the result, the later design is fabricated and its performance is measured.

7.3 Methodology

The design goal is to have wide band width operation and wide range of tuning capability. In literature this is achieved by using multiple matching networks, each having multiple sections, which will increase the design complexity, losses and size [93, 94]. By combining the varactor tuning approach (matching network) and the injection matching concept this problem can be solved. In this way, just a single varactor plus an inductor are used to tune the resonance frequency, and the SIMT is used to improve and widen the matching at that resonance. Another significant advantage of SIMT for the handset and chassis antennas is that it can be used to detune the antenna when an object (like the user's hand) affects the matching and radiation. This can be done by simply changing the relative phase between the sources. To achieve these goals using the SIMT, the antenna design presented in the literature is modified such that it satisfies the requirements for proper SIMT operation. The modification is accomplished using the following procedure. As described in section 4, SIM operation requires some signal to be coupled in to the

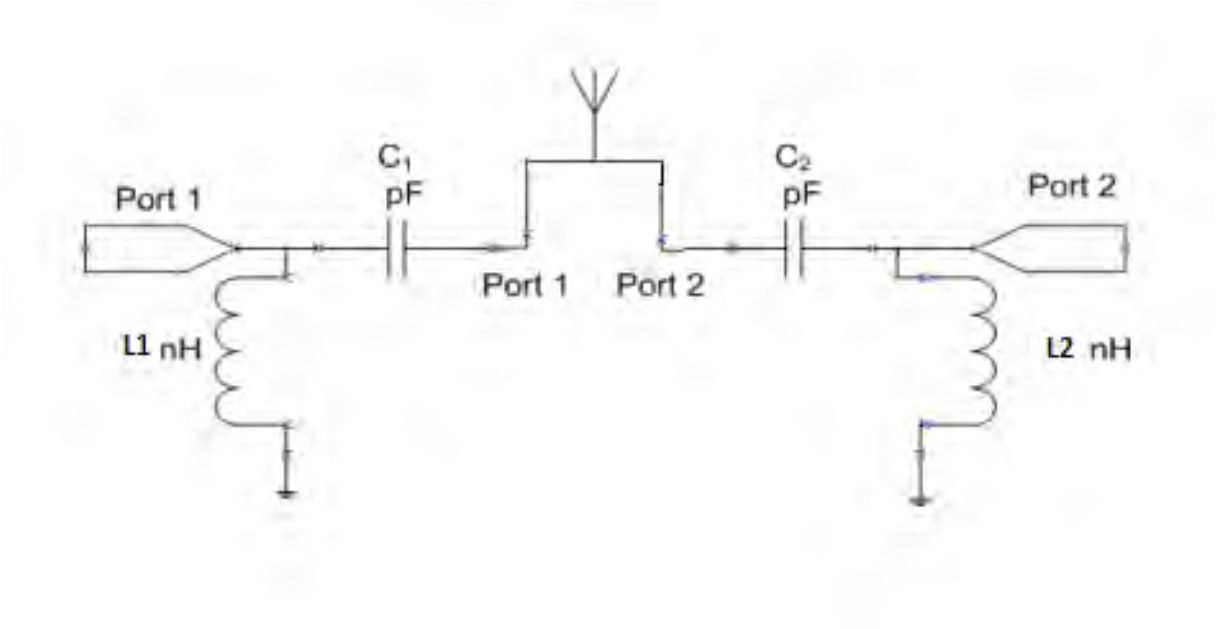

Figure 7.1: The configuration of the combined SIM varactor methodology

structure. Consequently, to have the widest tuning capability, the first port is introduced in to the structure where the lowest possible resonance is achieved, even if it is not good enough. Then the second port is introduced to the structure and its position is optimized such that the lowest achievable coupling between the ports is guaranteed (By trial and error it is understood that this condition can support wider bandwidth SIMT operation). Then one inductor and a varactor diode are located at the feed line of the antenna to tune the operating frequency as well as reducing the lowest possible achievable resonance (This will be expanded in section 7.3.1).

7.3.1 Design procedure

The goal here is to combine the varactor tuning approach and the SIMT tuning to get a wide tuning range with wide bandwidth of operation. To do so, the configuration illustrated in Fig.7.1 is proposed. In total, this approach can be accomplished via a minimum of two lumped elements as will be described.

As Fig.7.1 illustrates an, LC circuit including a varactor and an inductor is connected to the feeding points of the antenna. This configuration provides four parameters to

control the resonances at the ports. To have the potential of SIM operation there is a need of small degree of matching at the ports for the bands of interest. Therefore, the required initial matching can be provided via the proper values for C1, C2, L1, and L2. Once the vicinity of the desired resonance frequency is set by the values of the C1 and C2, the SIM operation can be accomplished to increase the bandwidth and improve the matching. In the normal varactor tuning antenna, as the resonance is getting far from the main resonance of the antenna due to the effect of tuning and varying the voltage across the varactor, the matching quality is reduced and -10 dB matching can not be met. Combining the SIM and varactor tuning techniques, brings two new variables γ and ϕ in which can significantly improve the matching and the bandwidth, when the resonance is far from the initial resonance due to the tuning or poor initial matching. Depending on the antenna structure and desired tuning band, C1 could be equal to C2 and L1 equal to L2. If this is the case, rather than using an LC circuit (C is the varactor) for each port (Fig. 7.1), one LC circuit can be shared for both ports.

It is also important to checked the initial tuning capability range that can be achieved with cooperating an LC circuit with the one port antenna (not under the SIMT operation). This should be checked for both ports. Therefore, at those frequencies the SIM operation will not be necessary. To have a clear and more generalized design procedure, for the optimum *combined varactor SIM operation* the following algorithm can be followed.

1. Choose the antenna structure desired to have reconfiguration capability(single port)

2. Find the feed point position for the single port antenna which leads to the widest initial matching even if it is not perfectly matched. (This means for instance 1 GHz bandwidth with S11 of -2dB is preferable to 0.5 GHz bandwidth with S11 of -10dB)

3. Introduce the second port of the antenna.

4. Find the position of the second port (via optimization or sweeping) such that it guarantees the lowest achievable coupling between the ports for the bands of interest.

5. Chose port 1 and set L1 such that it resonates with widest tuning range or at the desired band, with the available capacitance of the varactor diode. Frequencies with -10dB matching or better are called here as LC incorporated Port one resonance in the rest of this chapter.

6. Set L2=L1 and sweep the available capacitance range. (LC incorporated Port two resonance)

7. Keep C1=C2, monitor $|\Gamma_{e2}|$ and run sweeping with two sequences for C1 (available capacitance range with 10 samples) values and φ values every 36 degree. In total it would be (10*10) Γ_{e2} calculations.

8. If the tuning range and bandwidth is met, go to last step.

9. monitor $|\Gamma_{e2}|$ and run sweeping with three sequences for C1 and C2 (available capacitance range with 10 samples) values and φ values every 36°. In total it would be (10*10*10)

10. If the tuning range and bandwidth is met, go to last step.

11. monitor $|\Gamma_{e2}|$ and run sweeping with four sequences for C1 and C2 (available capacitance range with 10 samples) values and φ values every 36° and $\gamma = 1, 2, 3, 4$. In total it would be (10*10*10*4).

12. If the desired resonance and operating frequency in not in (LC incorporated) Port two resonance record the L1, L2, C1, C2, γ and φ.

This algorithm only needs a single full-wave 3-D simulation and there after just the faster circuit calculation is required. The most general way of using this technique is to run a sweep with five variables. When this is the case, the optimum way would be to use an optimization algorithm available in the simulation packages. However, in most cases, there is no need of five variables, and using 2 or 3 will lead to the desired result.

7.4 Examples of reconfigurable simultaneous injection matched antennas

7.4.1 One side feed chassis antenna

The first example is a chassis antenna in which two coupling elements are located at the bottom of the chassis to excite it. Ports one and two are connected to the longer and shorter coupling elements, respectively. The important parameter for having optimum SIM operation is the separation between the coupling elements, the separation between the ports and their distance to the chassis. To set these parameters the procedure described in the methodology section is followed. The geometry of the chassis and the feeding elements are shown in Fig. 7.2.

The goal of this example is to show how the SIMT can improve the tuning range and the bandwidth. For this purpose firstly, each port of the two port antenna is investigated separately to check the initial tuning potential of the antenna. Consequently, an LC circuit, with L=10 nH, is connected to the first and second port separately and the matching of these ports are monitored when C is changed from 0.2 pF to 18 pF while keeping L constant. These results are illustrated in Figs. 7.3 and 7.4 for port 1 and port 2 respectively. From the figures it is concluded that with an LC circuit the only frequency bands which can be covered by LC incorporated port one and two excitation, in total are (1-1.4)GHz, (2.2-2.4)GHz and (4-4.8)GHz. For the rest of the frequencies the matching is not acceptable. Therefore as was described earlier, the SIMT can be used to improve and widen the matching at these frequencies. Fig. 7.5 illustrates $|\Gamma_{e2}|$ for the combined SIM and varactor technique. Using this technique not only a very wide tuning range from (0.7-5) GHz is achieved, but also the bandwidth of operation is improved. In this example the design procedure is followed up to step 9. Therefore, a better result is also achievable if further steps have been taken. The results also can be improved if more samples are taken specially for φ.

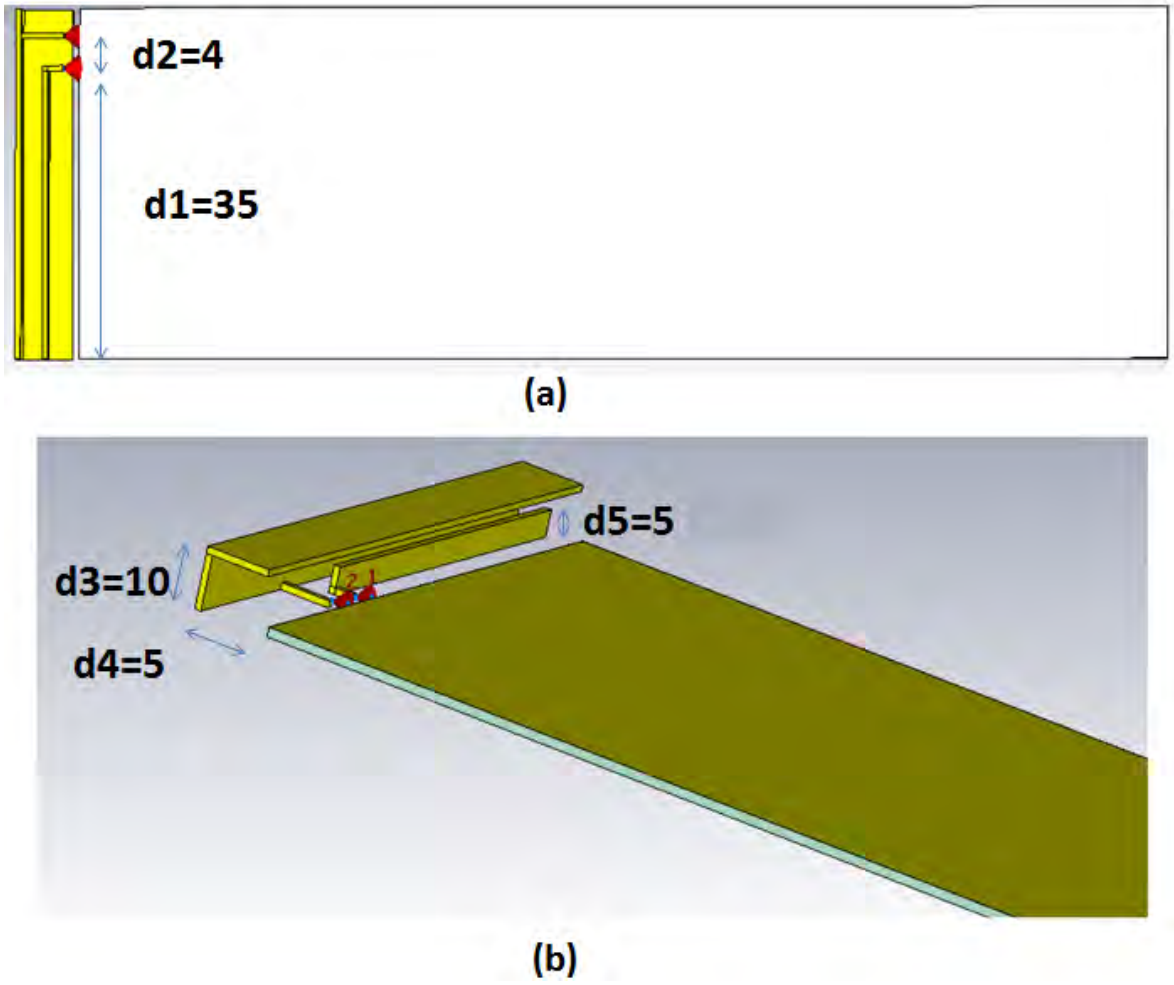

Figure 7.2: The antenna geometry and dimensions (a) plane view (b) 3D view

Previously, to cover a band from 0.7-2.5 GHz with much smaller band width and the same antenna size, 45 switched and lumped elements have been used [93, 94]. But here with just two varactors and one inductor and using the SIM technique a much wider tuning rage (almost twice) and much wider bandwidth for each band of operation is achieved. An approach for incorporating the LC circuit to the antenna is illustrated in Fig. 7.6. This will not increase the overall size. The coax pin is connected to the input of the LC circuit and via a wire, the output of the LC circuit is connected to the coupling element.

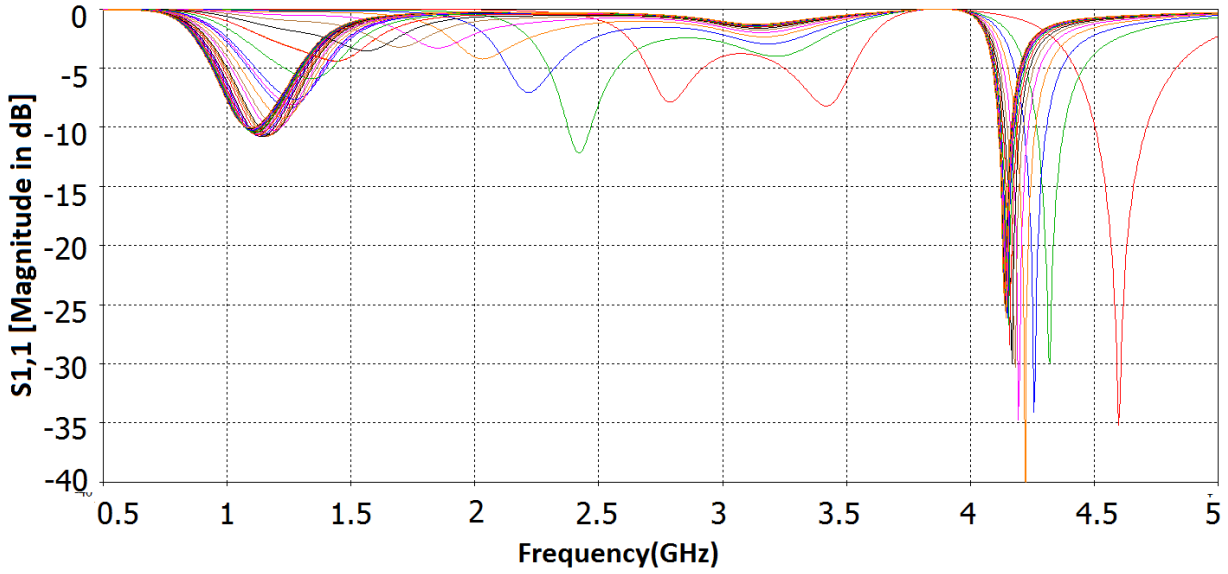

Figure 7.3: The Matching for port one of the single feed antenna incorporated with an LC circuit, L=10 nH while C is changed from 0.2 pF to 18 pF

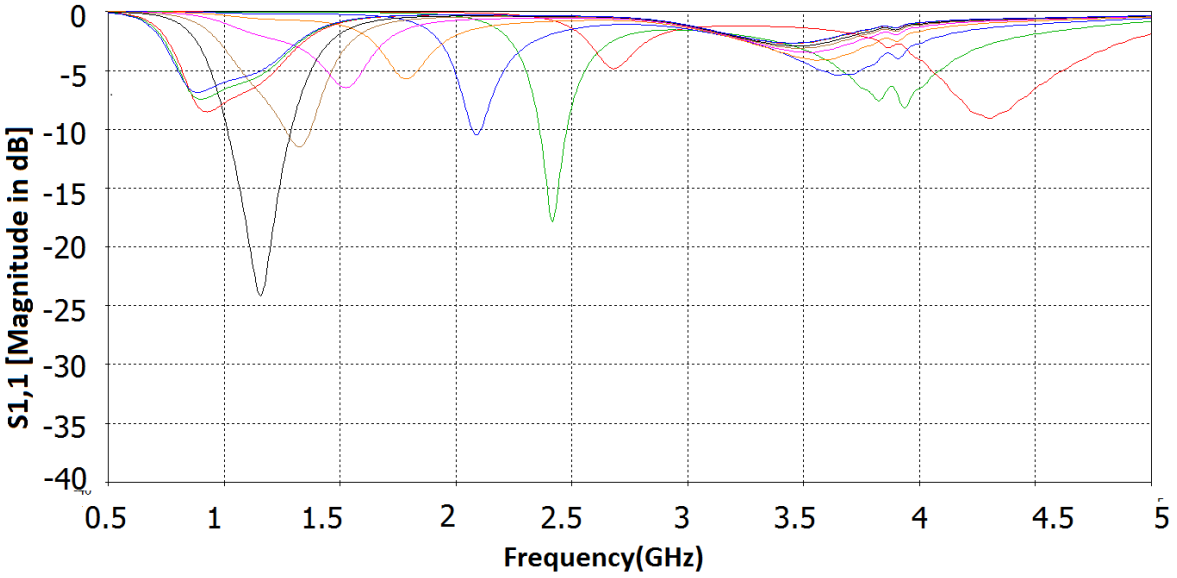

Figure 7.4: The Matching for port two of the single feed antenna incorporated with an LC circuit, L=10 nH while C is changed from 0.2 pF to 18 pF

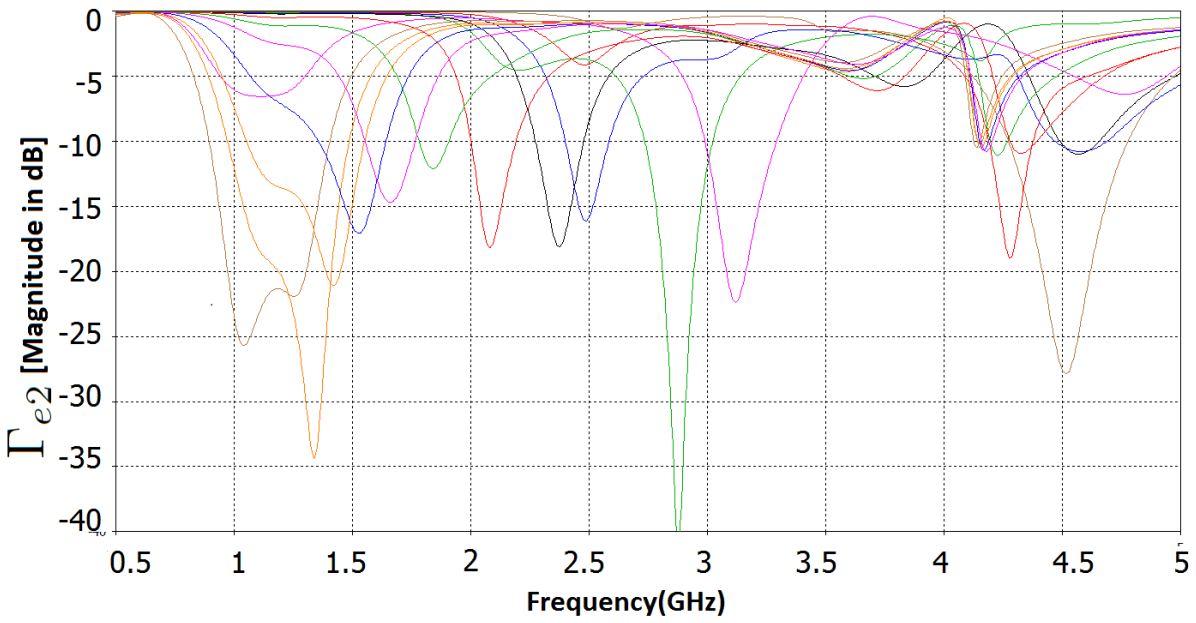

Figure 7.5: The Matching under the SIM condition for single sided feed antenna incorporated with LC circuit, L=10 nH while C is changed from 0.2 pF to 18 pF

7.4.2 Double sided feed chassis antenna

The second example has the same chassis size. However the coupling is changed such that, the tuning can be achieved via only 2 elements including an inductor and a varactor (up to step 7 of the design procedure). The inductance which is used here is 12 nH and the capacitance is varied from 0.1-18 pF . Moreover, this structure is designed such that it is much easier to fabricate. Fig 7.7 illustrates the geometry of this antenna. The dimensions of the coupling elements are 5mm x 20mm and they are placed 10mm above the chassis. Following the design procedure, the position of the ports are chosen such that they lead to the widest possible tuning range. Fig 7.8 shows the result of the matching of the antenna under the SIM condition while Fig 7.9 illustrates LC incorporated port one tuning when the capacitance is varied from 0.1-18 pF. By comparing these two figures it is clear that with one port tuning the bands which can be covered are 1.2-1.5 GHz and 3-4 GHz while

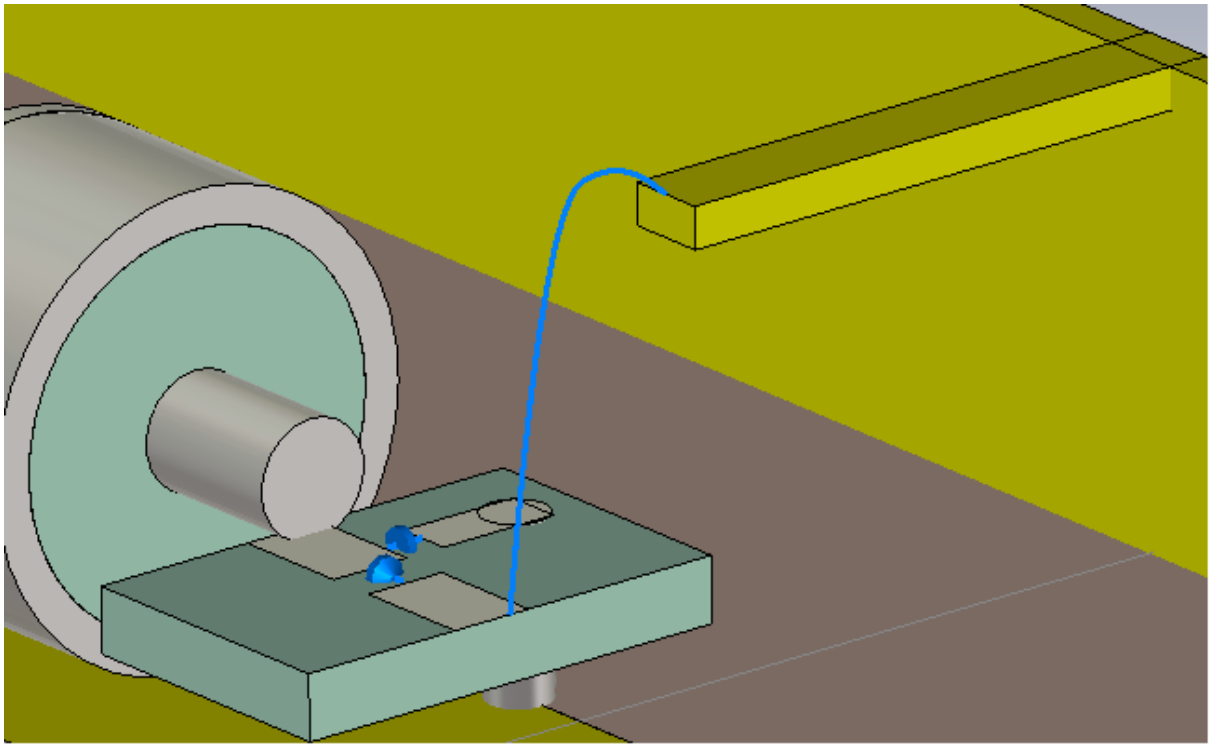

Figure 7.6: An approach for practical fabrication of the SIM antenna with the presence of the LC circuit

under the SIM condition the range of 0.7-5 GHz can be covered with even a wider band width of operation at each tuned band.

As discussed earlier, lower initial coupling between the ports is preferable for SIM operation and herein more distance between the ports can help to achieve this requirement. Therefore, the chassis is being excited from two sides to reduce the initial coupling between the ports at the very low frequency band (0.7-1 GHz) for possibility of SIM operation. If this band is not required, one side feed can be used and both ports can located on one side. This is shown in an example with the geometry illustrated in Fig 7.10. Fig 7.11 shows the matching of this example under the SIM operation when the capacitance is varied from 0.1-18 pF and L=12 nH. By comparing Fig 7.11 and Fig 7.8, it is clear that the double sided feed antenna can operate in lower frequencies (below 1 GHz) than the single sided due to the reason that was described. Moreover, it can be concluded that the position of the ports can affect the bandwidth and by comparing two resonances corresponding to the same capacitance value (the orange curve in both figures close to 2.5GHz), the -10 dB

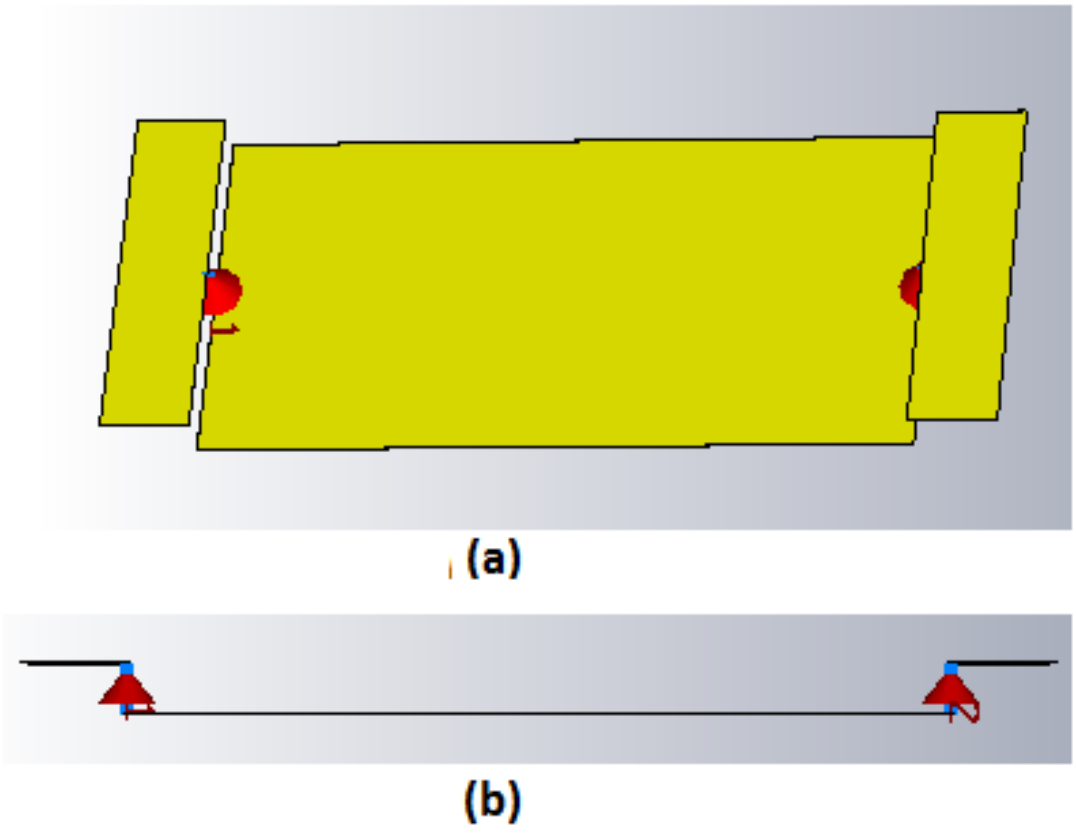

Figure 7.7: The geometry of the doubled sided feed SIM antenna (a) 3-D view and (b) side view

bandwidth is almost doubled in the second example. This gives an insight into how the band width of operation can be controlled by the relative position of the ports.

Experimental results

In order to validate the introduced approach this example is being fabricated. Figs 7.13 (a), (b) and (c) illustrate the SIM double sided fed antenna. Two thin substrate sheets are used to make the metallic chassis and the coupling elements. These two sheets are separated using Rohacell sheet with $\epsilon_r = 1$. Therefore, it will not affect the result.

The experimental result for the fabricated antennas is shown in Fig. 7.12. The solid cyan line shows the one port resonance of the antenna (S11) while the three marked curves illustrate the resonances under the SIM condition (Γ_{e2}). The SIM operation is performed at the frequencies where the natural matching of the antenna is not good (1-4 GHz). This

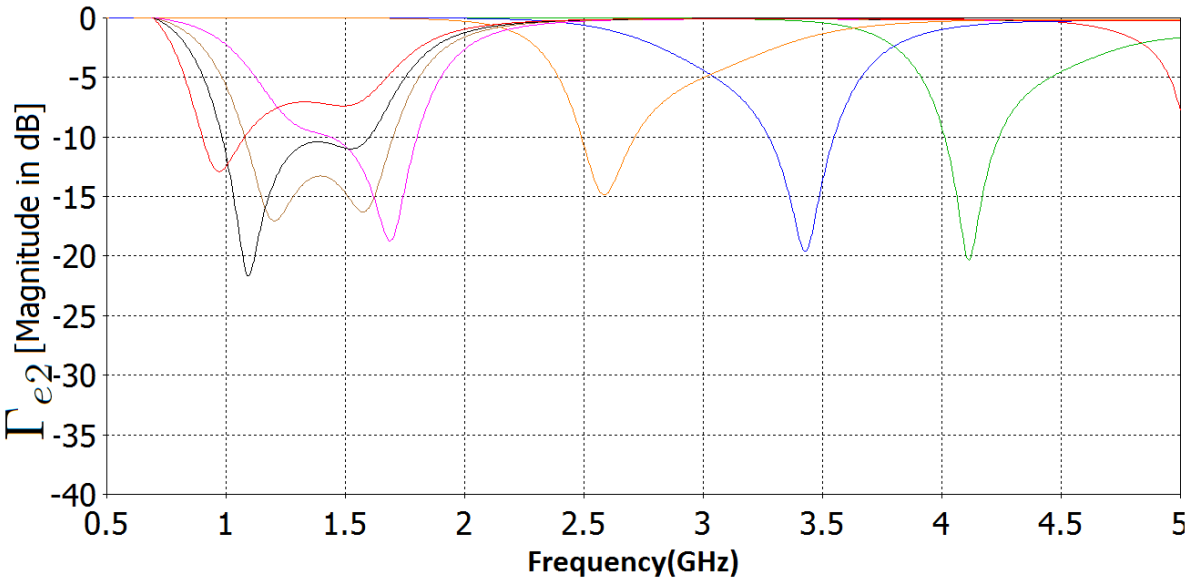

Figure 7.8: The Matching under the SIM condition for double sided feed antenna incorporated with LC circuit, L=12 nH while C is changed from 0.2 pF to 18 pF

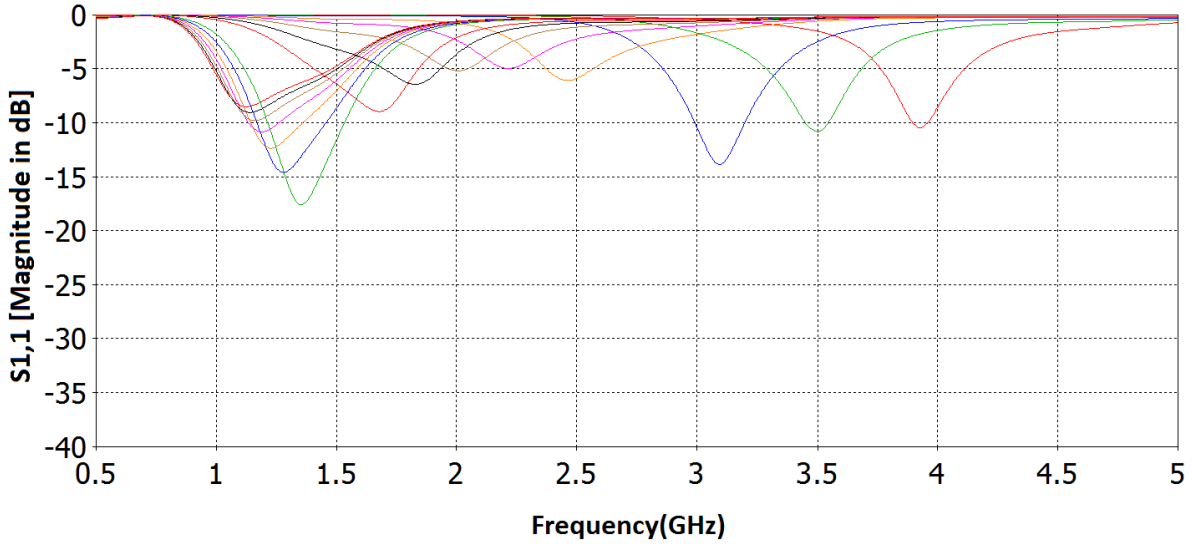

Figure 7.9: The matching for the single feed antenna

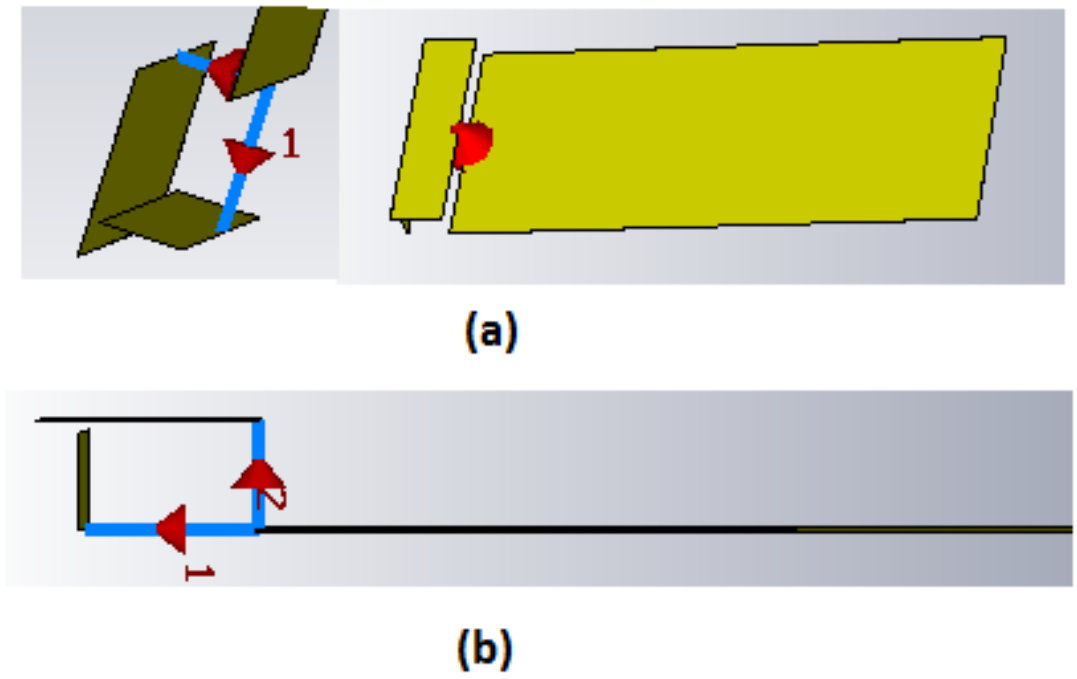

Figure 7.10: The geometry of the single sided feed SIM antenna that can share only one LC circuit (a) 3-D view and (b) side view

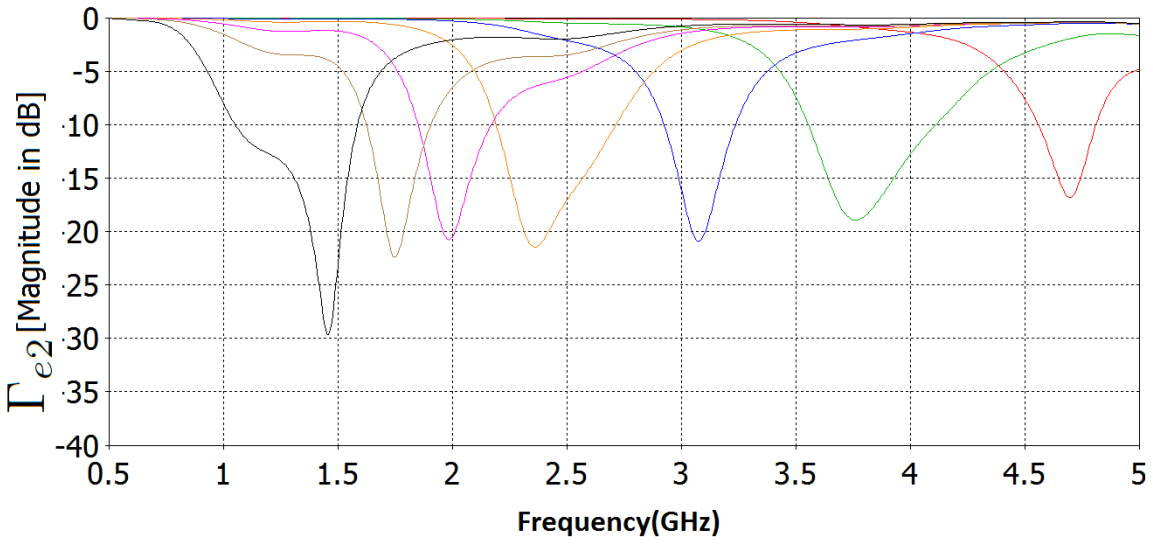

Figure 7.11: The Matching under the SIM condition for single sided feed antenna incorporated with LC circuit, L=12 nH while C is changed from 0.2 pF to 18 pF

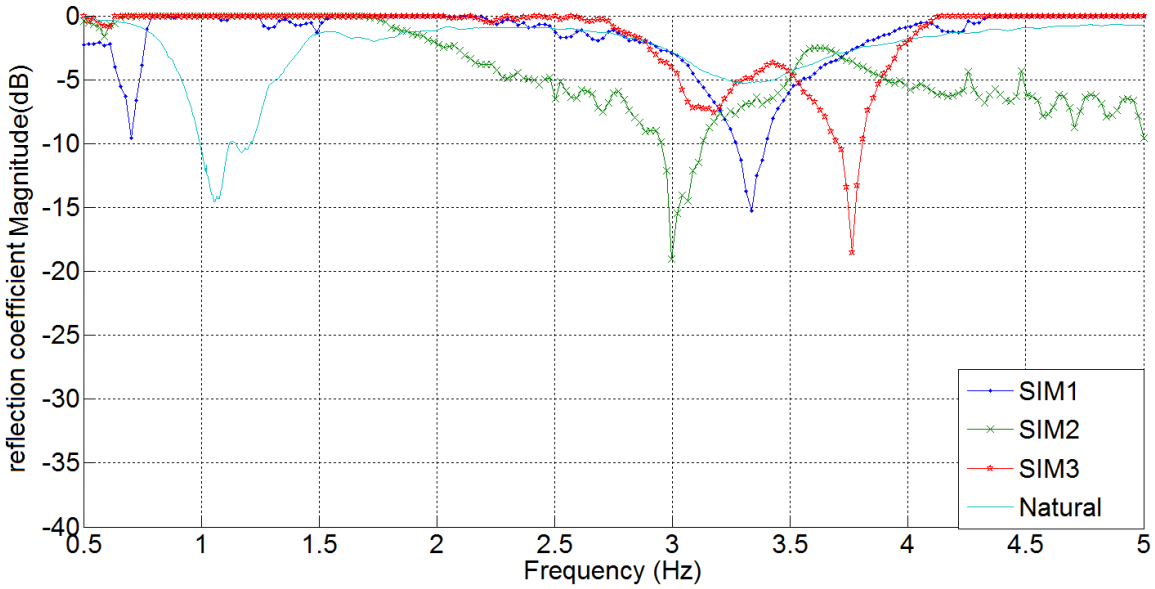

Figure 7.12: The measured data for matching under the SIM condition for and the natural resonance for the fabricated antenna

will validate the concept which was covered here. These are just three samples for the proof of concept and more samples could be taken to cover the whole band (1-5GHz). The radiation from the SIM antenna was covered and validated in previous chapters and therefore it is not discussed here.

7.5 Conclusion

In this chapter the potential of the SIMT for designing frequency reconfigurable antennas is discussed. For this propose the varactor tuning technique is combined with the SIM concept which results in a wide tuning range and wide bandwidth of operation. Then a design procedure is proposed for using this new concept and two examples are simulated and the results are verified. In the end for the validation of the theory one example is fabricated in which the measured results validate the concept.

The novel achievement introduced here is that the conventional varactor technique is combined with the SIMT concept to add at least one more degree of freedom, to increase the tuning range. In this fashion, for tuning the frequency, besides the variable

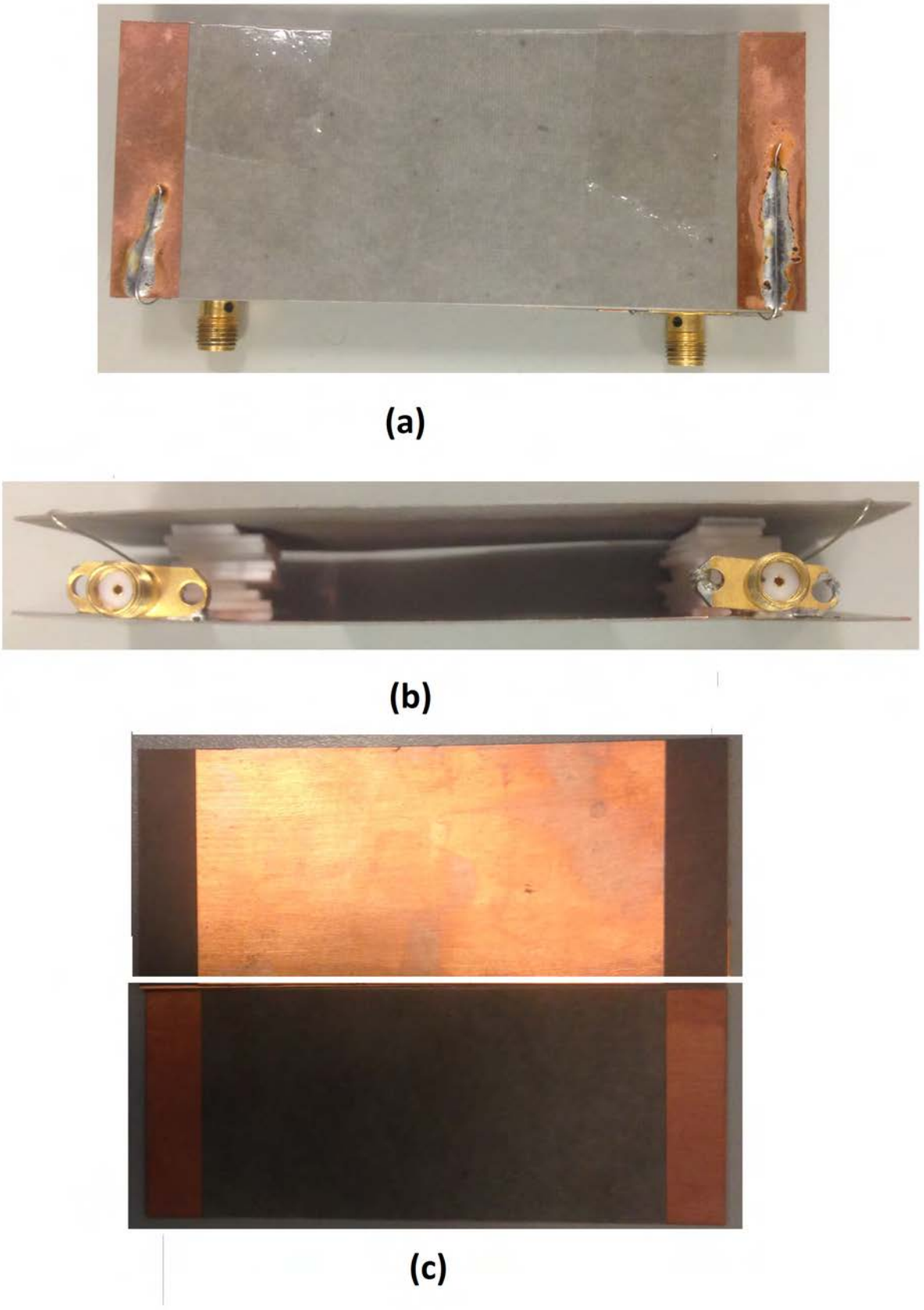

Figure 7.13: The fabricated two port SIM antenna

capacitance, the relative phase shift between the ports can be used. After applying this new technique, on a chassis antenna which uses only a varactor to tune the frequency, its overall tuning range bandwidth is improved significantly from 1.5GHz to 5.2GHz.

The purpose of this example was only to show how well the new concept can improve the bandwidth. However, if an antenna with a better initial tuning range was chosen, the overall tuning range could further improve. For further investigation, the relative amplitude of the ports can also be considered as another variable to tune the frequency.

Chapter 8

Conclusion

Nowadays mobile communication is an important and the most fast growing part of the telecommunication industry. On the top of conventional applications such as voice traffic, GPS, and paging, numerous new services have been added and this growth is expected to be continued.

The way people use mobile and wireless systems is affected by the societal development and therefore it regularly changes. The proliferation of indispensable services in our daily life, such as e-learning, e-banking and e-health will be continued. Entertainment and on-demand information will be also supported via mobile and wireless systems. These requirements and many others, will result in avalanche of mobile and wireless traffic volume and is predicted to grow steeply over the next decade [95, 96].

Moreover, it is expected that today's human centric communication system will be complemented with communicating machines in the close future. It is expected that 50 billion devices to get connected by 2020 to provide more efficient, convenient and safer every day life. This is known as the internet of things [97].

The coexistence of the machine and human in future communication system will open-up a vast range of new applications and communication characteristics. These new applications will impose very diverse requirements which need to be supported by the future evolution of the mobile network known as 5G. This system will need to be far more *fast,*

scalable, flexible and efficient. Therefore, high performance antennas are needed to address these requirements which need to be fitted within small mobile handsets. On the other hand, switched-off analogue communications provide an opportunity for re-using prime spectrum in UHF bands. Considering the size of hand-held devices, this will need aggressive miniaturization.

8.1 Solution for today's and future need

The main focus of the presented research in this thesis is to study and discover a methodology which could address the antenna's requirements that can be used in current and future mobile communication systems. For this purpose, a new theory called injection matching (IMT) is initially proposed in chapter 3 and complemented in chapter 4 as Simultaneous IMT (SIMT). This theory suggests a new way of controlling current distribution on the antenna structure that can be used to make wide-bandwidth, tunable, highly efficient and electrically small antennas. This is accomplished by the introduction of a second port to the antenna structure.

The theory is then verified over simulated and fabricated examples and validated via experimental data. This research shows significant advantages over other techniques which have been developed recently for the same proposes and therefore it opens up a new field of research.

The current and future requirements of mobile communication system and how well this thesis approached them are described in the following. For each of these requirement a practical chapter of this thesis is allocated to address and investigate these essential needs. This demonstrates the versatility of this thesis.

8.1.1 Faster service

To have faster service, antennas with wide-band width of operation are essential. However, due to small available size (compared with operating frequency) of the mobile devices, the

antennas are miniaturized and therefore suffer from poor matching.

In chapter 5, the proposed theory is applied on an antenna with poor initial matching and narrow bandwidth arises from its compact size. To improve the bandwidth of operation. From experimental data it is illustrated that the SIMT improves the initial -10 dB bandwidth by approximately 16% to 2.4:1 (130%). To achieve the equivalent bandwidth improvement with the conventional use of impedance matching networks, it was shown that, a minimum of three, 4-section matching networks are required which will make the antenna much bigger and lossy with a total of 21 lumped element components.

8.1.2 Highly efficient and miniaturized antennas

The heavily occupied mobile frequency bands create a demand to reuse the recently freed UHF bands used for analogue communication. This is a challenging demand as the handset dimensions limit the size and space available for the antenna design. The UHF wavelengths are much larger than the hand set devices and consequently miniaturization is required. On the other hand, limitations such as available battery life of a handset, requires the antenna to be highly efficient while being electrically small. This is the topic of chapter 6.

Numerous approaches have been suggested for miniaturizing the size of the antennas. A recently developed approach apart from using of Near Field Resonance Parasitic (NFRP) elements in which dispersion significantly limits the bandwidth, is to utilize active matching so that the antenna efficiency and bandwidth are no longer limited by the size. However, besides design complexity and fabrication losses, the active components such as NICs suffer from instability at high frequencies.

In Chapter 6, a highly miniaturized electrically small chassis antenna with $ka \simeq 0.67$ and $Q \simeq 1.6Q_{\text{Chu}}$ is produced based on the proposed theory. The theory is then verified based on the circuit point of view. It is illustrated that using the proposed technique not only can compensate for the reactive part of the input impedance but also it can increase the real part. It is then presented that via this technique, it is possible to improve the

overall efficiency of an electrically small antenna by almost 85 %. This can lead to highly efficient and wide bandwidth electrically small antennas without stability limitations.

8.1.3 Flexible

As the number of services and applications in mobile communications are growing dramatically, more than one antenna will be required to fully support these frequency bands allocated to various services and applications. To have a flexible service, there is a strong demand for antennas in which their frequency of operation can be tuned on demand. This can minimize the number of antennas required within a handset.

The frequency reconfiguration capability of this approach is illustrated in chapters 3 and 7. For this purpose the varactor tuning technique is combined with the SIMT concept which results in wide tuning range and wide bandwidth of operation. Then a design procedure is proposed in chapter 7 for using this new concept. Following this design procedure, a chassis antenna is designed which shows a tuning rage from 0.7 GHZ to 5 GHz. This is accomplished with the use of only 2 lumped elements including a varactor. To the best of our knowledge this tuning range with the use of only two lumped elements, has never been achieved before. This is because of the fact that in the developed technique two degrees of freedom are provided for tuning the frequency, by the varactor and the relative phase adjustment between the ports.

8.2 Further works

The influential outcomes and citations developed based on this thesis, promise that this work is likely to initiate a broad new research field. Moreover, an agile, efficient, highly miniaturized antenna can potentially fulfil a whole host of demanding applications for which no competing technology can offer solution.

The outcomes of this thesis are, a UK patent, an EPSRC proposal, an invited book chapter, and 8 publications in prestigious conferences and journals. Despite these influ-

ential outcomes, this thesis is just the starting point, and it opens up a newly discovered way of thinking. Therefore, there are still a great amount of ideas, opportunity and works that can be explored. Some of these ideas are illustrated in the following:

8.2.1 The theory and the limitation of the multi-port antenna

A significant step toward development and completion of the proposed theory is to formulate the radiation mechanism of an antenna under the forced excitation. This will provide opportunity to derive the fundamental limitations for such an antenna which can lead to an optimum and efficient design for a required application.

8.2.2 Pattern reconfigurability

In the next generation of mobile communication and with the introduction of small cells, there is strong demand for the use of pattern reconfigurable antennas. Such an antenna can increase the efficiency of the overall network by directing the pattern of the transmitter (receiver) toward the required location (source).

The proposed theory provides opportunity to have direct control on the current distribution and intuitively the pattern can be controlled. This can be achieved via controlling the relative phase, amplitude or positions of the ports. This was partially introduced in chapter 3 but has not been fully investigated due to the limited facilities available. There are many more variants that can be explored as the future work.

8.2.3 RF development of frequency dependent phase shifter and digital modulation

In the developed theory and examples, it was illustrated that changing relative phase between the ports can tune the frequency of operation and/or improve the initial matching. Via micro-control, it is possible to design a component with frequency dependent behaviour. In simpler words it can provide required phase-shift for a band of frequency.

If this could happen then it will be possible to provide the optimum phase shift that can lead to a good matching for various bands which can lead to overall significantly wide band width of operation.

It is shown that the injection matched antenna illustrates wide bandwidth of operation that is wide enough for modulation purposes. Further work is required on understanding the IM antenna performance in the context of digital modulation.

8.2.4 Closer to the limits

In this thesis, to ease fabrication and limited available technology, planar antennas were used to demonstrate the effectiveness of the developed theory and how well it can improve the required characteristics of the antenna. Therefore, these antennas were not a good candidate for demonstrating the maximum achievable performance. For instance, IMT applied to a volumetric antenna might allow the Q_{Chu} limit to be beaten.

Appendices

Appendix A

Different usage of multi-port configuration

In [98] an antenna is proposed which radiates and dissipate the incoming power in the common-mode and differential mode, respectively.

The structure is consisting of two lumped elements; a 100 Ohm resistor R which is used to absorb the differential-mode power and a capacitor C, for shifting the open-circuit-voltage standing wave, toward the location of the resistor in the antenna. The insets geometries are chosen such that they match the common-mode impedance of the coupled feed line. In the common-mode excitation, no current flows through the lumped elements and the spatially added input signals from the ports which leads to a current distribution similar to that of a conventional single port Microstrip patch with no gap. In differential-mode, an effective short-circuit is formed in the middle of the resistor and the capacitor. This will lead to a 50 Ohm resistor and a 2C capacitor to ground which is separated by a piece of transmission line(Fig. A.1 (a)). On the other hand, the center of the patch in the differential mode can be represented as short circuit, which is separated from the capacitor by another transmission line TL2. The equivalent circuit in the differential mode is presented in Fig. A.1 (b). In order to have the maximum power dissipation in the resistor, admittance YTL1 , the points where the resistor is attached, (see Fig.

A.1 (b)) should be zero. Hence, the dimensions and the values of the lumped elements are chosen so that the required admittance is achieved. The measured result shows a reflection coefficient of almost -20 dB in the operating frequency for both modes. The reflection coefficient for both modes are illustrated in Fig. A.1 (c). However, according to Fig. A.1 (d) it can be concluded that in the differential mode, the incoming power is deeply suppressed; while in common mode, a radiation pattern similar to single feed Microstrip antenna is shaped.

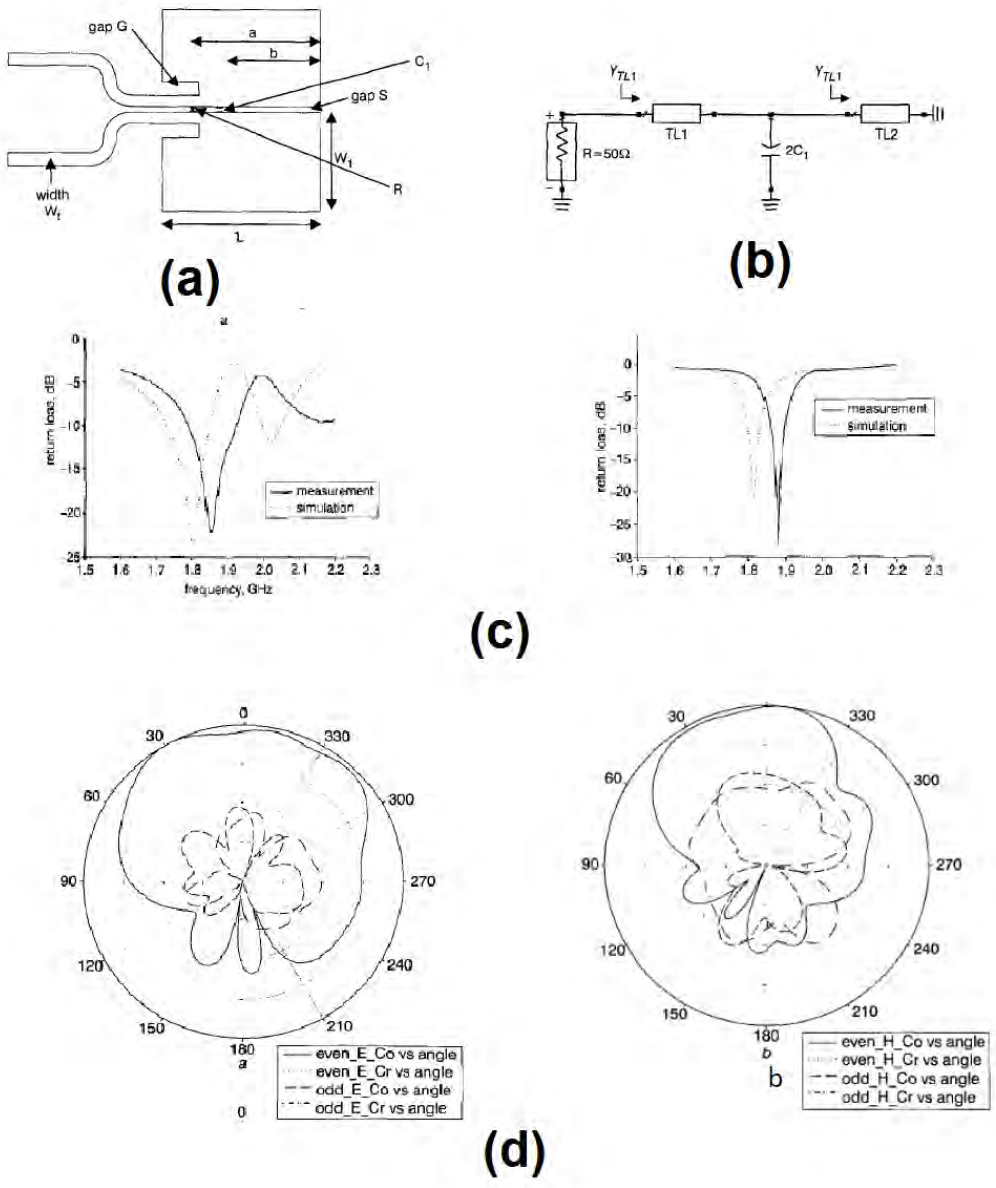

Figure A.1: (a) The geometry and (b) the equivalent circuit, (c) the reflection coefficient for even (right figure) and odd mode (left figure), (d)the E field for even and odd mode(left figure) and H field for even and odd mode (right figure) [98]

Appendix B

Different usage of multi-port configuration

In [99] a two port Microstrip patch antenna is presented. The proposed structure can be understood as the integration of a radiator and in-phase power divider/combiner with a high level isolation between the ports. The characteristics of the proposed antenna can be verified by considering half the patch once and the entire patch once. The dominant mode for radiation in the conventional rectangular patch is TM01. The first and second numbers after TM, illustrate the number of zero field intensity along the x-direction (width of the patch) and y-direction (length of the patch) respectively. In this mode, the two side edges behave as half wave length resonators, in which the maximum electric field intensity in y-direction occurs at both ends and the zero in the middle. In the x-direction the peak electric field remains constant. For the half patch analysis, the field distribution is distorted. It is concentrated on the left hand side in the y-direction and decays from maximum to almost zero in the x- direction. In this literature this is called the distorted TM01. The goal here is provide low coupling between the ports so that the ports can be used as power combiner/divider. This is provided at a specific frequency in which the TM01 is distorted and concentrated on one side of the structure. Fig. B.1 (a) illustrate the current distribution for the first three resonances when only the right handed port is

excited. The current distributions illustrate the TM10 and distorted TM01 and TM20 modes which occur at 2.3, 5.8 and 6.9 GHz respectively. In the distorted mode, when the entire patch is excited, the current is distributed mainly at the right side of the half patch, while for the TM10 and TM20 the current is distributed almost uniformly. In the distorted TM10 mode, the signals can be radiated effectively without serious power loss or leakage to the left hand port. As a result, port to port isolation is realizable. In comparison with two separated antenna (Fig. B.1 (b)), this technique shows lower coupling which makes it suitable for array application. This is illustrated in Fig. B.1 (c) The single feed matching, an the gain of the antenna is also illustrated in Fig. B.1 (d) which shows a good matching and high gain for the proposed antenna.

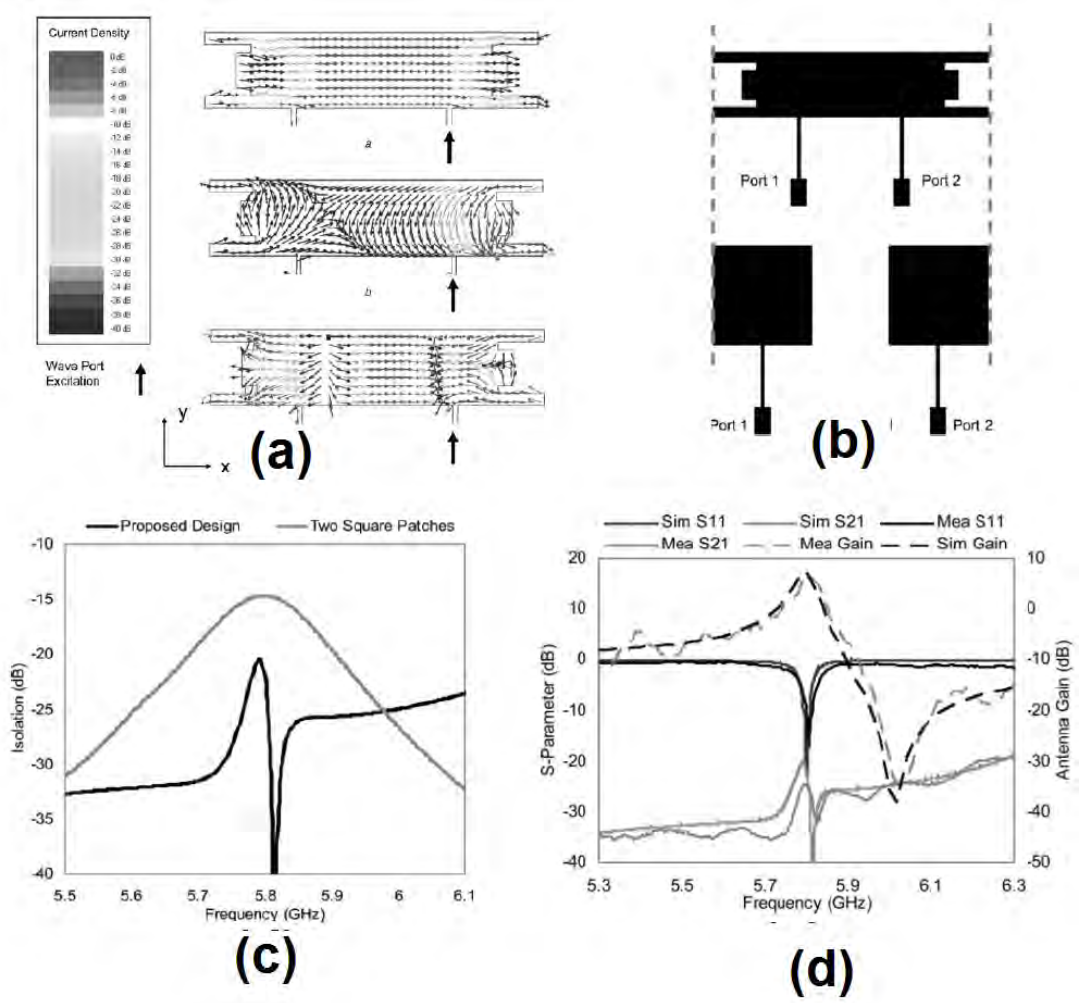

Figure B.1: the current path and electric field on the half patch an (b) the complete geometry of the proposed structure 11.(a)The measured and simulated result (b) the geometry of the connected and separated antenna (c) isolation of the separated and connected antenna (c) Current distribution for on the patch for TM10 , distorted TM01 and TM20 modes [99]

Appendix C

Return loss and insertion loss

When an electromagnetic wave enters a medium with different dielectric constant, part of it will pass and the rest will reflect. Reflection coefficient (Γ) is the ratio between the reflected wave and the incident wave while transmission coefficient (T) is the ratio of the transmitted power over the incident power.

When the travelling voltage signal in a transmission line meets impedance which differs from the line impedance the same situation will occur. The following equations illustrate the relations between the return loss (S11), insertion loss (S21) with the reflection and transmission coefficient. In practice these value are reported in negative form. In electrically small antenna design S11 below -6dB is considered as the operating frequency of the antenna [7].

$$S(1,1)_{dB} = 20log(|\Gamma|),$$

$$S(2,1)_{dB} = 10log(|T|),$$

Appendix D

CST and AWR software

CST transient solver is an EM simulator which is suitable for simulating field propagation through the structure. The simulation is performed by a fine frequency resolution signal which allows the users to derive the field results, with running only one simulation. Transient solver sends a quasi-impulse signal in the time domain and it calculates the desired measurements for the desired frequency range. Therefore it is much faster than frequency domain solver.

CST frequency domain solver like transient solver provides EM near field and far field as well as the S-parameter file. The advantage of frequency domain solver is that it is more suitable for electrically small structures and resonators. In frequency solver the structures is broken in to small pieces which are portions of the wave length. Therefore, in higher frequencies the structure is divided in to the smaller sections. Then the desired frequency range is sampled according to level of accuracy and the response of the structure is calculated for those frequencies. An example of frequency domain solver meshing is shown in Fig. D.1 [85, 100].

It is worth mentioning that AWR uses circuit analysis such as ABCD parameters which makes it suitable for the continuous structures. Consequently it would be much faster than CST with acceptable accuracy [100].

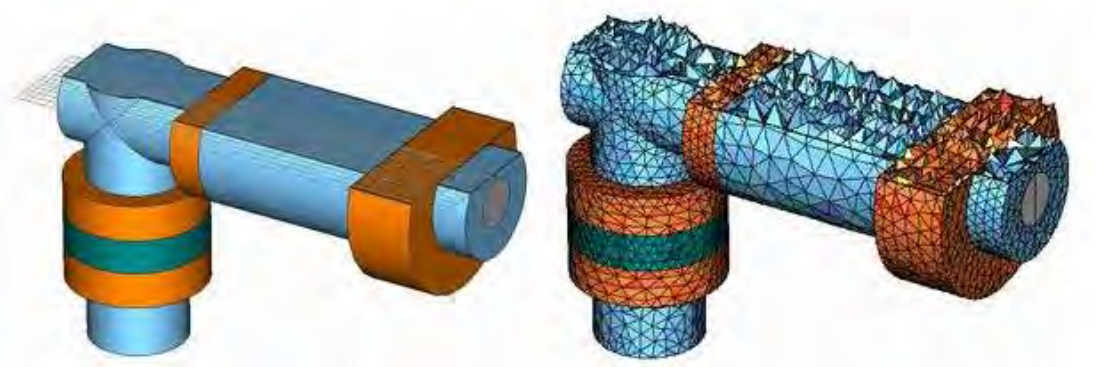

Figure D.1: An example of meshing in frequency domain solver [85]

Appendix E

The vector modulator

The important data for driving the vector modulator is provided in this appendix. Complete data sheet is available in [101]

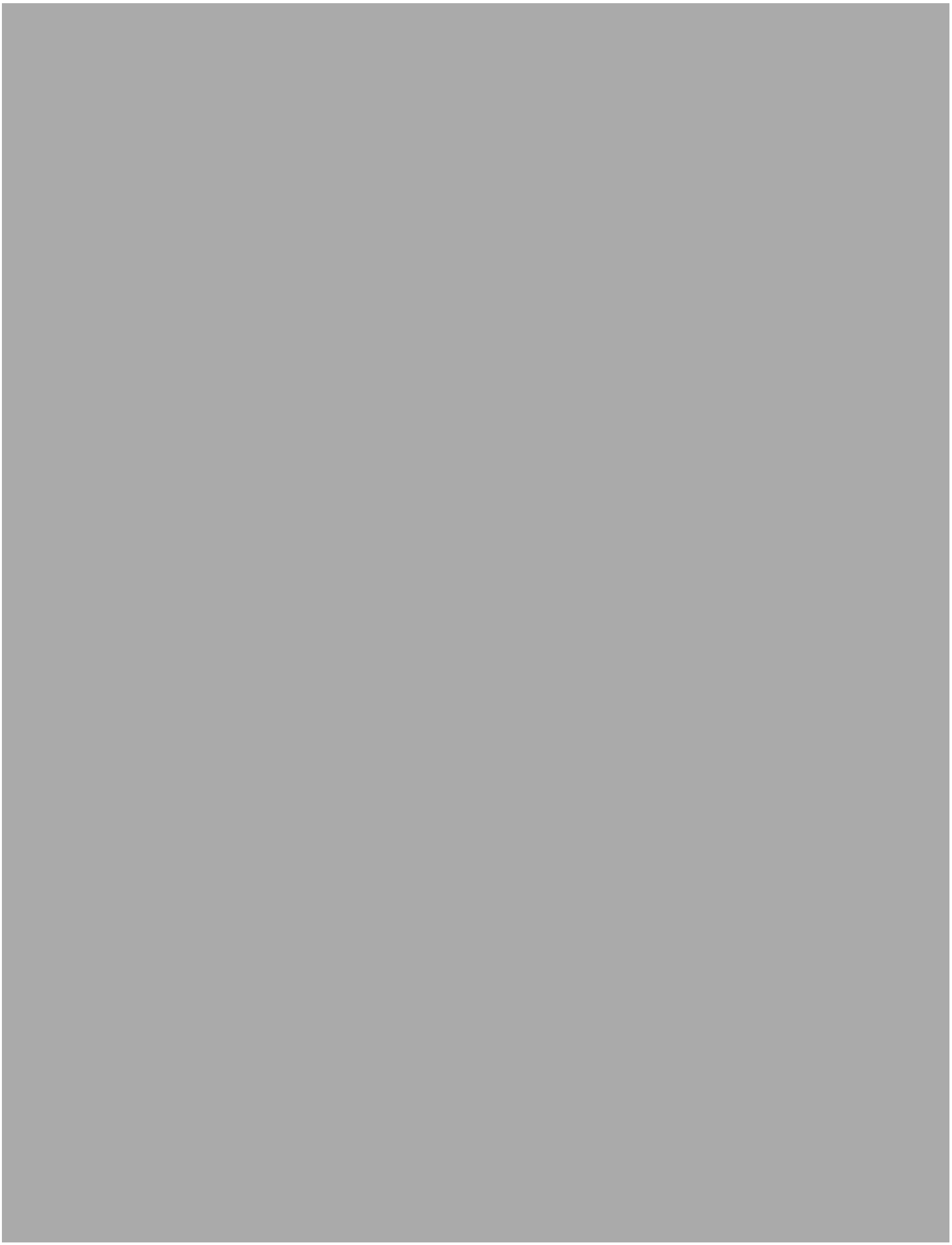

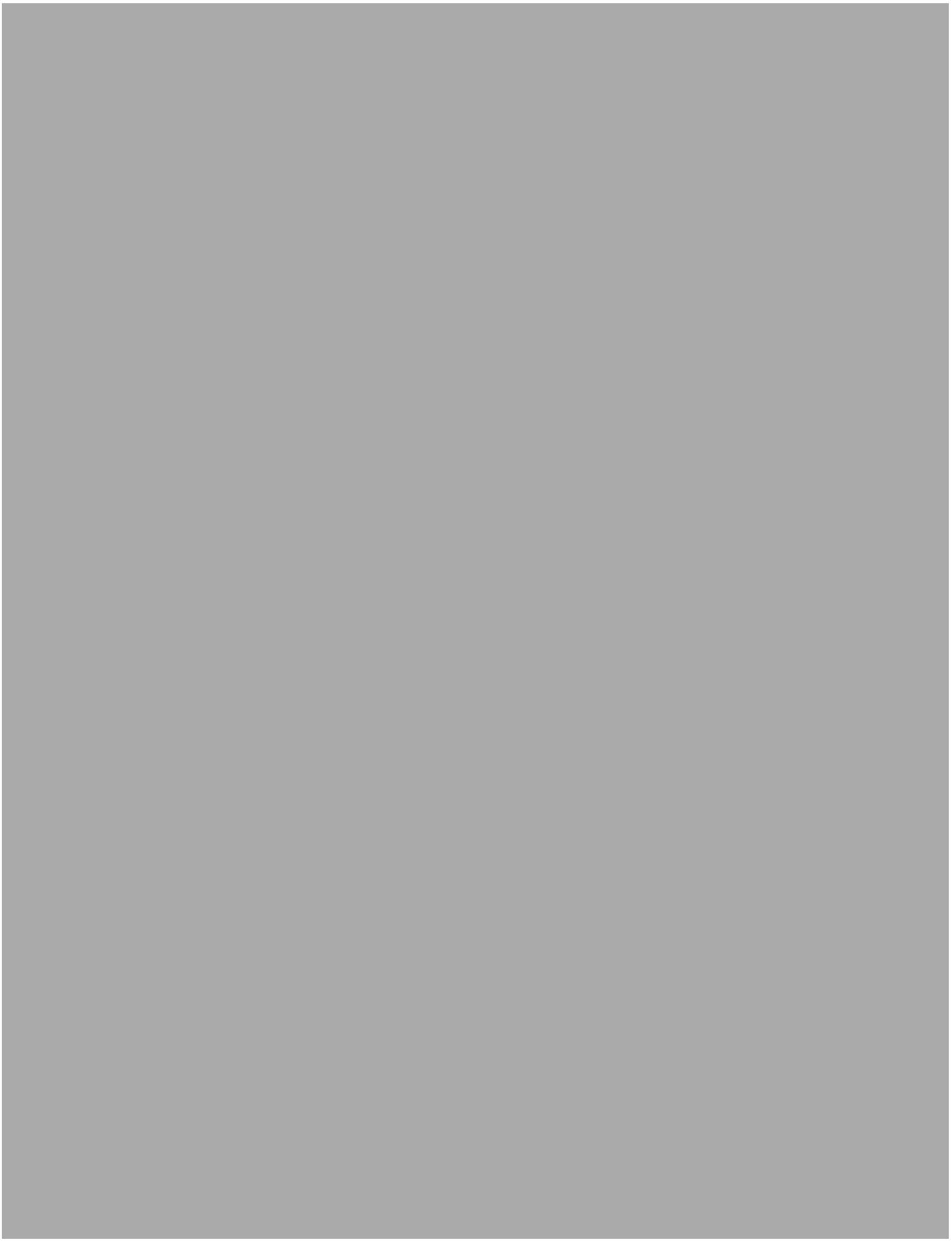

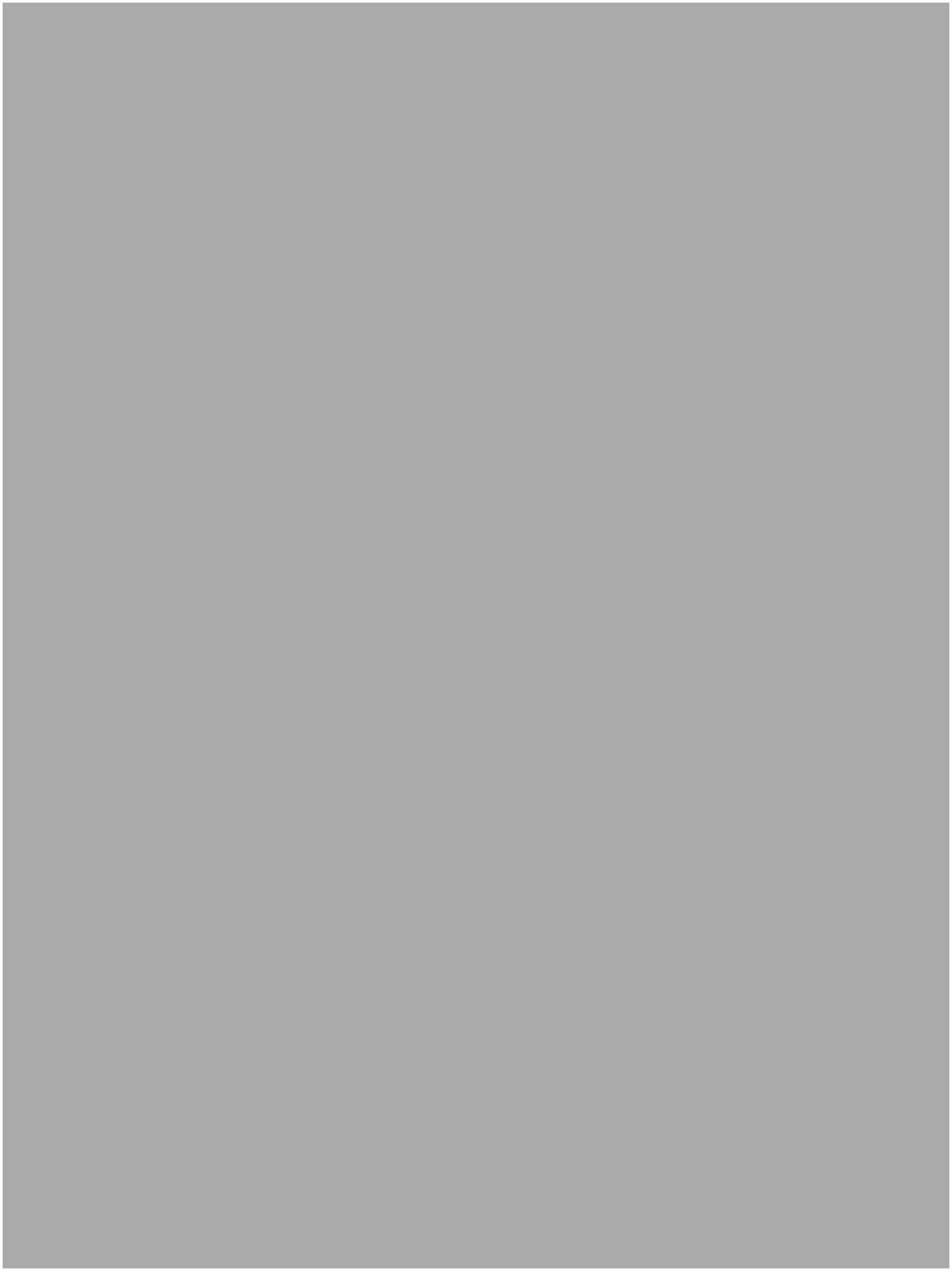

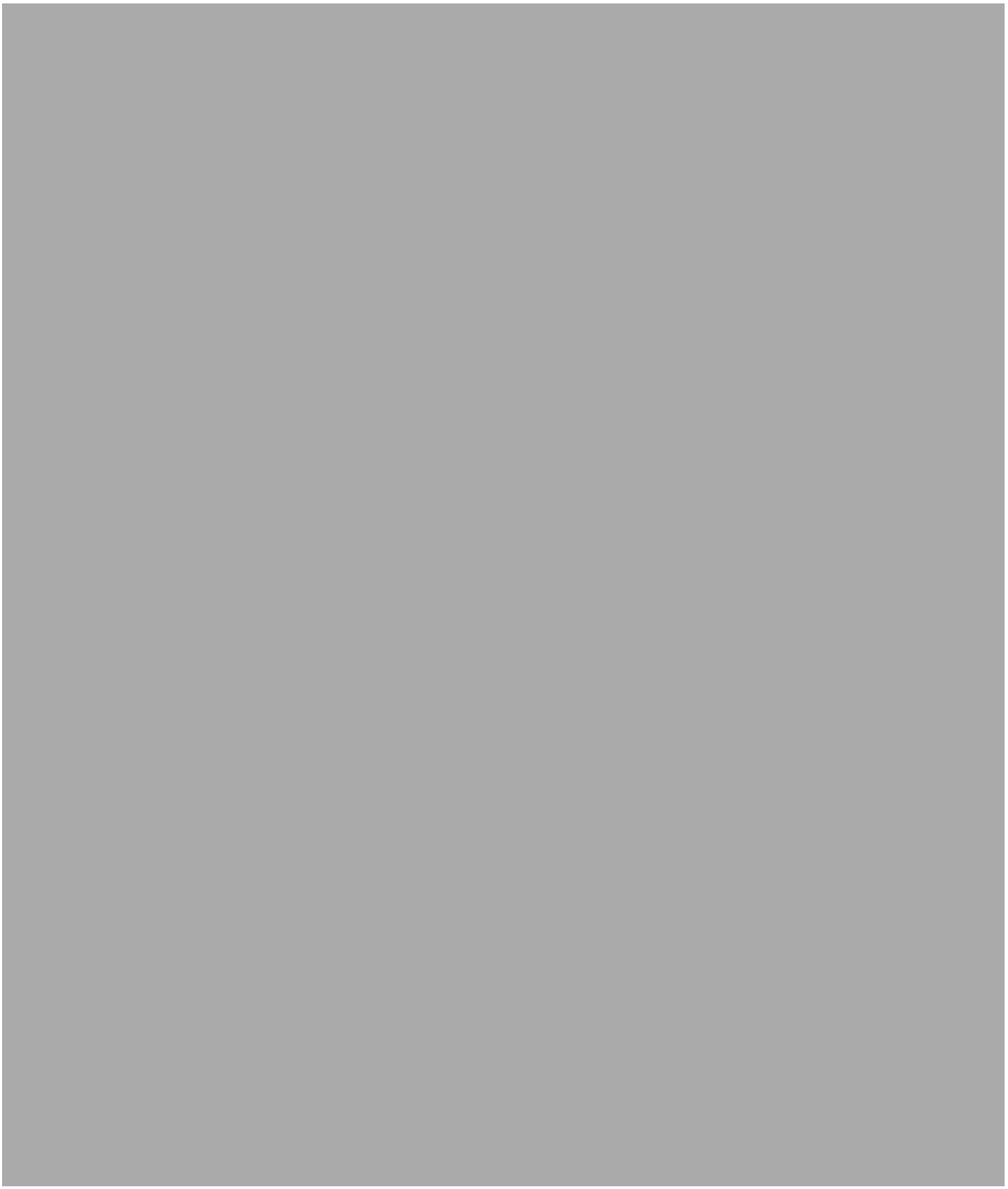

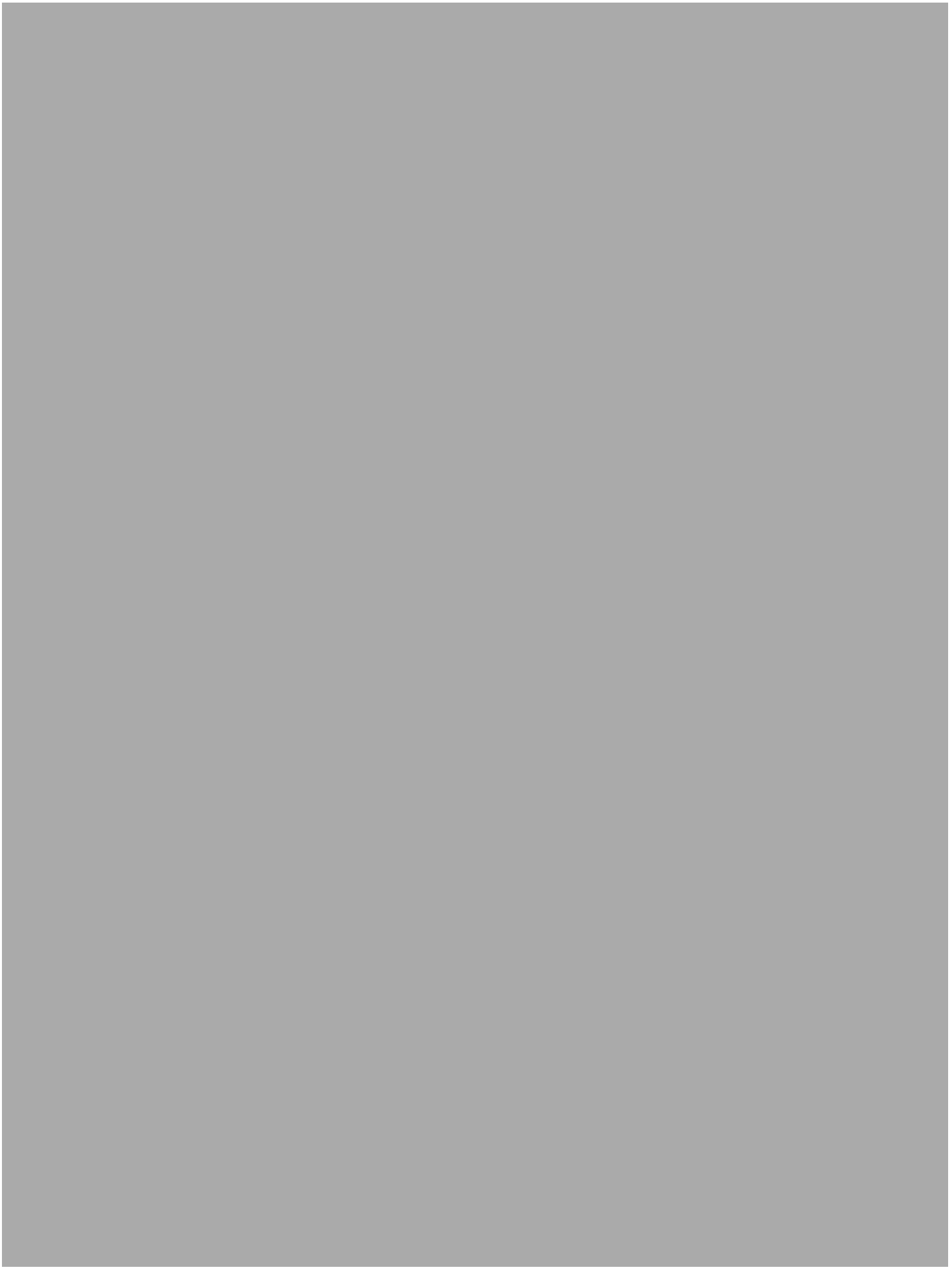

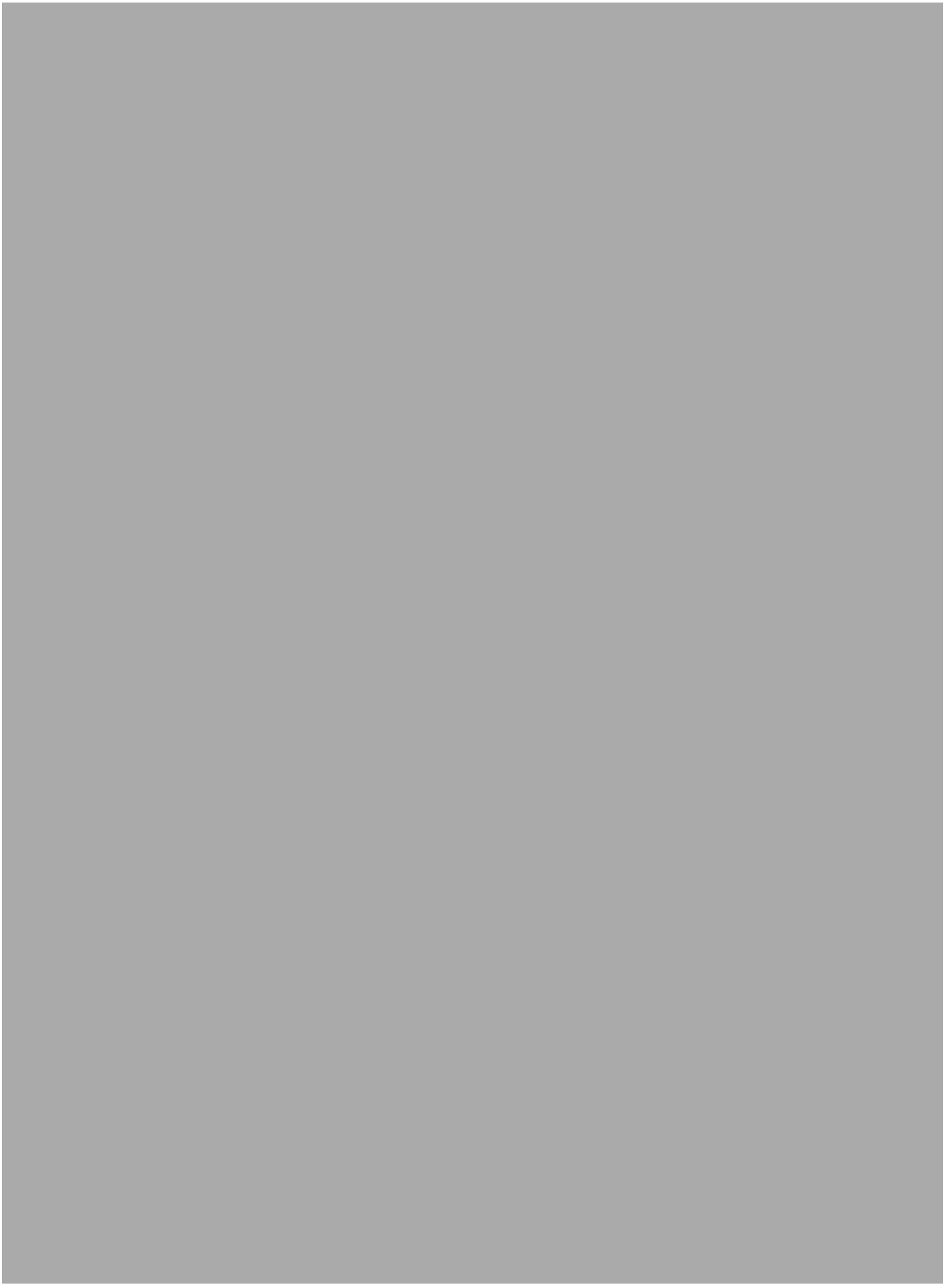

Appendix F

Feeding methods

Various feeding methods have been suggested for microstrip antennas. The most popular ones are: coax line, microstrips line, proximity coupled feed and aperture coupled feed. The advantages of microstrip feed lines is that they are easy to match with the patch only, by adjusting the inset point and they are also easy to fabricate. The drawback of them is that as the thickness of the substrate increases, the surface wave increases which leads to limitation of the bandwidth, unwanted radiations and lower efficiency. Coax lines are also easy to integrate and match to the patch. However, they are narrow bandwidth feed lines. The common disadvantages of probe fed and microstrip feed lines is that they cause cross polarized radiation . This problem can be tackled by utilizing an aperture-coupling feed and a proximity-coupling feed. In these feeding approaches, matching is achieved by changing the width and the length of the feed line. The reason that they are not as common as the first two methods is that they are difficult to fabricate. Figure 3(a, b, c, d) illustrates different feeding approaches [7]. Figure

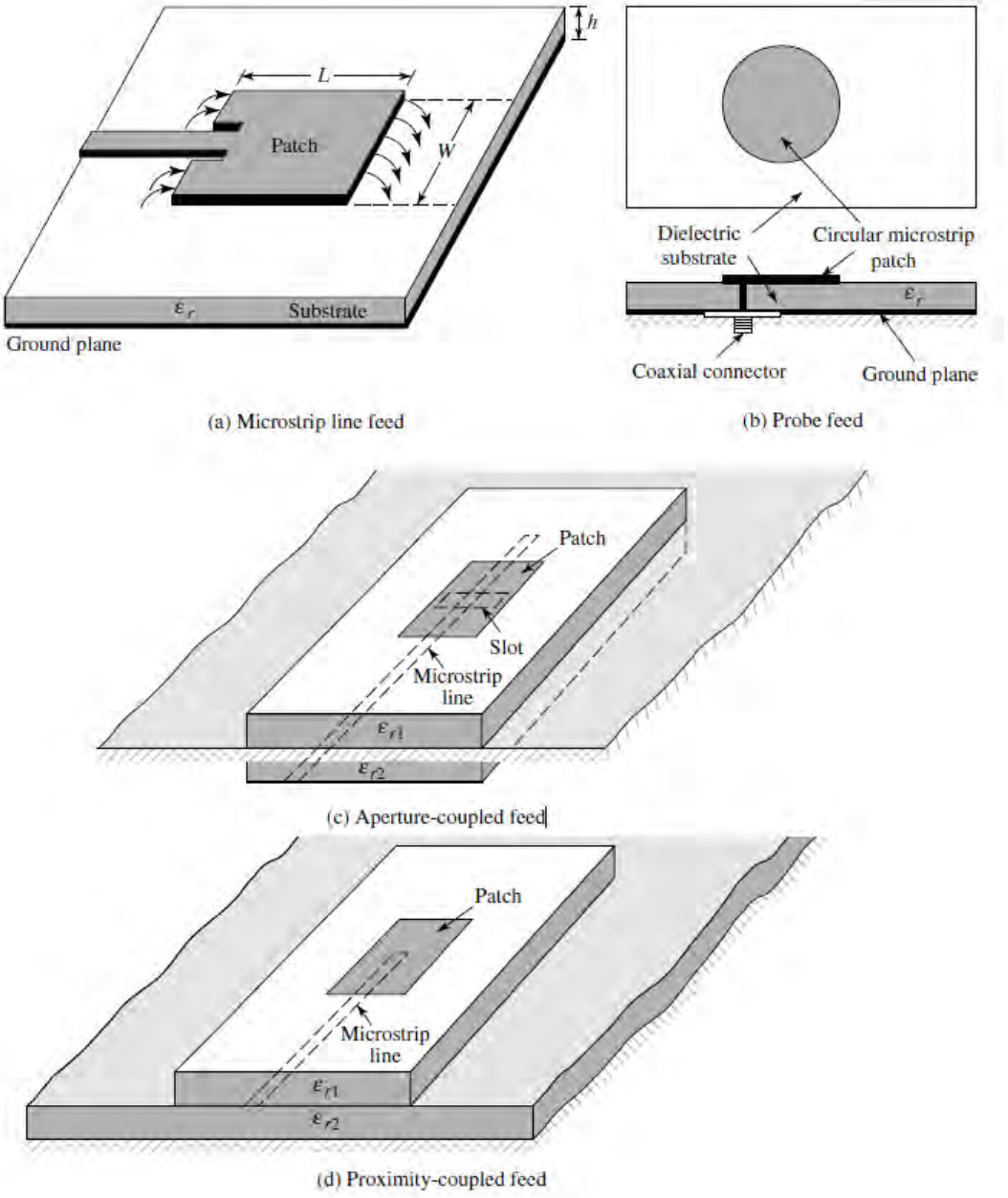

Figure F.1: Various feeding configuration. (a)Microstrip feed (b) Probe feed (c) Aperture-coupled feed (d) Proximity-coupled feed [7]

Appendix G

Design notes for wide band antenna design

To provide wideband bandwidth operation from a patch antenna the following design is developed based on the work presented in [89]

In the developed configuration (microstrip feed) presented in Fig. G.1 (a) the gap between the ground plane and the patch acts as an impedance matching network and it can tune the input impedance. Consequently, it has significant effect on the band width of the antenna. The other two important parameters on the antenna performance are the width of the ground and the size of the patch. These are important as the size of the patch is provides the lower resonance while width of the ground becomes important for higher harmonics. This can be understood from the current distribution on the modified design, demonstrated in Figs. G.1 (b) and (c). Fig. G.1 (b)is associated with the first resonance and the current distribution is concentrated on the patch and not the ground edge. This can be also understood from Fig. G.1 (d) which illustrates the dependence between resonance and the radios for the first harmonic. However for the higher harmonics, the current distributes on th ground and patch as can be seen in Fig. Fig. G.1 (b) which can be tuned by the gap in Fig. G.1 (a).

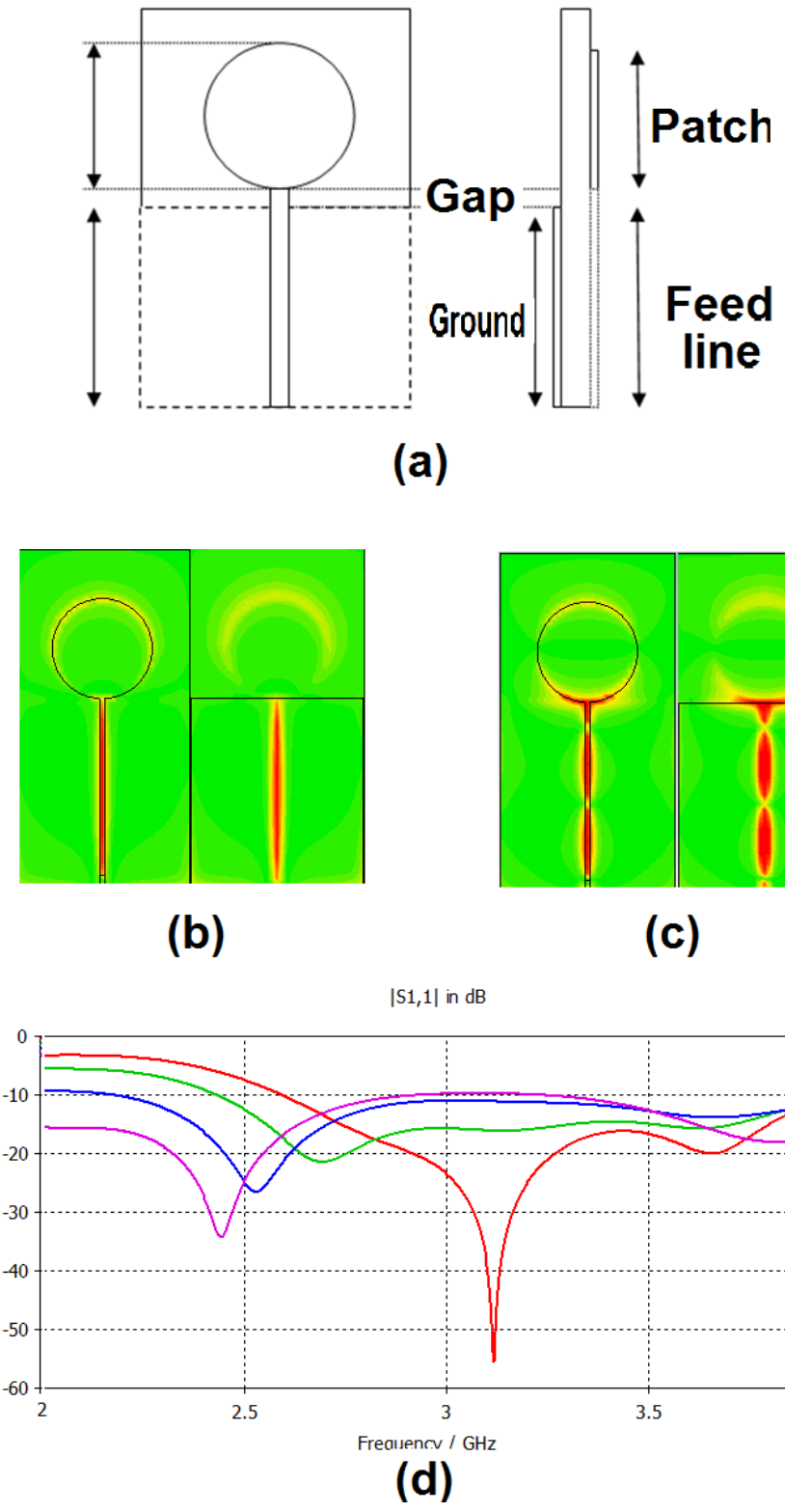

Figure G.1: (a)Design configuration of the wide band patch antenna(b) current distribution on front and back of the patch near (b) first resonant 1.9GHz (c) second resonant 3.7GHz (d) S11 for different radiuses of the patch

Appendix H

The varactor diodes

Table 3 shows some suitable Varactor diodes for tuning RF circuits which operates in UHF bands, from Skyworks Company [102].

List of References

[1] Rowell C, Lam EY. Mobile-Phone Antenna Design. IEEE Antennas and Propagation Magazine. 2012 Aug;54(4):14–34.

[2] Jofre L, Martinez M, Serrano R, Roqueta G. Handbook on small antennas. EurAPP Technical Working Group on Compact Antennas; 2012.

[3] Byford JA, Park KY, Chahal P, Rothwell EJ. Frequency reconfigurable patch antenna array. Electronics Letters. 2015;51(21):1628–1630.

[4] Bhellar B, Tahir FA. Frequency reconfigurable antenna for hand-held wireless devices. IET Microwaves, Antennas Propagation. 2015;9(13):1412–1417.

[5] Pal H, Choukiker YK. Design of frequency reconfigurable antenna with ambient RF-energy harvester system. In: 2016 International Conference on Information Communication and Embedded Systems (ICICES); 2016. p. 1–5.

[6] Behera AK, Agarwal M, Pandey G, Meshram MK. Frequency-reconfigurable triple band antenna for mobile handsets. In: 2015 IEEE Applied Electromagnetics Conference (AEMC); 2015. p. 1–2.

[7] Balanis CA. Antenna theory: analysis and design. John Wiley & Sons; 2016.

[8] Vainikainen P, Holopainen J, Icheln C, Kivekas O, Kyro M, Mustonen M, et al. More than 20 antenna elements in future mobile phones, threat or opportunity? In: Antennas and Propagation, 2009. EuCAP 2009. 3rd European Conference on; 2009. p. 2940–2943.

[9] Osseiran A, Boccardi F, Braun V, Kusume K, Marsch P, Maternia M, et al. Scenarios for 5G mobile and wireless communications: the vision of the METIS project. Communications Magazine, IEEE. 2014;52(5):26–35.

[10] Jin P, Ziolkowski RW. Low-Q, Electrically Small, Efficient Near-Field Resonant Parasitic Antennas. Antennas and Propagation, IEEE Transactions on. 2009;57(9):2548–2563.

[11] Chu LJ. Physical Limitations of Omni Directional Antennas. Journal of Applied Physics. 1948 Dec;19(12):1163–1175.

[12] Wheeler HA. Fundamental relations in the design of a VLF transmitting antenna. Antennas and Propagation, IRE Transactions on. 1958;6(1):120–122.

[13] Sievenpiper DF, Dawson DC, Jacob MM, Kanar T, Kim S, Long J, et al. Experimental Validation of Performance Limits and Design Guidelines for Small Antennas. Antennas and Propagation, IEEE Transactions on. 2012 Jan;60(1):8–19.

[14] Wheeler HA. Fundamental Limitations of Small Antennas. Proceedings of the IRE. 1947 Dec;35(12):1479–1484.

[15] Wheeler HA. The Radiansphere around a Small Antenna. Proceedings of the IRE. 1959 Aug;47(8):1325–1331.

[16] Wheeler HA. Small antennas. Antennas and Propagation, IEEE Transactions on. 1975 Jul;23(4):462–469.

[17] Wheeler HA. The Spherical Coil as an Inductor, Shield, or Antenna. Proceedings of the IRE. 1958 Sept;46(9):1595–1602.

[18] Pozar DM. Microwave engineering. Wiley. com; 2009.

[19] Collin R, Rothschild S. Evaluation of antenna Q. IEEE Transactions on Antennas and Propagation. 1964 Jan;12(1):23–27.

[20] Hansen RC. Fundamental limitations in antennas. Proceedings of the IEEE. 1981 Feb;69(2):170–182.

[21] McLean JS. A re-examination of the fundamental limits on the radiation Q of electrically small antennas. IEEE Transactions on Antennas and Propagation. 1996 May;44(5):672–.

[22] Goubau G. Multi-element Monopole Antennas. Proc Workshop on Electrically Small Antennas, ECOM, Ft Monmouth, NJ. 1976 May;(5):36–67.

[23] Mavridis GA, Anagnostou DE, Chryssomallis MT. Evaluation of the Quality Factor, Q, of Electrically Small Microstrip-Patch Antennas [Wireless Corner]. Antennas and Propagation Magazine, IEEE. 2011;53(4):216–224.

[24] Mavridis GA, Christodoulou CG, Chryssomallis MT. Area miniaturization of a microstrip patch antenna and the effect on the quality factor Q. In: Antennas and Propagation Society International Symposium, 2007 IEEE; 2007. p. 5435–5438.

[25] Mavridis GA, Anagnostou DE, Christodoulou CG, Chryssomallis MT. Quality factor Q of a miniaturized meander microstrip patch antenna. In: Antennas and Propagation Society International Symposium, 2008. AP-S 2008. IEEE; 2008. p. 1–4.

[26] Best SR. Low Q electrically small linear and elliptical polarized spherical dipole antennas. Antennas and Propagation, IEEE Transactions on. 2005;53(3):1047–1053.

[27] Kim OS. Low-Q Electrically Small Spherical Magnetic Dipole Antennas. Antennas and Propagation, IEEE Transactions on. 2010;58(7):2210–2217.

[28] Lim S, Rogers RL, Ling H. A tunable electrically small antenna for ground wave transmission. IEEE Transactions on Antennas and Propagation. 2006 Feb;54(2):417–421.

[29] Kim O. Low-Q Electrically Small Spherical Magnetic Dipole Antennas. IEEE Transactions on Antennas and Propagation. 2010 July;58(7):2210–2217.

[30] Hallbjorner P. Electrically small unbalanced four-arm wire antenna. IEEE Transactions on Antennas and Propagation. 2004 June;52(6):1424–1428.

[31] Altshuler EE. Electrically small self-resonant wire antennas optimized using a genetic algorithm. IEEE Transactions on Antennas and Propagation. 2002 Mar;50(3):297–300.

[32] Altshuler EE. A method for matching an antenna having a small radiation resistance to a 50-ohm coaxial line. IEEE Transactions on Antennas and Propagation. 2005 Sept;53(9):3086–3089.

[33] Sentucq B, Sharaiha A, Collardey S. Metamaterial-inspired electrically small antenna for UHF applications. In: Antenna Technology and Applied Electromagnetics (ANTEM), 2012 15th International Symposium on; 2012. p. 1–4.

[34] Ziolkowski RW, Erentok A. Metamaterial-based efficient electrically small antennas. IEEE Transactions on Antennas and Propagation. 2006 July;54(7):2113–2130.

[35] Jin P, Ziolkowski RW. High-Directivity, Electrically Small, Low-Profile Near-Field Resonant Parasitic Antennas. IEEE Antennas and Wireless Propagation Letters. 2012;11:305–309.

[36] Cutshall RT, Ziolkowski RW. Comparisons of the planar and 3D Egyptian axe dipole NFRP antennas' performance characteristics. In: Antennas and Propagation Society International Symposium (APSURSI), 2012 IEEE; 2012. p. 1–2.

[37] Jin P, Ziolkowski RW. Broadband, Efficient, Electrically Small Metamaterial-Inspired Antennas Facilitated by Active Near-Field Resonant Parasitic Elements. IEEE Transactions on Antennas and Propagation. 2010 Feb;58(2):318–327.

[38] Ziolkowski RW, Jin P, Lin CC. Metamaterial-Inspired Engineering of Antennas. Proceedings of the IEEE. 2011 Oct;99(10):1720–1731.

[39] Erentok A, Ziolkowski RW. Metamaterial-Inspired Efficient Electrically Small Antennas. IEEE Transactions on Antennas and Propagation. 2008 March;56(3):691–707.

[40] Jin P, Ziolkowski RW. Multi-Frequency, Linear and Circular Polarized, Metamaterial-Inspired, Near-Field Resonant Parasitic Antennas. IEEE Transactions on Antennas and Propagation. 2011 May;59(5):1446–1459.

[41] Sussman-Fort SE, Rudish RM. Non-Foster Impedance Matching of Electrically-Small Antennas. Antennas and Propagation, IEEE Transactions on. 2009 Aug;57(8):2230–2241.

[42] Bit-Babik G, Di Nallo C, Svigelj J, Faraone A. Small Wideband Antenna with non-Foster Loading Elements. In: Electromagnetics in Advanced Applications, 2007. ICEAA 2007. International Conference on; 2007. p. 105–107.

[43] Sussman-Fort SE, Rudish RM. Non-Foster impedance matching of electrically-small antennas. Antennas and Propagation, IEEE Transactions on. 2009;57(8):2230–2241.

[44] MacLean WR. The Reactance Theorem for a Resonator. Proceedings of the IRE. 1945 Aug;33(8):539–541.

[45] Elfrgani AM, Rojas RG. Non-Foster circuit embedded within electrically small antenna. In: Antennas and Propagation Society International Symposium (APSURSI), 2014 IEEE; 2014. p. 466–467.

[46] Tade OO, Gardner P, Hall PS. Negative impedance converters for broadband antenna matching. In: Microwave Conference (EuMC), 2012 42nd European; 2012. p. 613–616.

[47] Fan Y, Rajab KZ, Munoz M, Hao Y. Electrically small half-loop antenna design with non-foster matching networks. In: Antennas and Propagation (EUCAP), 2012 6th European Conference on; 2012. p. 126–129.

[48] Tomimoto K, Fukusako T. Electrically small and low-profile antenna using non -foster element (NFE). In: Electromagnetics (iWEM), 2014 IEEE International Workshop on; 2014. p. 54–55.

[49] Shen Y, Chio TH. Matching electrically small antenna using non-Foster circuit in the FM-band. In: Antennas and Propagation (EuCAP), 2014 8th European Conference on; 2014. p. 333–336.

[50] Mirzaei H, Eleftheriades G. A Resonant Printed Monopole Antenna With an Embedded Non-Foster Matching Network. IEEE Transactions on Antennas and Propagation. 2013 Nov;61(11):5363–5371.

[51] Elghannai EA, Rojas RG. Design of USB dongle antenna for WLAN applications using theory of characteristic modes. Electronics Letters. 2014 February;50(4):249–251.

[52] Mautz JR, Harrington RF. Modal analysis of loaded N-port scatterers. Antennas and Propagation, IEEE Transactions on. 1973 Mar;21(2):188–199.

[53] Obeidat KA, Raines BD, Rojas RG. Application of Characteristic Modes and Non-Foster Multiport Loading to the Design of Broadband Antennas. IEEE Transactions on Antennas and Propagation. 2010 Jan;58(1):203–207.

[54] Elghannai EA, Raines BD, Rojas RG. Multiport Reactive Loading Matching Technique for Wide Band Antenna Applications Using the Theory of Characteristic Modes. Antennas and Propagation, IEEE Transactions on. 2015 Jan;63(1):261–268.

[55] Tang MC, Zhu N, Ziolkowski RW. Augmenting a Modified Egyptian Axe Dipole Antenna With Non-Foster Elements to Enlarge Its Directivity Bandwidth. IEEE Antennas and Wireless Propagation Letters. 2013;12:421–424.

[56] Church J, Chieh JCS, Xu L, Rockway JD, Arceo D. UHF Electrically Small Box Cage Loop Antenna With an Embedded Non-Foster Load. IEEE Antennas and Wireless Propagation Letters. 2014;13:1329–1332.

[57] Cutshall RT, Ziolkowski RW. Performance Characteristics of Planar and Three-Dimensional Versions of a Frequency-Agile Electrically Small Antenna. IEEE Antennas and Propagation Magazine. 2014 Dec;56(6):53–71.

[58] Di Nallo C, Bit-Babik G, Faraone A. Wideband antenna using non-foster loading elements. In: Antennas and Propagation Society International Symposium, 2007 IEEE; 2007. p. 4501–4504.

[59] Ziolkowski RW, Zhu N. Electrically small antennas augmented with internal non-foster elements. In: Radio Science Meeting (Joint with AP-S Symposium), 2013 USNC-URSI; 2013. p. 225–225.

[60] Zhu N, Ziolkowski RW. Broad-Bandwidth, Electrically Small Antenna Augmented With an Internal Non-Foster Element. Antennas and Wireless Propagation Letters, IEEE. 2012;11:1116–1120.

[61] Zhu N, Ziolkowski RW. Broad-Bandwidth, Electrically Small Antenna Augmented With an Internal Non-Foster Element. IEEE Antennas and Wireless Propagation Letters. 2012;11:1116–1120.

[62] Barbuto M, Monti A, Bilotti F, Toscano A. Design of a Non-Foster Actively Loaded SRR and Application in Metamaterial-Inspired Components. IEEE Transactions on Antennas and Propagation. 2013 March;61(3):1219–1227.

[63] Zhu N, Ziolkowski RW. Active Metamaterial-Inspired Broad-Bandwidth, Efficient, Electrically Small Antennas. IEEE Antennas and Wireless Propagation Letters. 2011;10:1582–1585.

[64] Ayatollahi M, Rao Q, Wang D. A Compact, High Isolation and Wide Bandwidth Antenna Array for Long Term Evolution Wireless Devices. IEEE Transactions on Antennas and Propagation. 2012 Oct;60(10):4960–4963.

[65] Rao Q, Wang D. A compact dual-port diversity antenna for handheld devices. In: Antennas Propagation Conference, 2009. LAPC 2009. Loughborough; 2009. p. 181–184.

[66] Rao Q, Wang D. A Compact Dual-Port Diversity Antenna for Long-Term Evolution Handheld Devices. IEEE Transactions on Vehicular Technology. 2010 March;59(3):1319–1329.

[67] Wang R, Wang BZ, Gong ZS, Ding X. Compact Multiport Antenna With Radiator-Sharing Approach and Its Performance Evaluation of Time Reversal in an Intra-Car Environment. IEEE Transactions on Antennas and Propagation. 2015 Sept;63(9):4213–4219.

[68] Chattha HT, Nasir M, Abbasi QH, Huang Y, Alja'afreh SS. Compact Low-Profile Dual-Port Single Wideband Planar Inverted-F MIMO Antenna. IEEE Antennas and Wireless Propagation Letters. 2013;12:1673–1675.

[69] Li WW, Zhang B, Zhou JH, You BQ. High isolation dual-port MIMO antenna. Electronics Letters. 2013 July;49(15):919–921.

[70] Wen YQ, Wang BZ, Ding X. Planar Microstrip Endfire Antenna With Multiport Feeding. IEEE Antennas and Wireless Propagation Letters. 2016;15:556–559.

[71] Hall P, Gardner P, Kelly J, Ebrahimi E, Hamid M, Ghanem F, et al. Reconfigurable antenna challenges for future radio systems. EuCAP 2009. 2009;.

[72] Costantine J, Tawk Y, Barbin SE, Christodoulou CG. Reconfigurable Antennas: Design and Applications. Proceedings of the IEEE. 2015 March;103(3):424–437.

[73] Al-Husseini M, Ramadan A, Zamudio ME, Christodoulou CG, El-Hajj A, Kabalan KY. A UWB antenna combined with a reconfigurable bandpass filter for cognitive radio applications. In: Antennas and Propagation in Wireless Communications (APWC), 2011 IEEE-APS Topical Conference on; 2011. p. 902–904.

[74] Gardner P, Feresidis A, Hall PS, Jackson TJ, Tade O, Mavridou M, et al. Frequency reconfiguration in single and dual antenna modules. In: Antennas and Propagation (EuCAP), 2013 7th European Conference on; 2013. p. 2006–2009.

[75] Ebrahimi E, Hall PS. A dual port wide-narrowband antenna for cognitive radio. In: Antennas and Propagation, 2009. EuCAP 2009. 3rd European Conference on; 2009. p. 809–812.

[76] Hamid MR, Gardner P, Hall PS, Ghanem F. Vivaldi Antenna With Integrated Switchable Band Pass Resonator. IEEE Transactions on Antennas and Propagation. 2011 Nov;59(11):4008–4015.

[77] Hamid MR, Gardner P, Hall PS, Ghanem F. Switched-Band Vivaldi Antenna. IEEE Transactions on Antennas and Propagation. 2011 May;59(5):1472–1480.

[78] Hall PS, Gardner P, Hu Z, Song P, Kelly J, Hamid MR. Reconfigurable antennas for wideband wireless systems. In: Adaptable and Tunable Antenna Technology for Handsets and Mobile Computing Products, 2009 IET Seminar on; 2009. p. 1–31.

[79] Tawk Y, Costantine J, Christodoulou CG. A frequency reconfigurable printed monopole with pattern diversity. IEEE Trans Antennas Propag. 2015;.

[80] Piazza D, Mookiah P, D'Amico M, Dandekar KR. Two Port Reconfigurable Circular Patch Antenna for MIMO Systems. In: Antennas and Propagation, 2007. EuCAP 2007. The Second European Conference on; 2007. p. 1–7.

[81] Osman MN, Rahim MKA, Hamid MR, Yusoff MFM, Majid HA. Compact Dual-Port Polarization-Reconfigurable Antenna With High Isolations for MIMO Application. IEEE Antennas and Wireless Propagation Letters. 2016;15:456–459.

[82] Doherty WH. A New High Efficiency Power Amplifier for Modulated Waves. Radio Engineers, Proceedings of the Institute of. 1936;24(9):1163–1182.

[83] Kabiri Y, Gardner P, Constantinou C. A novel approach for wideband tunable Electrically Small Antennas. In: Antennas and Propagation (EuCAP), 2014 8th European Conference on; 2014. p. 3633–3637.

[84] Kabiri Y, Gardner P, Constantinou C. Injection matched approach for wideband tunable electrically small antennas. Microwaves, Antennas Propagation, IET. 2014 August;8(11):878–886.

[85] CST Microwave Studio 2013 By Computer Simulation Technology;. Http://www.CST.com.

[86] AWR Design Envinronment Microwave Office 2010 By AWR Corporation;. Http://www.awrcorp.com.

[87] Kabiri Y, Gardner P, Constantinou C. Investigation of radiation from an injection matched antenna. In: Antennas and Propagation Conference (LAPC), 2014 Loughborough; 2014. p. 52–54.

[88] Rotaru MD, Sykulski JK. Band widening technique for small integrated packaged antennas. In: 2015 IEEE 17th Electronics Packaging and Technology Conference (EPTC); 2015. p. 1–4.

[89] Liang J, Chiau CC, Chen X, Parini CG. Study of a printed circular disc monopole antenna for UWB systems. Antennas and Propagation, IEEE Transactions on. 2005 Nov;53(11):3500–3504.

[90] Rodriguez JL, Garcia-Tunon I, Taboada JM, Obelleiro Basteiro F. Broadband HF Antenna Matching Network Design Using a Real-Coded Genetic Algorithm. Antennas and Propagation, IEEE Transactions on. 2007 March;55(3):611–618.

[91] Vector Network Analyzers Operating Manual; 2015. Available from: `http://cdn.rohde-schwarz.com`.

[92] Hu ZH, Kelly J, Song CTP, Hall PS, Gardner P. Equivalent circuit modeling of chassis-antenna with two coupling elements. In: Antennas and Propagation Society International Symposium (APSURSI), 2010 IEEE; 2010. p. 1–4.

[93] Hu ZH, Kelly J, Song CTP, Hall PS, Gardner P. Novel wide tunable dual-band reconfigurable chassis-antenna for future mobile terminals. In: Antennas and Propagation (EuCAP), 2010 Proceedings of the Fourth European Conference on; 2010. p. 1–5.

[94] Hu ZH, Song CTP, Kelly J, Hall PS, Gardner P. Novel reconfigurable dual-port UWB chassis-antenna. In: Antennas and Propagation Society International Symposium (APSURSI), 2010 IEEE; 2010. p. 1–4.

[95] Osseiran A, Boccardi F, Braun V, Kusume K, Marsch P, Maternia M, et al. Scenarios for 5G mobile and wireless communications: the vision of the METIS project. IEEE Communications Magazine. 2014 May;52(5):26–35.

[96] Cisco CVNI. Global mobile data traffic forecast update, 2013–2018. white paper. 2014;.

[97] Ericsson L. More than 50 billion connected devices. Ericsson White Paper. 2011;.

[98] Chiw ST, Gardner P, Gao SC. Compact power combining patch antenna. Electronics Letters. 2002 Nov;38(23):1413–1414.

[99] Chiu L, Xue Q, Chan CH. Dual-fed patch antenna with distorted patch mode for balanced circuits. IET Microwaves, Antennas Propagation. 2010 July;4(7):809–816.

[100] Office M. AWR Design Environment;. Available from: `http://www.awrcorp.com`.

[101] RF Vector Modulator Analog device technology;. Available from: `http://www.analog.com/media/en/technical-documentation/evaluation-documentation/AD8341.pdf`.

[102] Varactor Sky works technology;. Available from: `http://www.skyworksinc.com`.